GENERATION OF LOW FREQUENCY WAVES BY ENERGETIC PARTICLES IN SPACE PLASMAS

A THESIS

SUBMITTED TO THE UNIVERSITY OF MUMBAI

FOR THE

Ph.D. (SCIENCE) DEGREE IN PHYSICS

Submitted by

T. SREERAJ

Under the guidance of

Prof. SATYAVIR SINGH

Indian Institute of Geomagnetism (IIG)

Plot No. 5, Sector 18, Near Kalamboli Highway

New Panvel (W), Navi Mumbai- 410 218,

Maharashtra, India

February 2019

To my father, mother and all my well wishers...

STATEMENT BY THE CANDIDATE

As required by the University Ordinances 770, I wish to state that the work embodied in this thesis titled "Generation of Low Frequency Waves by Energetic Particles in Space Plasmas" forms my own contribution to the research work carried out under the guidance of Prof. Satyavir Singh at the Indian Institute of Geomagnetism, New Panvel, Navi Mumbai. This work has not been submitted for any other degree of this or any other University. Wherever references have been made to previous works of others, it has been clearly indicated as such and included in the Bibliography.

Signature of Candidate

Full Name: T. Sreeraj

Certified by

Signature of Guide

Name: Prof. Satyavir Singh

Statement required under 0.770 **Statement No. 1**

I hereby declare that the work described in the thesis has not been submitted previously to this or any other University for Ph.D or any other degree.

Statement required under 0.771 **Statement No. 2**

"Whether the work is based on the discovery of new facts by the candidate or of new relations of facts observed by others, and how the work tends to the general advancement of knowledge".

The thesis explores the propagation characteristics and generation of various plasma waves in diverse space plasma environment. Chap. 1 provides an introduction to subject of plasma physics explaining the various sources of plasma, theoretical approaches used to investigate it and describing about various waves that are under study. Chaps. 2 to 5 elaborate on the original work done by the candidate. The conclusion and suggestion for future work are provided in Chap. 6 of the thesis.

A brief summary of the important new findings is given below:

- The study of coupling of electrostatic ion cyclotron and ion acoustic waves has been carried out in solar wind plasma. It is seen that with the increase in the angle of propagation, the strength of coupling decreases and for perpendicular propagation the the coupling vanishes. Furthermore, except for Helium cyclotron mode, effect of Helium ion concentration is negligible, where the frequency of Helium cyclotron mode increases with increase in Helium ion concentration. The decrease in the superthermality index decreases the frequencies of all modes, except for slow ion acoustic mode for which there is insignificant effect of superthermality. The effect of helium ion temperature is significant on the frequency of helium cyclotron mode and it increases with increase in temperature

- For the first time, electron beam driven electrostatic waves are studied through a theoretical multi-component plasma model in the lunar wake. The theoretical model de-

veloped here is applied to electrostatic waves observed by ARTEMIS mission in the first flyby. Our analysis shows that the observed low (high) electrostatic waves could be electron beam driven slow (fast) ion acoustic modes, which falls in the frequency range reported by Tao et al. (2012).

- We have studied the linear dispersion relation characteristics and instability of harmonics of electrostatic ion cyclotron waves in three component magnetized plasma comprising of consisting of beam electrons, protons and doubly charged Helium ions. We have shown that there is an interesting pattern for Helium harmonics as largely odd harmonics are getting exited for the relevant plasma parameters whereas for proton harmonics both odd and even harmonics are excited. To the authors knowledge, this kind of behavior has not been reported earlier neither theoretically/experimentally nor in space observations.

- Moreover, we have observed that with change of angle of propagation, the peak growth rate not necessarily always maximizes at $k\rho_p \sim$ n; n being the harmonic number, in contrast with what was reported by Okuda et al. (1981b). The theory developed here can be applied to EIC observations in laboratory plasmas (Suszcynsky et al., 1989) as well as space plasmas (Gavrishchaka et al., 2000; Backrud et al., 2005a; Tang et al., 2015).

Statement required under 0.771 **Statement No. 3**

"The source from which this information has been derived and to the extent to which he has based his work on the work of others, and shall indicate which portion or portions of his thesis he claims as original".

The information mentioned is derived by the candidate during the course of research work which is reported in the thesis. Some of the results presented in the thesis are published in the following research articles:

- **Papers Published and communicated in Journals**

1. **T. Sreeraj**, S. V. Singh, and G. S. Lakhina, Coupling of electrostatic ion cyclotron

and ion acoustic waves in the solar wind, *Phys. Plasmas*, 23, 082901 (2016); doi: 10.1063/1.4960657

2. **T. Sreeraj**, S. V. Singh, and G. S. Lakhina, Electrostatic waves driven by electron beam in lunar wake plasma, *Phys. Plasmas*, 25, 052902 (2018); doi: 10.1063/1.5032141

3. G. S. Lakhina, S. V. Singh, R. Rubia, and **T. Sreeraj**, A review of nonlinear fluid models for ion-and electron-acoustic solitons and double layers: Application to weak double layers and electrostatic solitary waves in the solar wind and the lunar wake, *Phys. Plasmas*, 25, 080501 (2018); doi: 10.1063/1.5033498

4. **T. Sreeraj**, S. V. Singh, and G. S. Lakhina, A study of higher harmonic instability of electrostatic ion cyclotron waves, *Pramana – J. Phys.*, Manuscript accepted for publication (2018)

• **Papers presented in National and International conferences:**

1. **T. Sreeraj**, S. Devanandhan, S. V. Singh and G. S. Lakhina, *Ion Cyclotron and Ion Acoustic Waves In magnetised Plasma With Kappa Distribution Of Electrons* presented at 29^{th} National Symposium On Plasma Science & Technology- PLASMA-2014 held at International & Inter University Centre for Nanoscience and Nanotechnology, School of Pure & Applied Physics, Mahatma Gandhi University, Kottayam, Kerala, India (December 08-11, 2014)

2. S. Devanandhan, **T. Sreeraj**, S. V. Singh and G. S. Lakhina, *Influence Of Superthermal Electrons On Obliquely Propagating Ion-Acoustic Solitary Waves In Space Plasmas* presented at 29^{th} National Symposium On Plasma Science & Technology- PLASMA-2014 held at International & Inter University Centre for Nanoscience and Nanotechnology, School of Pure & Applied Physics, Mahatma Gandhi University, Kottayam, Kerala, India (December 08-11, 2014)

3. **T. Sreeraj**, S. V. Singh and G. S. Lakhina, *Electrostatic Ion Cyclotron Waves in Solar Wind* presented at 2^{nd} URSI Regional Conference on Radio Science, (URSI- RCRS-2015) held at Jawaharlal Nehru University, New Delhi, India (November 16-19, 2015).

4. S. Devanandhan, **T. Sreeraj**, S. V. Singh, G. S. Lakhina, *Oblique Propagation of Ion Acoustic Solitons in Magnetized Superthermal Plasmas* presented at American Geophysical Union- Fall Meeting held at San Francisco, USA (14-18, December, 2015)

5. **T. Sreeraj**, S. V. Singh, G. S. Lakhina, *Harmonics of electrostatic ion cyclotron waves in three component magnetised plasma* presented at 42nd COSPAR Scientific Assembly held at Pasadena, California, U. S. A on (14-22 July, 2018)

6. **T. Sreeraj**, S. V. Singh, G. S. Lakhina, *Electron beam driven electrostatic waves in the lunar wake plasma* presented at 42nd COSPAR Scientific Assembly held at Pasadena, California, U. S. A on (14-22 July, 2018)

7. **T. Sreeraj**, S. V. Singh, G. S. Lakhina, *Kinetic Study of Electrostatic Waves in Lunar Wake Plasma with Kappa electrons and Kappa Beam Electron* presented at 100th AGU Fall meeting held at Washington D.C., U. S. A on (10-14 December, 2018)

Statement required under 0.771 **Statement No. 4**

"Where a candidate presents joint work, he shall clearly state the portion which is his own contribution as distinguished from the portion contributed by his collaborators."

The complete analytical and numerical computations are done by the candidate in the papers mentioned in Statement No. 3. Prof. Satyavir Singh helped in formulating the research problems and taught various theoretical methods. The derivation of dispersion relation of the modes listed in the thesis is carried out by student. Prof. G. S. Lakhina helped in the interpretation of the results obtained during the course of research work presented in this thesis.

(Prof. Satyavir Singh) **(T. Sreeraj)**

Guiding Teacher **Candidate**

Acknowledgments

Some moments are nice, some are nicer, some are even worth writing about:-

Charles Bukowski, *War All the Time*

The journey towards submitting the Ph.D. was a memorable one. It is now the time to look back and thank those who had played a significant role in helping me to achieve this feat.

First, I am indebted to Prof. Satyavir Singh, my research guide at IIG, who accepted my request to work under him. Before coming to IIG, plasma, for me, was just a 'fourth state of matter' and the term 'magnetosphere' was completely alien to me. He taught me the ABCs of plasma physics and continually motivated me during all the hard times. Prof. G. S. Lakhina, emeritus scientist, is another person who has further enriched my knowledge in plasma physics. The discussions with him was always a source of new insights into this subject. Both Prof. G. S. Lakhina and Prof. Satyavir Singh gave me very crucial suggestions towards advancement of my thesis work and I feel privileged to work with them.

I also acknowledge Prof. R. V. Reddy for the help rendered during the course of my tenure here. I express my sincere thanks to Prof. Amar Kakad, who has always helped me in understanding and writing the Mathematica codes. I always cherish the random discussions I had with Prof. Suktisama Ghosh in the canteen. We have talked about everything under the sun. Dr. B. Remya (or Remyaechi) also helped me to clarify some doubts about the codes that I have used for my studies. I wish to thank Prof. D. S. Ramesh, Director, IIG for his cooperation and for permitting me to avail the facilities in the institute for successful completion of my work. Department of Science and Technology (DST), Government of India provided financial support that I received in the form of stipends and travel grant. For this, I would like to acknowledge the common man of my nation.

How can one forget the experience of being surrounded by many loving persons and many well-wishers? I was fortunate to be enjoying the company of many people. My sincere thanks to Selva bhai (R. Selva Kumaran), Sneha didi (Sneha Gokani), Chinmay bhai (Chinmaya Kumar Nayak) and Remyaechi for the hospitality that was offered to me. I want to express my deep gratitude to Dr. Devanandhan, who have always helped me and provided constant support. Many thanks for Sandeepaettan (Sandeep Sathian) and Mahesh bhai (J. L. V. Mahesh Babu) for the moral support provided on the hour of need.

Trekking was a new revelation to me. To me, it is a way to interact much with Nature and a great stress buster. I have to thank Singhji (Dupinder Singh) for including me in his many trekking adventures. I cannot forget the first trekking that I ever had to nearby Nevali hills along with the wonderful company of Kuttiyaettan (Mohd. Kutty), Sunilaettan (Sunil Kumar A. S.) and Sukanta bhai and seeing the IIG from top of the hills. In addition, Sunilaettan was the first contact that I made in IIG and has always been there whenever I needed any help. The company along with Priyeshaettan (K. Priyesh) has been always a memorable one and I am grateful to him for this. Thanks to Vijay (P. Vijaya Kumar), my roommate for putting up with me though our daily routine timings were 180° phase shifted. I want to thank Singhji, Vijay and Megha Pandya for helping me with Matlab program. The company of Nagarjuna and Ramsingh were the one that I will always cherish. Kamalam, Hari (Harikrishnan), Dhanya, Padma, Ajish, Rubia, Krushna, Biswajit, Debrup bhai have been new additions to my friends circle. The discussions about anything with Kamalam and Hari always brought new insights. Thanks to Kamalam for providing me an untiring support during my course. Thanks to Hari for giving me a hand when I started learning Mathematica programming. Thanks to Dhanya and Padma for helping me through this entire course. Thanks also to Ajithaettan (Ajith K. K.), Steffy and Radhika. Thanks also to mama in the canteen who has served me even in the wee hours. I would like to thank unknown people at StackExchange community for answering my questions. My sincere thanks to people at Wolfram community and also at MathWorks community.

My teachers were always kind enough to guide me throughout my lifetime and it will be an injustice not to mention them. My sincere thanks to Prof. Mani at Salafi English Medium School, who motivated me to pursue physics. When I joined for B.Sc. at S.N. College, Kannur, Prof. B. Dheepak opened up a new window to physics world. I also thank

Remya miss for all the discussions about exciting topics in physics. Sincere thanks to Nithya miss. At this stage, I also fondly remembers the company of Praveen, Hithin, Nishanth, Anju, Dinsha, Chethan, Rakhi, Sudhina & Priyanka and all other people and memorable moments at SN college.

Ashokan Sir, Madhu Sir, Deepesh Sir and Aneesh Sir at TASC, Taliparmaba, introduced me to the higher level of physics and their teaching helped me to understand many concepts. I thank Sreejith, Arunaettan and Sijithaettan for the friendship they offered to me at TASC. I would like to thank Dr. Ravi Krishna Menon for teaching me to the problem solving skills in physics. Thanks also to Dr. K. M. Udayanandan, who gave me the first taste about how to tackle the research problem while doing M.Sc. project under his supervision. Also, he introduced me softwares like Mathematica and LaTeX.

Coming to the family side. At the onset, I would like to remind that no written acknowledgment could articulate the appreciation I feel for these people. I am highly indebted to my father (Mr. Sreedharan), who has given all of his life for the betterment of the family. I will be ever grateful to him, and am sorry that he has not lived to see me submitting thesis, which he always wanted. I owe a debt of grateful to my mother (Mrs. Rajamani Sreedharan) and sister (Mrs. Reeshma Vaisakh) for supporting me through this entire process. Valyaettan (Vinod Kumar T) has given me the suggestion to read the Vignettes in Physics by G. Venkataraman, which has significantly changed the way I look the subject of physics and had been a constant motivator for my research work. Kunhaettan (Vineeth Kumar T) was also there whenever I needed any help and thanks for those Bangalore days. I express my sincere gratitude to my uncles Ananthakrishnan and Madhavan and also to T. V. Padmanabhan.

And, finally, thank God...

(T. Sreeraj)

(February, 2019)

Contents

Chapter 1

Introduction

1.1 How it all started...

A long time ago sailors were crisscrossing the oceans in search of new lands. They were always guided by some scientific techniques/instruments and more over by superstitions. Most of the wonders that they viewed were attributed to some sort of mysterious phenomenon. The following observations made by them were not different: during a typical thunderstorm, the mast of the ship acquires a strange colour and glows like fire. Sailors regarded this as religious phenomenon and they considered this to be a good omen as St. Erasmus of Formia, a protector saint for sailors, was with them. So they named this phenomenon as 'St. Elmo's fire'. The first person to demystify this phenomenon was Benjamin Franklin: he discovered that iron rods which are pointed would light up during lightening storm. In his opinion this was similar to what was seen by sailors. A pioneer in static electricity he was, Franklin concluded that these were electrical phenomenon. These phenomenon also caught by the curios eyes of Charles Darwin during his voyages to study about the evolution (Thompson, 1828; Darwin, 1839). The first recorded figure of St. Elmo's fire were drawn by Zimmermann (1868) (Fig. 1.1).

When all this was happening, many discoveries were made in the field of science and in particular, physics. When a large DC voltage is applied between two electrodes kept in sealed glass tube which contains gas at lower pressure, a glowing phenomenon starts to appear inside it. These glass tubes were known as *discharge lamps/tubes* and these lights

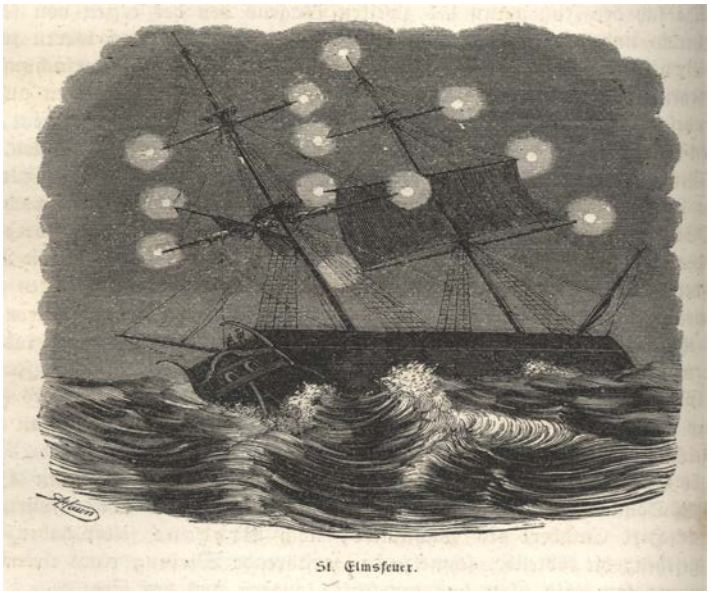

Figure 1.1: Painting of St. Elmo's fire (Zimmermann, 1868). (Figure courtesy: Official Flickr account of NOAA- https://www.flickr.com/ photos/51647007@N08/11951797835/)

were known as *cathode rays*. Though the apparatus became familiar towards the middle of nineteenth century, the reason for this glowing phenomenon was not understood. Sir William Crookes took first step in understanding this strange phenomenon. He ascertained that these cathode rays are a flux of particles. Crookes went extra-mile by developing the Crookes tube to investigate further about cathode rays. He delivered a lecture before the British Association for the Advancement of Science at Sheffield Friday August 22, 1870 titled 'On Radiant Matter'. In that lecture he said that "So distinct are these phenomena from anything which occurs in air or gas at the ordinary tension, that we are led to assume that we are here brought face to face with **Matter in a Fourth state** or condition, a condition as far removed from the state of gas as a gas is from liquid" (Crookes, 1879) [emphasis is mine]. Sir William Crookes was the first person to coin the term fourth state for this phenomena and that name struck.

Even though the technologies based on this discovery were increasing, the theoretical advances were none- notable exceptions were the work done by John Sealy Edward Townsend, Clement D. Child, Lewi Tonks. These were the people working in the field of gas discharge. But it was Irving Langmuir who took up a pivotal role in shaping the field of discharge tubes and consequently on fourth state. His fundamental achievements can be noted as follows (Morozov, 2013): -

1. Developed a new vacuum technology by which one could produce pure vacuum efficiently.

2. He saw the glowing discharge in Crooks tube that moulds itself to the shape of the Crooks tube. And consequently coined the term **plasma** in 1928 as it reminded him of blood plasma (and blood plasma were named after a Greek word, which means 'mouldable substance' or 'jelly'). Langmuir described his observations as: "Except near the electrodes, where there are sheaths containing very few electrons, the ionized gas contains ions and electrons in about equal numbers so that the resultant space charge is very small .We shall use the name plasma to describe this region containing balanced charges of ions and electrons"(Langmuir, 1928).

3. He modified the electrostatic probes, which were used to measure plasma parameters, viz. electronic temperature, electric potential and density of plasma. This is the reason why electrostatic probes are referred to as 'Langmuir' probes.

4. Along with Lewi Tonks, Langmuir conducted many studies. It is worthwhile to mention that it was with Tonks, Langmuir found out what is known as plasma oscillation, which now has the name Langmuir oscillation and calculated the frequency of it (Tonks and Langmuir, 1929).

Now the reason for the St.Elmo's fire were clear: it was nothing more than bluish-white plasma caused by the release of electrons in a strong electric field.

1.2 What is plasma?

In the early days scientists classified the matter which was seen around them into solid, liquid and gas. The solid is closely packed with strong inter-molecular force of attraction, molecules in liquid is not so strongly attracted with other liquid molecules while in gaseous states the molecules are very loosely packed with very less intermolecular force of attraction. The transition from one sate to another was also well defined: when you heat the solid to a sufficiently high temperature you will get liquid, if you heat liquid to sufficient high temperature you will get gas. In each transformation, we are supplying energy to the molecules to break the inter-molecular force of attraction. So, when the question was raised what will

happen if we heat the gas to again higher temperature, it was shown that the excess energy that has been supplied will strip off the electrons from the atoms and gas gets ionized. This ionized gas was considered to be the fourth state of matter, i.e., plasma. As one can see from the previous Sect. 1.1, people began to consider plasma, which is a ionized gas, as the fourth state of matter. It turns out that there is a bit of ionization in all gases. So, a much rigorous definition of plasma were taken into consideration and now it is (Chen, 1984):

plasma is a quasi-neutral gas of charged and neutral particles that exhibits collective behavior.

Quasi-neutrality is a tendency of plasma to remain electrically neutral in such a way that the density of ions and electrons are roughly the same. Mathematically:

$$\sum_{\substack{\text{all negative}\\ \text{species}}} n_e = \sum_{\substack{\text{all positive}\\ \text{species}}} n_i \tag{1.1}$$

Here n_e and n_i are number density of negatively charged particles and positively charged ions, respectively (in this thesis we adopt a convention that positive ions are denoted with a general subscript i). The n_i appearing in the Eq. (1.1) can be proton or a combinations of other positively charged particles. When the plasma is composed of ions which are multiply charged, then we have to multiply the individual charge with the charge number. If there is any deviation from quasi-neutrality, then large electric field will be set up in such a way that plasma restores this deviation.

Collective behavior can be illustrated as follows: the force of interaction between the particles in an ordinary gas is van der Waals force, which varies as sixth power of inverse of inter-particle distance. And also, this is a short range force. The case is different in plasma, where the constituent particles are charged. The interacting force between the particles are of electrostatic in nature, which decays as second power of inter-particle distance, which makes it a long range force. This also means that the each particle in the plasma can interact with many numbers of particles. Consequently, to any external perturbing agency, plasma shows a collective behavior, which is a cooperative response of an individual particle in plasma (Piel, 2017).

The above mentioned definition is a qualitative one. How do we make it quantitative? For that we have to look into the time and length scales which are prominent in plasma.

Consider a test charge (with positive charge) that is introduced in plasma. Once it is introduced, the positive ions in the plasma moves away from it (due to electrostatic repulsion) and electrons in the vicinity will come closer to the test charge. This will effectively shield the test charge and neutralize it. This means that effects of the electrostatic force is screened off and plasma remains quasi-neutral. *Debye length* is the scale length in plasma beyond which the effect of test particle decreases. This is given by the expression:

$$\lambda_{Ds} = \sqrt{\frac{\varepsilon_0 k_B T_s}{n_{0s} e^2}} \tag{1.2}$$

In Eq. (1.2), k_B is the Boltzmann's constant, ε_0 is the permittivity of the free space, e is the fundamental charge, T_s and n_{os} is the temperature and density of the s^{th} species. Now imagine a scenario, where the scale length, 'L', of the plasma is lesser than that of Debye length, λ_{Ds}. In this case, the cumulative charge of electron that is surrounding the test charge will not be equal to that of the the positive test charge. Hence, quasi-neutrality is violated and therefore strong electrostatic field that will be formed in this region. So, in short, the quasi-neutrality is violated in the length scale smaller than the Debye length. Hence, for a ionized gas to be called as plasma one need to have plasma system length higher than that of Debye length: $\lambda_{Ds} << L$.

This length is clearly dependent on the density of particles in the plasma. If there are not enough charges to shield the test charge, the electric field will leak out and makes it presence felt through out the plasma. This destroys the collective behavior nature of plasma. The number of particles required to make Debye shielding to be effective can be calculated in this way: imagine a sphere which is having the radius of Debye length. Then, the number of particles in this "Debye sphere" is given by:

$$N_{Ds} = n_{0s} \frac{4}{3} \pi \lambda_{Ds}^3 \tag{1.3}$$

For collective behavior to take place, it is required that $N_{Ds} >> 1$.

Consider a plasma comprising of electrons and protons in a equilibrium state. Let us assume that the overall quasi neutrality is disturbed by some external forces. Then, the electrons will respond to this change more quickly than protons because electrons are much lighter compared to protons. The electron will move to restore the quasi-neutrality with the help of electric field that has been generated by the external force. But due to their inertia

they will move back and forth about their equilibrium position. This collective response of electrons manifests into what is known as *plasma oscillations*, whose frequency is given by the expression:

$$\omega_{pe} = \sqrt{\frac{n_{0e}e^2}{\varepsilon_0 m_e}} \tag{1.4}$$

Here, m_e is the mass of electrons. This expression was first discovered by Tonks and Langmuir (1929). Now, if there are significant amount of neutral particles, then there is a possibility of damping of these collective oscillations of electrons due to collisions between the electrons and neutrals. So, the frequency of electron-neutral collision must be smaller than the electron plasma frequency. This condition is usually expressed as: $\omega_{pe}\tau >> 1$. Here, τ is the inverse of electron-neutral collision frequency, which is also the average time an electron travels between collisions with neutrals.

Then, the conditions under which an ionized gas becomes plasma are (Chen, 1984):

1. $\lambda_{De} << L$
2. $N_{De} >> 1$
3. $\omega_{pe}\tau >> 1$

So, these make the definition of plasma more robust.

The discussion of plasma cannot conclude without some words about the Saha ionization formula. Under the condition of thermal equilibrium, the fraction of ionized particles or degree of ionization is given by the expression (Chen, 1984):

$$\frac{n_i}{n_n} \approx 2.4 \times 10^{21} \frac{T^{3/2}}{n_i} e^{-U_i/k_B T} \tag{1.5}$$

Here n_i and n_n are the densities of ionized atoms and neutral atoms (in per m^3), T is the gas temperature (in kelvin, K) and U_i is the ionization energy of the gas. From Eq. (1.5), it is clear that there will be a finite number of ionized particles even when ionization energy U_i is greater than that of thermal energy of the constituent particle, but the number is too low [for calculation, see Chen (1984)]. However, with the increase in the temperature, the ionization becomes much larger.

(a) The flame goes to one side with the application of electric field, which is characteristic of plasma. (Figure courtesy: http://www.askamathematician.com/2013/05/q-is-fire-a-plasma-what-is-plasma/)

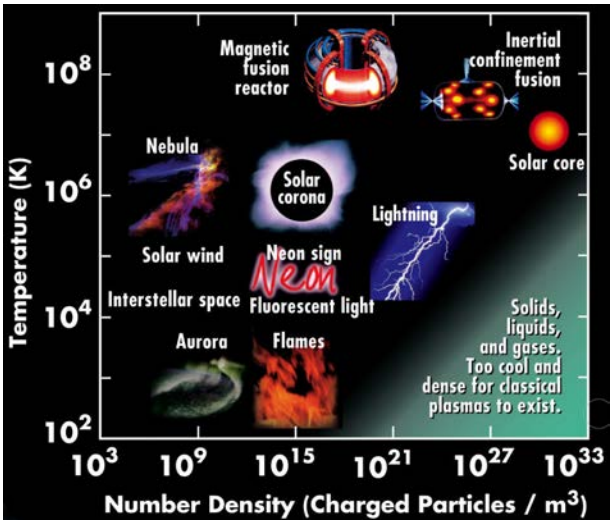

(b) Occurrence of plasma. Figure courtesy: http://www.cpepphysics.org/images/cpep-fusion-2016-sm.jpg

Figure 1.2: Plasma

1.3 Occurrence of plasma

Where can we find plasma? The answer may look strange, but the fact is that 99% of the visible universe is in plasma state: this means that majority of stars, nebulae, interplanetary space, interplanetary medium, supernovae etc. are in the form of plasma. In near Earth environment, its occurrence is rather limited to magnetosphere, ionosphere, lighting bolt, fire (Fig. 1.2). In the next section, examples of naturally occurring plasma are given:

1.3.1 The Sun

In our proximal space, Sun is the biggest reservoir of plasma. Since the solar wind (Sect. 1.3.2) coming from Sun directly interacts with Earth's magnetosphere (Sect. 1.3.3), it is vital to know the processes and the phenomenon happening in Sun. For astronomers, Sun is just another star which belongs to spectral class G2 among millions of stars in the Universe- or, in short, it is our local star. With the advent of newer and newer technologies, it has been possible to understand the Sun in whole new perspective. This has created a paradigm shift in the understanding the workings of Sun. The Sun weighs approximately 1.9×10^{30} kg which is equivalent of 300,000 Earth masses and accounts for 99% of solar system's mass.

The relative abundance of various elements in the composition of Sun is 92.1% is Hydrogen, 7.8% Helium and remaining mass is dominated by Oxygen, Carbon and Nitrogen. The radius of Sun is about 696,000 km (=1 $R_{\odot}$)(Moldwin, 2008). The surface acceleration due to gravity at Sun is 28 times that on Earth. Since Sun is not a solid structure like our Earth, the rotational velocity varies at different regions of Sun. This means that the speed at which matter rotates at Sun's equator is not the same at poles. This effect is known as *differential rotation*. Due to this, at equator, rotational speed is around $\approx$ 26 days and at poles it is $\approx$ 36 days(Priest, 1995).

A single statement holds the key towards understanding the structure of Sun- ***the structure of the Sun is a matter of balance***(Kay et al., 2016). Inside the Sun, thermal pressure (produced by the nuclear reaction) is in tug-of-war with the gravity. The Sun would collapse if the gravity were stronger than the pressure and if it is the other-way around, the Sun would blow itself apart. The balance between these two oppositely acting forces is called hydrostatic equilibrium. So, the pressure at any point within the interior of Sun is in such a way to hold up the weight of all layers above that point. If this was not the case, the forces inside the Sun would not be in balance and the surface of Sun would move. Since we dont see the size of the Sun changing from one day to another, we can be pretty sure that the Sun's interior is indeed in hydrostatic equilibrium(Kay et al., 2016).

For the scientists who were studying the energy production in Sun, it was a shock to know that the amount of energy produced by Sun at every second is $\approx 3.85 \times 10^{26}$ W (Kay et al., 2016). The primary source of energy is the fusion of proton to form Helium nucleus with release of energy through a series of processes known as p-p (proton-proton) chain(Kay et al., 2016). The fusion process in the Sun is going on for around 4.5 billion (4.5×10^9) years(Moldwin, 2008) and it is estimated that it will continue to do so for another 4.5 billion years(Moldwin, 2008).

Sun's interior can be divided into(Priest, 1995) (Fig. 1.3):

- Solar core: This is the place where above mentioned p-p chain reaction takes place. The solar core has radius of about 0.25 $R_{\odot}$ (which is approximately about 1,74,000 km) with mass density of 150,000 kg m^{-3}. This enormous density means that temperature is also extremely high- core has a temperature of 15 million(15×10^6) K. At this temperature(energy), the protons overcome the electrostatic repulsion between them

thereby paving way for short-range nuclear force to act and combine to form Helium atoms. This reaction will release the energy in accordance with Einstein's mass energy equation.

The energy released from the fusion at core is taken out either by convection (transfer of energy via by movement of matter), conduction (transfer of energy via collision of particle) or by radiation (transfer of energy via electromagnetic radiation). The next layers of Sun is classified according to these physical processes.

- Radiative Zone: Transfer of energy by radiation depends how freely radiation can move from one point to another in matter. The degree to which matter impedes the flow of radiation or photons is called opacity. The opacity of a material depends a host of different parameters (e.g. the density of the material, its composition, its temperature, and the wavelength of the photons moving through it etc.). The opacity is very low in the layers just above Sun's core. So here the major portion of the transfer of energy happens in the form of radiation and hence this region is known as *radiative zone*. This region has a thickness of 0.5 $R_{\odot}$ (350,000 km). Temperature of the radiative zone gets reduced to 6 million K towards the bottom of the radiative zone and reduces further to 5,00,000 K at the outer margins of the radiative zone. But due to the interaction with the matter here, a single photon may take 1,00,000 years to come out to outer layers of the Sun!

- Convective zone: Since the temperature further reduces after radiative zone, the atoms are no longer ionized and hence the opacity increases. In this part, it is the convection that drives the energy transfer and hence this area is known as *convective zone*, which is of 0.25 $R_{\odot}$ thickness. The hotter material near the top of the radiation zone (the bottom of the convection zone) rises up and the cooler material sinks to the bottom. As the hot material reaches the top of the convection zone it begins to cool and sink, and as it sinks it heats up again and will rise. The transition from radiative zone and the convective zone is known as *tachocline* .

  A point worth to ponder is the generation of magnetic field in the Sun. The magnetic field of the Sun is very high and complex. The mechanism that produces the magnetic field is known as *solar dynamo*, which operates in tachocline region. The exact mech-

anism of how the solar dynamo works is still not clearly understood. But one thing that is certain is that the magnetic field coming out of the Sun will be twisted and stretched due to the plasma flowing in the convection zone.

The radiation will again take over as the primary mode of energy transfer after the convective zone.

Then comes the atmosphere of Sun which consists of (Fig. 1.3):

- Photosphere: The visible surface of the Sun is called *photosphere*. This has a thickness of 500 km, where the temperature ranges from 6600 K at the bottom to 4300 K at the top. The sun spots, which are cooler and much less brighter part of photosphere, are found here. Sun spots are regions of intense magnetic activity. The sunspots can be as large as 20,000 km across with magnetic field strength which can go up-to 0.3 tesla (T) (for comparison, the diameter of Earth is $\approx$ 13,000 km and the magnetic field is 3×10^{-6} T)(Priest, 1995).

- Chromosphere: Just above photosphere, lies *chromosphere*. Since, it's a very thin layer around the Sun, it is essentially transparent to all wavelengths. The trend in variation of temperature is reversed in chromosphere: temperature at bottom is about 4300K and towards the edge of photosphere, it is around 40,000K at the height of 2500 km.

- Corona: This is the outermost layer of Sun, which is at a temperature of approximately 1 million K. The temperature of corona is, surprisingly, much higher than that chromosphere or photosphere. This is a puzzling aspect and this is known as coronal heating problem. Many mechanisms have been proposed to explain this phenomenon: acoustic wave heating, Alfven body waves, surface Alfven waves etc.

1.3.2 Solar Wind

It was earlier thought that the space between the Sun and Earth was completely void. But it turns out a highly conducting plasma which is ejected by Sun, called as *solar wind*, fills this void. This outflow is mainly caused by expansion of corona. In this way, we can call the solar wind as extension of Sun's corona. The magnetic field, which is produced in Sun, are

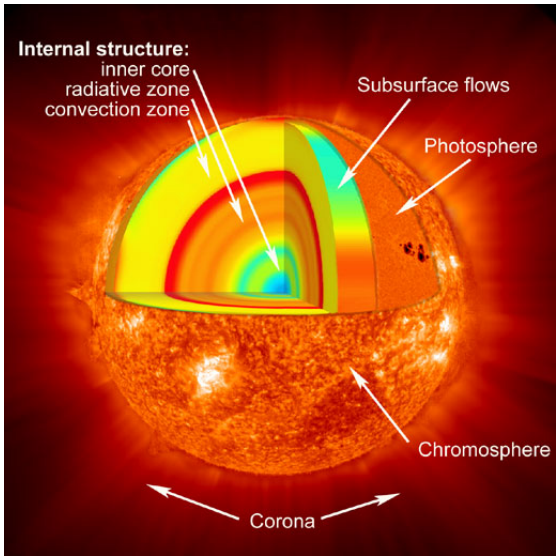

Figure 1.3: Artist's impression of layers of Sun. (Figure courtesy: Official Flickr account of NASA's Marshall Space Flight Center- https://www.flickr.com/photos/nasamarshall/2689379453)

frozen into the solar wind (due to its high conductivity) and is carried over to the entire solar system. Some typical parameters which characterizes solar wind plasma are as follows: electron density 7.1 cm^{-3}, proton density 6.6 cm^{-3}, radial flow speed 450 kms^{-1}, magnetic field 7 nT (all parameters near at 1 astronomical unit (1 AU =1.5×10^8 km) (Hundhausen, 1995). Trace amount of heavy ions can also be seen along with these elements. These solar wind will cause the disturbance of terrestrial magnetic field and it can lead to catastrophic effects. This was first suggested by Sydney Chapman in 1918, when not even the concept of plasma was established. The outflow of the solar wind has an interesting pattern. If the Sun was not rotating, the outflow of solar wind will be in radial direction. However, Sun is rotating with rotational period of 26 days at equatorial region and 36 days at polar regions (see 1.3.1). Therefore, solar wind is twisted in form of Archimedean spiral, which is also known as *Parker spiral*. Once the magnetic field of Sun (which is embedded in solar wind plasma) is detached from the surface of the Sun, it is called as *Interplanetery Magnetic Field (IMF)* (Fig. 1.4). The magnetic field in the solar wind plasma makes an angle with the imaginary line drawn between Earth and Sun. This has a magnitude of 45°(Russell, 2013).

The solar wind comes in two different forms: *fast solar wind* and *slow solar wind*. The differentiation is not just in bulk speed, but in various other aspects. The fast solar

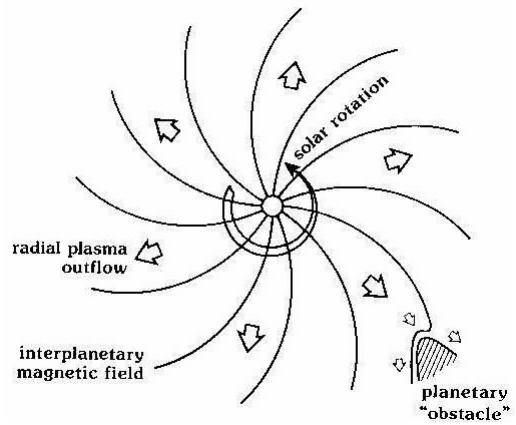

Figure 1.4: Solar wind with interplanetery magnetic field. Figure courtesy https://pwg.gsfc.nasa.gov/istp/outreach/ images/ Gusts/ windsprl.jpg

wind has a velocity of 750 kms^{-1} and originates in the polar regions of the Sun, within the open magnetic field line regions identified by coronal holes (Feldman et al., 2005). On the other hand, slow wind picks up the velocity of about 400 kms^{-1}(Feldman et al., 2005) and originates from the equatorial part of Sun (Bruno and Carbone, 2013). The fast solar wind has proton temperature anisotropy, with $T_{p\perp} > T_{p\parallel}$, whereas for the slow solar wind, this condition is reversed (here, $T_{p\perp}$ and $T_{p\parallel}$ respectively denotes the temperature of protons perpendicular and parallel to the ambient magnetic field). The temperature of protons is more than temperature of electrons in slow solar wind, whereas protons is much cooler than electrons in slow solar wind (Marsch, 2006). Other solar wind parameters are listed in Tab. 1.1.

Table 1.1: Typical values of solar wind parameters as measured by Helios 2 at 1 AU (Bruno and Carbone, 2013).

Parameter	**Slow Solar wind**	**Fast Solar wind**
number density	~ 15 cm^{-3}	~ 4 cm^{-3}
bulk velocity	~ 350 kms^{-1}	~ 600 kms^{-1}
proton temperature	$\sim 5 \times 10^4$ K	$\sim 2 \times 10^5$ K
electron temperature	$\sim 2 \times 10^5$ K	$\sim 1 \times 10^5 K$
α-particle temperature	$\sim 2 \times 10^5 K$	$\sim 8 \times 10^5 K$

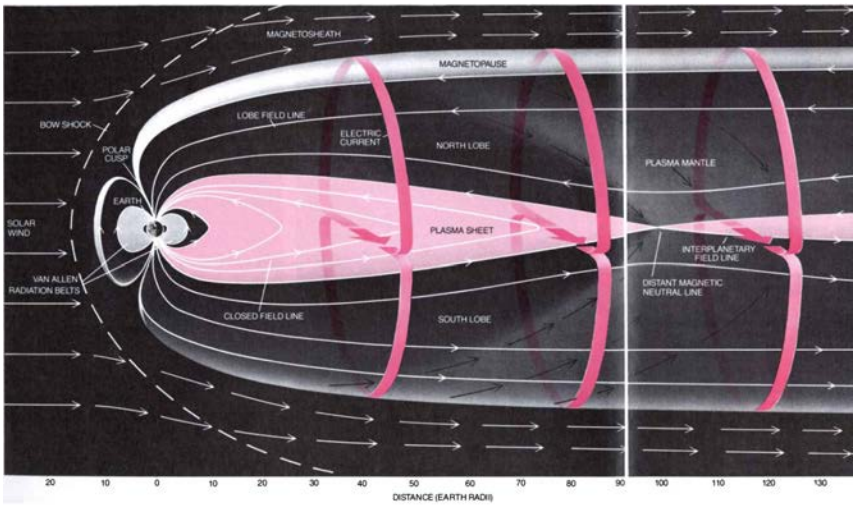

Figure 1.5: Earth's magnetosphere(Hones, 1986).

1.3.3 Magnetosphere

The solar wind coming through the interplanetary space has the magnetic field "frozen" into it. The solar magnetic field interacts with the magnetic field of our Earth and forms a region known as *magnetosphere*. In other words, magnetosphere is the vast region of space magnetically connected to the Earth. It is the magnetic field in the solar wind that deforms otherwise perfectly dipolar magnetic field of the Earth and results in tear drop-like structure with elongated tail. The term magnetosphere was first coined by Gold (1959).

The Fig. 1.5 shows the cross-section of Earth's magnetosphere. Here the north pole is located at the top and the Sun is on left. The extent of Earth's magnetosphere will depend upon the the solar wind pressure. During "quite" period of Sun, the magnetosphere will extend up-to 15 R_E in the Sunlit side or day-side (R_E is the radius of Earth which is $\approx$ 6370 km) and extends up-to 100 R_E in the night side. The upcoming solar wind when stopped by magnetic field of Earth creates what is known as *bow shock*. This is the first contact point of magnetic field of solar wind and Earth's magnetic field and it is located at 13 R_E. The solar wind plasma is slowed down substantially here and it is diverted around the Earth's magnetosphere. The boundary which separates the solar wind and Earth's magnetosphere is known as *magnetopause* and is located at $\approx$ 10 R_E on the day-side. Here the pressure of the geomagnetic field balances that of solar wind. The region between bow shock and magnetopause is known as *magnetosheath*. Since the solar wind plasma is substantially slowed down due to the interaction with Earth's magnetic field, the magnetosheath plasma is hotter

compared to solar wind plasma in order that conservation of energy to hold. Earth's magnetic field is compressed on the day side and in the night side the magnetic field is stretched down to form a long tail known as *magnetotail*. Magnetotail is roughly 30 R_E across and extends more than 100 R_E in the downwind direction (Hargreaves, 1992). Magnetotail consists of upper/north lobe and lower/south lobe. These two lobes have different magnetization- in upper/north lobe the magnetic field is directed towards Sun and in lower/south lobe it is directed away from Sun. These two regions are separated by the *plasma sheet*.

In the regions inside the magnetopause, the Earth's magnetic field behaves roughly in dipolar fashion. This region is known as *inner magnetosphere*, whereas the regions that has been mentioned in the above section is called *outer magnetosphere*.

The co-rotating region of torus shaped cold plasma near to the Earth's surface is known as *plasmasphere*. This region has high densities of plasma ($\sim 10^3$ cm^{-3}) with an average energy of ~ 1 eV and its major constituents are mostly Hydrogen and Helium and also significant amount of Oxygen that has got enough energy to escape from Earth's ionosphere(Moldwin, 2008; Wolf, 1995). The outer boundary of plasmasphere is marked by a sharp decrease in the number density of the particles where the density can go from $\sim 10^3$ cm^{-3} to $\sim 10^{-1}$ cm^{-3} within a short radial span of 0.5 R_E(Wolf, 1995). This region is known as *plasmapause*. The plasma in the plasmasphere is of ionospheric origin, rather than of solar wind origin.

Near to the Earth's surface, there exist a region of energetic particles with kinetic energy more than 30 keV. This appears in the form of a belt and is known as *Van Allen radiation belt* (after it's discoverer J. A. Van Allen) or simply *radiation belt*, which often overlaps with the plasmasphere. The outer belt consists of energetic electrons and has it's inner edge around 3 R_E. The outer edge is highly variable which usually located beyond geosynchronous orbit. The inner belt comprises of energetic electrons and protons and it extends up from 1.1 R_E to 2.5 R_E. The *slot* region is the region between the inner and outer radiation belt, that is devoid of any energetic particle. This slot region may disappear during geomagnetic storms, which results in the overlapping of inner and outer radiation belt (Fig. 1.6).

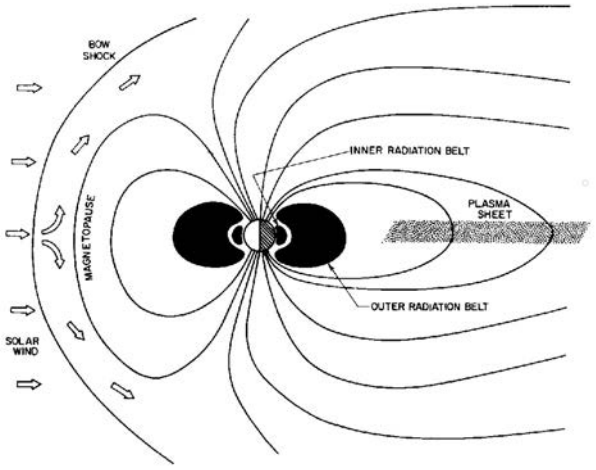

Figure 1.6: Radiation beltVan Allen (1991)

1.3.4 Ionosphere

Just above the atmosphere starting from 50 km, we have the last natural reservoir of plasma. The solar radiation impinging on the atmosphere, ionizes it and forms a layer of partially ionized plasma known as *ionosphere*. Generally, the ionosphere is divided into following layers (Zolesi and Cander, 2014):

1. D layer (50-70 km): The neutral component of this region consist mainly of N_2, O_2, Ar, CO_2, He. It also consist of O_3 as well as H_2O, whose quantities are highly variable. The charged particle comprises of NO^+ acting like a major positive charge carrier, with electrons, O_2^- and possibly other negative ions acts like particle carrying the negative charges. The main source of ionization in this layer is solar L-alpha (121.6 nm) radiation for NO; solar X-rays (<0.8 nm) for N_2, O_2 and Ar; solar ultraviolet (UV) radiation (< 111.8 nm) for unstable O_2 and galactic cosmic rays for ionizing all the atmospheric constituents.

2. E layer (90-140 km): This layer was initially called as Kennelly-Heaviside or the Heaviside layer. E layer is formed by X-rays in the 8-10.4 nm range and UV radiation from 80 nm to L-beta (102.6 nm). This produces the principal NO^+, O_2^+ and secondary O^+, N_2^+ ion components.

3. F layer: The F layer is divided into F1 layer and F2 layer.

   F1 layer (140-210 km)

F2 layer (210-500 km)

These all layers co-exist mutually on day time. During night time, F layer (combination of F1 and F2 region) and E layer only exist.

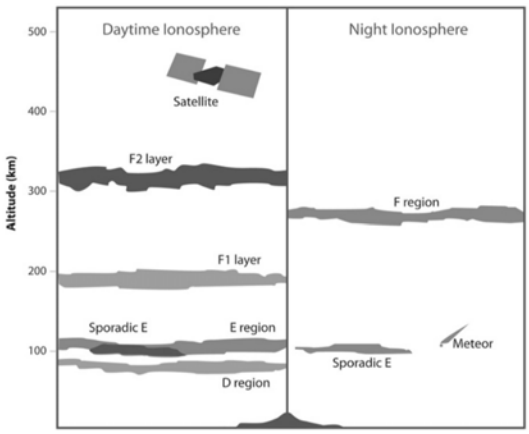

Figure 1.7: Various Layers of ionosphere (Zolesi and Cander, 2014)

1.4 Theoretical approaches

The various theoretical approaches to investigate plasma are listed in this section. These have varying degree of application depending upon the problem under consideration.

1.4.1 Kinetic theory

The plasma comprises of many particles. At this very statement itself, it is evident that some sort of 'statistical' approach is required because it is close to impossible to track the trajectories of all the particles and also, we no longer require the information of individual particle. Kinetic theory of particles forms a primer to this method. In kinetic approach, instead of solving the equation of motion for each individual particle, it considers the development of the distribution function for the system of particles in phase space.

For a single particle, complete description in classical mechanics requires knowledge of its position (defined by x, y, z or $\mathbf{r}$ in general) as well as velocity (v_x, v_y, v_z or $\mathbf{v}$) at all times. This can be represented by a single point at any given time t in a six-dimensional *phase space* spanned by three spatial axes and three velocity axes. Lets assume a collection of 'N' particle

of s^{th} species that makes up plasma. Then, the entire system of particles is described by the group of representative points in phase space. The *distribution function* $f_s(\mathbf{r},\mathbf{v},t)$ which is a function of position and velocity, is the density of representative points in the phase space. This means that the number of particles having the velocities lying between $\mathbf{v}$ and $\mathbf{v}+d\mathbf{v}$ positioned between $\mathbf{r}$ and $\mathbf{r}+d\mathbf{r}$ is given by:

$$dN_s = f_s(\mathbf{r},\mathbf{v},t)d\mathbf{r}d\mathbf{v} \tag{1.6}$$

This is also the the number of particles of s^{th} species inside the volume element $d\mathbf{r}d\mathbf{v}$ surrounding the phase space coordinates $(\mathbf{r},\mathbf{v})$ at any instant. The distribution function contains all the information about the plasma under consideration and the measurable macroscopic quantities of plasma can be deduced from this.

The distribution function, in general, is a function of position vector, $\mathbf{r}$ and if this is the case, then this type of distribution function is called as *non-uniform distribution function*. A distribution function which is independent of position is called a *uniform distribution function*. The distribution function is said to *anisotropic*, when it depends on the orientation of the velocity vector. When it is independent of orientation of velocity vector but dependent upon it's magnitude, then it is called as *isotropic distribution function* (Goossens, 2003). Further description of distribution function is given in Sect. 1.5

The evolution of the distribution function is governed by the partial differential equation, known as classical Boltzmann equation or *kinetic* equation:

$$\frac{\partial f_s(\mathbf{r},\mathbf{v},t)}{\partial t} + \mathbf{v}.\nabla f_s(\mathbf{r},\mathbf{v},t) + \frac{\mathbf{F}}{m}.\nabla_{\mathbf{v}} f_s(\mathbf{r},\mathbf{v},t) = \left(\frac{\partial f_s(\mathbf{r},\mathbf{v},t)}{\partial t}\right)_{collision} \tag{1.7}$$

This equation has it's roots in statistical mechanics, which one can derive from first-principles (see: Goossens (2003); Baumjohann and Treumann (2012); Chiuderi and Velli (2015)).The term on the right hand side of Eq. (1.7) gives the contribution from all the collision of the particles in plasma. The above equation hold good for fluids as well as for a plasma. In-order to incorporate electromagnetic forces in plasma, one has to add to the force term:

$$\mathbf{F} = q(\mathbf{E}+\mathbf{v}\times\mathbf{B})+\mathbf{f} \tag{1.8}$$

The first term is the Lorentz force term, which is of electromagnetic in origin and the second term will be the forces having non-electromagnetic origin which is acting on plasma (Chiuderi and Velli, 2015). Neglecting the non-electromagnetic force, the Eq. (1.7) can be written

as:

$$\frac{\partial f_s(\mathbf{r},\mathbf{v},t)}{\partial t} + \mathbf{v}.\nabla f_s(\mathbf{r},\mathbf{v},t) + \frac{\mathbf{q}}{m}\Big(\mathbf{E}+\mathbf{v}\times\mathbf{B}\Big).\nabla_{\mathbf{v}} f_s(\mathbf{r},\mathbf{v},t) = \left(\frac{\partial f_s(\mathbf{r},\mathbf{v},t)}{\partial t}\right)_{collision} \tag{1.9}$$

The collision-less Boltzmann equation is known as *Vlasov equation*:

$$\frac{\partial f_s(\mathbf{r},\mathbf{v},t)}{\partial t} + \mathbf{v}.\nabla f_s(\mathbf{r},\mathbf{v},t) + \frac{q}{m}\Big(\mathbf{E}+\mathbf{v}\times\mathbf{B}\Big).\nabla_{\mathbf{v}} f_s(\mathbf{r},\mathbf{v},t) = 0 \tag{1.10}$$

Vlasov equation is invariant under the inversal of time ($t \to -t$) which subsequently means that entropy of the system remains invariant.

The electric and magnetic field in Eqs. (1.8) to (1.10) are the averaged field experienced by the particle which satisfies Maxwell's equation:

$$\nabla.\mathbf{E} = \frac{\rho}{\varepsilon_0} \tag{1.11a}$$

$$\nabla.\mathbf{B} = 0 \tag{1.11b}$$

$$\nabla\times\mathbf{E} = -\frac{\partial\mathbf{B}}{\partial t} \tag{1.11c}$$

$$\nabla\times\mathbf{B} = \mu_0\left(\mathbf{J}+\varepsilon_0\frac{\partial\mathbf{E}}{\partial t}\right) \tag{1.11d}$$

Eqs. (1.10) and (1.11) coupled with charge density and current density given by Eq. (1.12) forms the complete set of self-consistent equation required for description of plasma:

$$\rho(\mathbf{r},t) = \sum_s q_s \int_{\mathbf{v}} f_s(\mathbf{r},\mathbf{v},t)d\mathbf{v} \tag{1.12a}$$

$$\mathbf{J}(\mathbf{r},t) = \sum_s q_s \int_{\mathbf{v}} \mathbf{v} f_s(\mathbf{r},\mathbf{v},t)d\mathbf{v} \tag{1.12b}$$

Much of kinetic theory of plasma physics centers around extracting out necessary physics from distribution function. Distribution function, as it stands, is not directly observable quantity. Then how is possible to extract out the information from this? Answer is given by taking the *velocity moments* of the distribution function. For example, the particle density $n_s(\mathbf{r},t)$ and mass density ρ_s for s^{th} species can be calculated as (Goossens, 2003):

$$n_s(\mathbf{r},t) = \int f_s(\mathbf{r},\mathbf{v},t)d^3\mathbf{v} \tag{1.13a}$$

$$\rho_s(\mathbf{r},t) = n_s(\mathbf{r},t)m_s \tag{1.13b}$$

Eq. (1.13a) is known as *zero-order moment*.

The macroscopic flow velocity of s^{th} species in the neighborhood of the position vector $\mathbf{r}$ at instant t is called the *bulk flow velocity* or *average velocity*, which is given by *first-order moment*(Baumjohann and Treumann, 2012):

$$\mathbf{v}_b(\mathbf{r},t) = \frac{1}{n_s(\mathbf{r},t)} \int \mathbf{v} f_s(\mathbf{r},\mathbf{v},t) d^3v \tag{1.14}$$

Second-order moment gives the pressure tensor, which is the contributions of fluctuation of velocities from this mean velocity(Baumjohann and Treumann, 2012):

$$\mathbf{P} = m \int (\mathbf{v}-\mathbf{v}_b)(\mathbf{v}-\mathbf{v}_b) f(\mathbf{v}) d^3v \tag{1.15}$$

The distribution function play a central part in the kinetic theory. Complete description of state of system is obtained from distribution function and it's evolution in time. By definition it seems to be a highly theoretical concept, but one can measure the particle flux in a system and relate it to distribution function (Baumjohann and Treumann, 2012; Parks, 2004).

1.4.2 Fluid theory

The kinetic description of plasma amounts to the most fundamental description of plasma. However, many times solving the Eq. (1.10) is not that straight forward. As mentioned earlier (see Sect. 1.4.1), it centers around distribution function, which itself is not a measurable quantity. But there are some other quantities which are measurable and these are calculated from the velocity moments of distribution function. It gives the information about the plasma system that one is seeking (albeit many information's are lost). So, sometimes it is not necessary to understand the exact evolution of the distribution function to know about the system. Hence, we resort to other methods and found that by taking the velocity moments of 'Vlasov equation' (i.e. Eq. (1.10)), one can find out the macroscopic transport equation. These describe the time and spatial evolution of macroscopic quantities. These are similar to the fluid equations that one encounters in hydrodynamics and this kind of approach is known as *fluid theory* and provides a immediate physical picture. Here, we consider the collection of particles to be electrically conducting fluid. The fluid theory is approximate

theory in which macroscopic quantities are continuous function of position and time. Unlike kinetic theory, this will lead to equations in three spatial dimensions and time, which is a great simplification over the seven dimensional description of plasma in phase space.

The zero-order moment of Vlasov equation is derived by multiplying the Vlasov equation by $m_s\mathbf{v}^0$ and integrating over the velocity space:

$$\frac{\partial n_s}{\partial t} + \nabla.(n_s\mathbf{v}_s) = 0 \tag{1.16}$$

Note that we do not make any distinction between the bulk flow velocity $\mathbf{v}_b(\mathbf{r},t)$ and individual particle velocity, and hence the subscript b is dropped and subscript s is introduced to differentiate between various species. This is the *equation of continuity*, which describes the the conservation of the number of particles. This states that the number density of particles as well as mass and charge densities will remain the same during the motion of fluid, in absence of any **interaction process** (Baumjohann and Treumann, 2012).

Moving further, the first-order moment of Vlasov equation is calculated by multiplying Eq. (1.10) by $m_s\mathbf{v}^1$ and integrating over the velocity space. This will give *equation of motion* or *momentum density conservation equation*:

$$m_s n_s\left[\frac{\partial \mathbf{v}_s}{\partial t} + (\mathbf{v}_s.\nabla)\mathbf{v}_s\right] = q_s n_s(\mathbf{E} + \mathbf{v}_s \times \mathbf{B}) - \nabla.P_s \tag{1.17}$$

$\nabla.P_s$ is the force associated with the *pressure tensor* of the fluid per unit volume.
We could, in principle, proceed in the similar fashion to find out the higher moments of Vlasov equation, but it is sufficient to stop at this moment.

Fluid equations Eqs. (1.16) and (1.17) as it stands possess an intrinsic problem: they are incomplete. While calculating the zero-order moment of Vlasov equation, i.e. Eq. (1.16), we got expression containing the first-order moment of distribution function, Eq. (1.14). So we seek to find another equation for the velocity of the fluid. This is given by first-order moment of Vlasov equation (Eq. (1.17)). But it turns out that this equation contains the next higher moment of the distribution function, Eq. (1.15). This process can go on indefinitely. So, at all the time when we obtain a new equation by taking the velocity moments, a new unknown appears and consequently number of equations are always less than the number of unknowns. Because of this, one has to close these set of expression (Eqs. (1.16) and (1.17)) at some stage. This problem is known as *closure problem*. This problem can be overcome by

using the equation of the state for pressure, whose actual form depends whether the pressure tensor is isotropic or anisotropic (Baumjohann and Treumann, 2012).

The above equations [Eqs. (1.12), (1.16) and (1.17)], with Eq. (1.11) and appropriate pressure equation provides the approximate description of plasma.

1.4.3 Single particle approach

In-order to understand the dynamics of plasma, sometimes it is vital to know about the individual motion of constituent particles under the action of electric and magnetic field. This approach is best suited to understand the very low dense plasma. Strictly speaking, this is not a plasma physics approach as the basic criterion's of plasma are not met here. Here one can neglect the field produced by the stationary charged particle as well as moving charged particle in contrast with the externally imposed field.

Next, we describe particle distribution function which have been used in this thesis.

1.5 Distribution function

We return back to the distribution function that was discussed in Sect. 1.4.1. This amounts to immense importance in kinetic theory and it is the time evolution of distribution function, which gives the measurable quantities of plasma.

1.5.1 Maxwell-Boltzmann distribution function

A system which is free from any external forces will attain a thermal equilibrium. In this equilibrium state, the distribution function is given by Maxwell-Boltzmann distribution function as under:

$$f(\mathbf{v}) = \left(\frac{m_s}{2\pi k_B T_s}\right)^{\frac{3}{2}} e^{\left(-\frac{mv^2}{2k_B T_s}\right)} \tag{1.18}$$

Here $v_{ts} = \sqrt{\frac{k_B T_s}{m_s}}$ gives the thermal velocity of the species (see Fig. 1.8a).

This concept can be further be extended by observing that sometimes in a plasma a stream of particles move with a velocity v_0. In this case, the distribution function will be

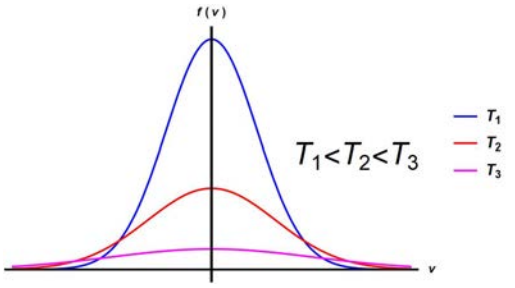

(a) Maxwell-Boltzmann distribution function

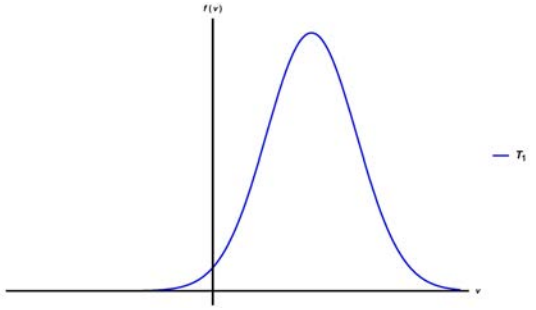

(b) Drifting Maxwell-Boltzmann distribution function

Figure 1.8

modified as (Fig. 1.8b):

$$f(\mathbf{v}) = \left(\frac{m_s}{2\pi k_B T_s}\right)^{\frac{3}{2}} e^{\left(-\frac{m_s(v-v_0)^2}{2k_B T_s}\right)} \tag{1.19}$$

Further, we also have anisotropic distribution function. Other types of distributions such as bi-Maxwellian, losscone-distribution, ring distribution and kappa-distribution are also encountered in space plasmas. The distributions which depart from Maxwellian are known as nonthermal distributions. One such distribution will be described in the next section.

1.5.2 Non thermal distribution function

Sometimes the particle distribution that is seen in the magnetospheric, solar wind and astrophysical plasma (or in short, space plasma) exhibits deviation from Maxwell-Boltzmann distribution function. They reside in stationary state which are not in thermal equilibrium (by stationary, one means that their statistics are at least temporarily time invariant (Livadiotis, 2015)). These distributions are in general called as *non thermal distribution* owing to the above mentioned fact as has been described earlier..

In the late 1960s, the experimental data that was poured in from various satellite measurements showed that the distribution of electrons in the space plasmas cannot be fitted by Maxwell-Boltzmann distribution. By analyzing the data used from IMP-1 and IMP-2 (Interplanetary Monitoring Platform) satellite, it was found that electron density profile cannot be matched with that of Maxwell-Boltzmann, but rather with another different distribution function which has a non Maxwell-Boltzmann tail. So in 1966, Olbert has hypothesized what

is now known as *kappa distribution function* or *generalized Lorentzian distribution function* (S. Olbert in unpublished notes as reported by Binsack (1966)). This form of a new distribution function was used by Vasyliunas (1968) to study about electrons of low energy observed by OGO 1 and OGO 3 (Orbiting Geophysical Observatory) satellites in the magnetosphere. The form for this expression is (Vasyliunas, 1968) (Fig. 1.9a):

$$f(\mathbf{v}) = \frac{n_s}{\pi^{\frac{3}{2}}} \frac{1}{\theta_s^3} \frac{\Gamma(\kappa+1)}{\kappa^{\frac{3}{2}}\Gamma(\kappa-\frac{1}{2})} \left(1+\frac{v^2}{\kappa\theta_s^2}\right)^{-(\kappa+1)} \tag{1.20}$$

Here, $\theta_s = \sqrt{\frac{2\kappa-3}{2\kappa}} v_{ts}$, where v_{ts} is the thermal velocity of s^{th} species. From the definition of θ it is clear that in order to have a meaningful definition for thermal velocity, one should have $\kappa > \frac{3}{2}$. The kappa distribution tends to Maxwell-Boltzmann distribution as $\kappa \to \infty$. Though initially it was used to explain the electron distribution observed by IMP-1 (Olbert, 1968), IMP-2 (Binsack, 1966) and OGO 1 & OGO 3 (Vasyliunas, 1968), this has gone beyond the Earth's magnetospheric realm. Now, this has been observed in corona, solar wind, outer heliosphere, magnetosphere of other planets, and supernova (Fig. 1.9b; also see (Livadiotis, 2015) and references therein).

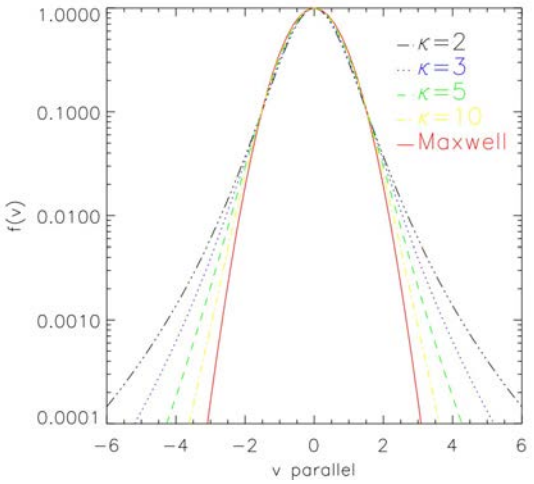

(a) Kappa distribution function Pierrard and Lazar (2010)

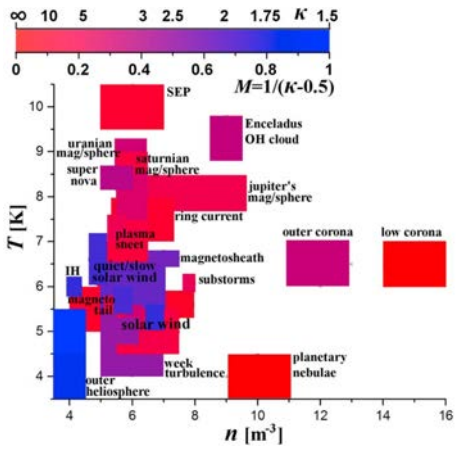

(b) Extent of kappa distribution function in space plasmas (Livadiotis, 2015)

Figure 1.9

In the section below, a brief description of waves and their classification is presented.

1.6 Waves in plasma

Waves are important aspects of any medium. A lot can be inferred from the waves that is being propagated through it. Plasma waves are no exception to this. Between the different regions of space, plasma waves acts as a mode of energy transfer. Not only this, wave behaves as a diagnostic tool to study about plasma. For example, as mentioned earlier, in plasma we do have what is known as plasma frequency, Eq. (1.4). This quantity is directly proportional to the square root of number density. This means that observations of plasma frequency is a direct measure of plasma density in the medium.

A plasma can support a wide variety of waves. These are essentially time-dependent evolution of various parameters such as electric and magnetic field, density etc. Waves in plasma are generated by disturbance which should fulfill at least two conditions (Baumjohann and Treumann, 2012):

- It must be solution of appropriate equation of plasma (i.e. modes should be given by the dispersion relation of the plasma)
- It's amplitude should be higher than the level of thermal fluctuation which is present in plasma. If the amplitude is small and there is no mechanism to amplify the disturbance, then the disturbance will die out and there won't be any wave.

General procedure to study about the properties of wave is by examining the response of plasma under the action of small perturbation. Assume that the plasma parameters can be written in the form (Tjulin, 2003):

$$a(\mathbf{r},t) = a_0 + a_1(\mathbf{r},t) \tag{1.21}$$

Here, with reference to a_0, $a_1(\mathbf{r},t)$ is a small perturbation. The perturbations are assumed to be of the form:

$$a_1(\mathbf{r},t) = a_1 e^{i(\mathbf{k}.\mathbf{r}-\omega t)} \tag{1.22}$$

If one substitute this quantities in the equation Eq. (1.10),Eq. (1.16) or Eq. (1.17), one can infer that time derivative($\frac{\partial}{\partial t}$) and spatial derivative(∇) can be replaced by $-i\omega$ and $i\mathbf{k}$ respectively. Considering only linear perturbation, which means that one neglect the terms containing perturbed quantity's second order or higher terms, we can derive the *dispersion*

relation. Basically, these are the relations between angular frequency of wave mode ω and propagation vector or wave vector $\mathbf{k}$. Dispersion relation provides many insights into the plasma system under consideration. For example, dispersion relation provides you the various plasma modes in the system, it gives you information about unstable modes in the system, it can also give you whether there is any coupling between various modes etc.

Before getting any further, let us define some terms that is used frequently with reference to plasma physics. When one talks about waves that are *parallel* and *perpendicular*, this is with reference to the undisturbed magnetic field $\mathbf{B}_0$. *Transverse waves* are those in which the oscillating electric field $\mathbf{E}_1$ has it's orientation perpendicular to the wave vector, $\mathbf{k}$, whereas for *longitudinal waves* $\mathbf{E}_1$ is parallel to $\mathbf{k}$.

The most broad classification of plasma waves is *electrostatic*, *electromagnetic* and *hydrodynamic* waves. For electrostatic waves there will not be oscillating magnetic field, on the other hand, for electromagnetic waves, there will be finite oscillating magnetic field.

Electromagnetic plasma waves are further differentiated into *right handed* wave and *left handed* wave based upon the rotation of electric field. For right handed waves electric field rotates in clockwise direction as we look along the ambient magnetic field direction and vice-versa for left handed wave.

Another type of wave that is present in the plasma is hydromagnetic or MHD waves. This occurs only in a magnetized plasma which have frequency very small compared to that of ion cyclotron frequency. Here, the inertia is provided by the positive ions and the current density time magnetic field ($J \times B$) term which comes from momentum equation gives the restoring force. These oscillations may be regarded as oscillations of magnetic lines of force which acts as stretched strings loaded with charged particles (Inan and Gołkowski, 2010).

As far as kinetic theory is concerned, the derivation of dispersion relation is much more involved. For an unmagnetized plasma, the dispersion relation can be written as:

$$1 - \sum_s \frac{\omega_{ps}^2}{n_{0s}} \int_{-\infty}^{\infty} \frac{f_{0s}(v)}{(\omega - kv)^2} dv = 0 \tag{1.23}$$

For a plasma with Maxwell-Boltzmann distribution, the dispersion relation can be written as:

$$1 + \sum_s \frac{1}{k^2 \lambda_{Ds}^2} (1 + \zeta Z(\zeta)) = 0 \tag{1.24}$$

Here ζ stands for ratio of phase velocity of the wave to the thermal velocity of s^{th} species,

i.e. $\zeta = \frac{\omega}{kv_{ts}}$ and $Z(\zeta)$ is the plasma dispersion function defined by:

$$Z(\zeta) \equiv \frac{1}{\sqrt{\pi}} \int_{-\infty}^{\infty} \frac{e^{-\xi^2}}{\xi - \zeta} d\xi \tag{1.25}$$

Here $\mathrm{Im}(\xi) > 0$. The properties of Eq. (1.25) are described in Baumjohann and Treumann (2012). When there exist a beam in the system, expression for ζ gets modified into $\zeta = \frac{\omega - k_{\|} U_s}{kv_{ts}}$, where U_s is the velocity of beam. The derivation of electrostatic dispersion relation for a magnetized plasma is much more involved. The dispersion relation for hot, magnetized anisotropic plasma is given by (Swanson, 2003):

$$1 + \sum_s \frac{\omega_{ps}^2 e^{-\lambda_s}}{k^2 v_{ts}^2} \sum_{n=-\infty}^{\infty} \Big[1 + \frac{\omega + n\Omega_s (1 - T_{\|s}/T_{\perp s}) - k_{\|} U_s}{k_{\|} v_{ts}} Z(\xi_{ns}) \Big] I_n(\lambda_s) = 0 \tag{1.26}$$

Here, $\Omega_s = \frac{z_s q_s B_0}{m_s}$, where z_s, q_s and m_s represents the charge multiplicity, fundamental charge and mass of s^{th} species, respectively. B_0 is the ambient magnetic field and $\lambda_s = \frac{1}{2}(k_{\perp} \frac{v_{ts}}{\Omega_s})^2$

As one can see from Tab. 1.2, there exist a plethora of plasma waves, even for a 2-component plasma. When the plasma comprises of more than 2 components, a combination of one or more mentioned waves can be observed.

Classification	Oscillating Species	Conditions	Dispersion Relation	Name
Electrostatic	electrons	$\mathbf{B}_0 = 0$ or $\mathbf{k}\|\|\mathbf{B}_0$	$\omega^2 = {\omega_{pe}}^2 + \frac{3}{2}k^2{v_{te}}^2$	Plasma Oscillation or Langmuir wave
	electrons	$\mathbf{k} \perp \mathbf{B}_0$	$\omega^2 = {\omega_{pe}}^2 + {\Omega_e}^2 = {\omega_h}^2$	Upper Hybrid Oscillation
	ions	$\mathbf{B}_0 = 0$ or $\mathbf{k}\|\|\mathbf{B}_0$	$\omega^2 = k^2{v_s}^2$	Ion Acoustic Wave
	ions	$\mathbf{k} \perp \mathbf{B}_0$ (nearly)	$\omega^2 = {\Omega_i}^2 + k^2{v_{ti}}^2$	Electrostatic ion Cyclotron Wave
	ions	$\mathbf{k} \perp \mathbf{B}_0$ (exactly)	$\omega^2 = [(\Omega_e\Omega_i)^-1 + {\omega_{pi}}^{-2}]^{-1}$	Lower Hybrid Oscillation
Electromagnetic	electron	$\mathbf{B}_0 = 0$	$\omega^2 = {\omega_{pe}}^2 + k^2c^2$	light wave
	electron	$\mathbf{k} \perp \mathbf{B}_0$, $\mathbf{E}_1\|\|\mathbf{B}_0$	$\frac{c^2k^2}{\omega^2} = 1 - \frac{{\omega_{pe}}^2}{\omega^2}$	O Wave
	electron	$\mathbf{k} \perp \mathbf{B}_0$, $\mathbf{E}_1 \perp \mathbf{B}_0$	$\frac{c^2k^2}{\omega^2} = 1 - \frac{{\omega_{pe}}^2}{\omega^2}\frac{\omega^2-{\omega_{pe}}^2}{\omega^2-{\omega_h}^2}$	X wave
	electron	$\mathbf{k}\|\|\mathbf{B}_0$ (right circ. polarization)	$\frac{c^2k^2}{\omega^2} = 1 - \frac{\frac{{\omega_{pe}}^2}{\omega^2}}{1-(\frac{\Omega_e}{\omega})}$	R wave Whistler
	electron	$\mathbf{k}\|\|\mathbf{B}_0$ (left circ. polarization)	$\frac{c^2k^2}{\omega^2} = 1 - \frac{\frac{{\omega_{pe}}^2}{\omega^2}}{1+(\frac{\Omega_e}{\omega})}$	L wave
	ions	$\mathbf{B}_0 = 0$		none
	ions	$\mathbf{k}\|\|\mathbf{B}_0$	$\omega^2 = k^2{v_A}^2$	Alfven Wave
	ions	$\mathbf{k} \perp \mathbf{B}_0$	$\frac{\omega^2}{k^2} = c^2\frac{{v_s}^2+{v_A}^2}{c^2+{v_A}^2}$	Magnetosonic Wave

Table 1.2: Waves in Plasma. Adapted from Chen (1984)

1.7 Waves in question in this thesis

A brief description of various waves which are relevant for our work presented in the thesis is given in the below sections.

1.7.1 Ion acoustic waves

Ion acoustic waves, along with Langmuir waves, constitutes one of the most fundamental waves in unmagnetized plasma, which has a frequency less than that of plasma frequency of ions, ω_{pi} with the condition $T_e >> T_i$ (André, 1985). These waves have a frequency range between 1-10 kHz depending on different plasma conditions (Gurnett et al., 1979, 1993; Hess et al., 1998; Huttunen et al., 2007; Rehman et al., 2018b) and are observed in various space plasma environments- solar wind (Gurnett and Frank, 1978; Gurnett et al., 1979, 1993; Yadav and Sharma, 2013), magnetosphere(Anderson et al., 1981; Fuselier et al., 1987), auroral region (Bergmann, 1984; Villain et al., 1990; Wahlund et al., 1994; Backrud et al., 2004, 2005a,b), heliosphere (Hess et al., 1998; Lin et al., 2001) and comets (Scarf et al., 1986; Scarf, 1989)along with variety of laboratory plasma conditions (Song et al., 1991; Sato, 1994; Castro et al., 2010). Theoretical studies also indicate the presence of ion acoustic waves in various plasma configurations (Lee and Kan, 1981; André, 1985; Hellberg and Mace, 2002; Sultana et al., 2010; Rehman et al., 2018a). The free energy for the ion acoustic waves is given by electron heat flux (Gurnett et al., 1979). Ion acoustic mode can also be driven unstable by electrons or ion beams (Gurnett and Frank, 1978; Fuselier et al., 1987) along with density gradients (Vranjes, 2013). Ulysses space craft observed plasma waves, which are of electrostatic in nature, with frequencies between the electron and ion plasma frequency in the vicinity of interplanetary shock waves in three dimensional heliosphere (Hess et al., 1998). These modes are interpreted as Doppler shifted ion-acoustic waves (Hess et al., 1998). These observations show the ratio of electron temperature to proton temperature to be less than 1, which is in sharp contrast with what is said in theory. So, they have speculated the presence of two temperature electrons. In a three component plasma comprising of electrons, denser core ions and less dense beam ions, it was shown by Gary and Omidi (1987) that if the beam temperature is sufficiently low with reference to core ion temperature, then ion acoustic modes can be driven unstable even when the ratio of electron temperature to

ion temperature is lesser than 1. In a series of papers, Backrud et al. (2004, 2005a,b),have analyzed the Cluster observation of ion acoustic waves in auroral region and they have found that broadband wave emissions are a combination of various linear waves and ion acoustic waves are observed in small regions of auroral plasma without suprathermal electron, whose energies are of the order of tens of eV. The electric field which was observed has a significant parallel component in all the events considered.

Ion acoustic waves were observed in the plasma modeled by hot and cool electron along with positive ions, Jones et al. (1975). They have summarized that presence of even small fraction of cold electrons drastically affect the properties of ion acoustic waves. Ion acoustic waves were also observed in a two component magnetized plasma for oblique propagation(Lee and Kan, 1981). The space plasmas are often characterized by non-thermal distributions such as kappa-distribution as has been discussed by Thorne and Summers (1991). They employed the kappa distribution to study the electrostatic waves in a hot unmagnetized plasma and have shown that damping of ion-acoustic waves is strongly dependent on the ion temperature and high-energetic tail of non-thermal distribution only has a slight effect on the damping. This work was latter extended to incorporate the kappa-Maxwellian distribution function Hellberg and Mace (2002). In a magnetized plasma comprising of cold ions and kappa electrons, Sultana et al. (2010) have shown that there is a decrease in the frequency of ion acoustic waves with the increase in the angle of propagation and decrease in the value of superthermality index. It was shown by Hadi et al. (2017) that the ion acoustic modes gets damped in a non-thermal plasma modeled by Cairn's distribution with the increase in the non-thermality factor. With the aid of kinetic theory in a plasma modeled by singly ionized electrons, drifting helium ions and drifting protons, Rehman et al. (2018b) have shown that phase speed of ion acoustic waves increases with the increase in the drift velocity. Moreover, plasma density and temperature does not affect the phase speed to the extend effected by streaming.

In a multi ion plasma, two different kinds of ion acoustic wave modes can be seen-slow ion acoustic mode and fast ion acoustic mode (André, 1985; Mishra and Chhabra, 1996). The phase speed of the slow mode lies between the thermal speeds of the two ion species, whereas for the fast mode it lies between thermal speeds of the hotter ions and the electrons (Nsengiyumva et al., 2014). The evidence for this mode came into light while

studying the propagation and damping of ion wave in a plasma comprising of electron and two ions (D'Angelo et al., 1966). Fast ion acoustic modes have decreased Landau damping rate compared with that of slow ion acoustic mode (D'Angelo et al., 1966; Yoshimura et al., 1997; Misra et al., 2012). This hints at possible application of slow ion acoustic wave for heating of ions in a plasma. In a plasma comprising of proton and oxygen beam along with background hot electron, Bergmann et al. (1988) had shown that there exist slow and fast ion acoustic mode. They had found that for the fast waves the dissipation due to Landau damping is negligible on account of higher phase velocity of fast modes compared with the ion thermal velocity. The slow modes propagate with a frequency below the negative ion frequency and they do propagate without any instability. In auroral region, Freja satellite measured broadband extremely low frequency (BB-ELF) plasma wave in high-resolution (Seyler and Wahlund, 1996; Wahlund et al., 1998). Seyler and Wahlund (1996) have differentiated the wave regime of propagation of electrostatic plasma waves on the basis of propagation angle lesser or greater than $\varepsilon = \sqrt{m_e/m_i}$, where the angle is with respect to magnetic field. Waves with propagation angles greater than ε correspond to either the electrostatic ion cyclotron wave or the shorter wavelength oblique ion acoustic wave, which are termed as fast ion cyclotron or fast ion acoustic waves respectively. On the other hand, waves propagating at angles less than ε correspond to the inertial Alfven wave which is called the slow ion cyclotron wave and in the short wavelength limit is called the slow ion acoustic wave. Numerical and experimental analysis of ion acoustic waves in a four component plasma comprising of electron, F^-, SF_6^- and a positive ion species (Ar^+ or Xe^+) were undertaken by Ichiki et al. (2001). They had found the coexistence of fast ion acoustic mode and slow ion acoustic mode in this plasma and also speculate the possibility of existence of fast and slow ion acoustic modes in single negative ion plasma. The existence of fast and slow ion acoustic modes were also reported in plasma comprising of positive and negative ions, electrons and immobile dust (Misra et al., 2012). Shahmansouri and Tribeche (2014) investigated the properties of ion acoustic waves in bi-ion plasma comprising of hot and cold ion and kappa electron and found out that the plasma supports fast ion acoustic mode and slow ion acoustic mode. When the thermal effects are neglected, the system supports only fast mode.

1.7.2 Electron acoustic waves

In a plasma with electrons having two different temperatures, there can exist another wave mode known as *electron acoustic* wave mode.

The existence of electron acoustic mode were pointed out in seminal paper by Fried and Gould (1961), where it was shown along with the Langmuir mode and ion acoustic mode. Electron acoustic mode was shown to a heavily damped electrostatic wave mode in their unmagnetized electron- ion plasma model. If the plasma comprises of different electrons, then electron acoustic modes becomes weakly damped. Later it was reported by Watanabe and Taniuti (1977) that in plasma comprising of ions and electrons at different temperatures- one hot and other cold, electron acoustic wave, indeed, can be observed. The temperature range which substantiates the existence of these modes is $T_h >> T_c$, where T_h and T_c corresponds temperature of hot and cold electrons respectively. Yu and Shukla (1983) have undertaken a linear study of electron acoustic wave in a three component unmagnetized plasma comprising of hot and cold electrons and ions. Assuming that the phase velocity of waves lies in the range $v_{tc} << \omega/k << v_{ti} << v_{th}$, they too found the existence of electron acoustic mode. Sharma et al. (1983) have shown that an inhomogeneous plasma immersed in magnetic field can also produce electron acoustic mode when the temperature of ions is hotter than the electrons. Gary and Tokar (1985) also found similar temperature regime, but also found the number density regime which supports the electron acoustic mode. In an extended work, Gary (1987) had shown that if there is relative drift between hot and cold electrons, electron acoustic instability will arise. Electron acoustic waves and instabilities were studied in a 3 component plasma comprising of cold drifting Maxwellian electron, hot electrons and ions by Schriver and Ashour-Abdalla (1989). Through simulation, it was shown that, with the residual heating of background ions, cold electron beam free energy source is eliminated rapidly by these instabilities. Considering a plasma comprising of a hot electron beam and stationary cool electrons and ions (with both electrons and ions magnetized and beam drifting along the external magnetic field), Bharuthram (1991) has studied the characteristic of the electron-acoustic instability. He has found that wave growth reduces with increase in the temperature anisotropy of hot beam and cool electrons.

Electron acoustic modes have been used to explain various wave phenomena occurring in different parts of magnetosphere. The Dynamic Explorer-1 satellite has observed the

electrostatic auroral hiss emissions at frequencies below the electron plasma frequency near the polar cusp. By correlating between hiss and upward flowing electron beam, Lin et al. (1984), have shown that auroral hiss emissions are whistler waves propagating near the resonance cone. A comprehensive study of electron acoustic mode which drives electrostatic hiss in the day-side polar cusp were undertaken by Tokar and Gary (1984). They have shown that, using linear kinetic theory, the unstable mode is the electron acoustic mode, rather than the whistler mode. The Broadband Electrostatic Noise (BEN) were observed in the day-side auroral zone and it was suggested that in the generation of BEN, nonlinear effects play a significant role (Dubouloz et al., 1991a). Subsequently, the higher frequency side of BEN, which is observed in the day-side auroral zone, were interpreted with the help of electron acoustic solitons, which is a non linear counter part of electron acoustic mode by Dubouloz et al. (1991b). Electron acoustic waves were also studied in laboratory experiments ((Derfler and Simonen, 1969; Henry and Trguier, 1972; Chowdhury et al., 2017)) and magnetospheric regions ((Dubouloz et al., 1991a,b; Tokar and Gary, 1984; Singh and Lakhina, 2001)). Singh and Lakhina (2001) have studied generation of electron acoustic waves in the magnetosphere. They have found that electron beams in the day-side auroral region, polar cusp and plasma sheet boundary layer can generate electron acoustic waves.

1.7.3 Electrostatic ion cyclotron (EIC) waves

In the presence of external magnetic field, variety of plasma waves are possible. One prominent among them is electrostatic ion cyclotron (EIC) wave which propagates almost perpendicularly with reference to external magnetic field, with dispersion relation (Nicholson, 1983):

$$\omega^2 = \Omega_s^2 + k^2 c_s^2 \tag{1.27}$$

Here, $\Omega_s = \frac{z_s q B_0}{m_s}$ is the cyclotron frequency of s^{th} species with z_s, q and m_s being multiplicity, charge and mass of the species respectively. B_0 being the ambient magnetic field and c_s is the acoustic speed defined by $c_s = \sqrt{k_B T_e / m_s}$.

EIC waves are one of the important waves that have been observed in the magnetized plasma which have a frequency near to the ion cyclotron frequency. EIC waves have a small finite wave number along the magnetic field. D'Angelo and Motley (1962) and Motley and

D'Angelo (1963) were the first one to observe these waves in laboratory plasma with cesium and potassium. Thereafter, EIC waves were observed in high latitude ionosphere by Mosier and Gurnett (1969).

EIC waves have been observed in various regions of the Earth's magnetosphere by many satellites, e.g., S3-3 (Kintner et al., 1978, 1979; Temerin et al., 1979), ISEE-1 (Cattell et al., 1991), Viking (André et al., 1987), Polar (Mozer et al., 1997), FAST Cattell et al. (1998) and GEOS 1 and 2 (Young et al., 1981; Roux et al., 1982), THEMIS (Tang et al., 2015). The interest in the study of EIC waves grew due to their importance in heating of the ions in the magnetosphere (Hinata, 1980; Dakin et al., 1976; Ungstrup et al., 1979; Roux et al., 1982). Electrostatic ion cyclotron instability (EICI) space plasmas can be generated by various sources of free energies, such as electron beam (Singh et al., 1985), field aligned currents (Drummond and Rosenbluth, 1962; Kindel and Kennel, 1971), ion beams (Okuda and Nishikawa, 1984; Lakhina, 1987), velocity shear (Gavrishchaka et al., 1997) and density gradients (Tang et al., 2015), inverse Landau damping of electrons (Kindel and Kennel, 1971; Drummond and Rosenbluth, 1962). The EICI also has lowest threshold among the various current driven instabilities (Kindel and Kennel, 1971).

EIC waves have also been studied in plasmas with particles having nonthermal distributions e.g., kappa-Maxwellian (particle distribution in the parallel direction is modeled by the kappa distribution, where as those in perpendicular direction is modeled by Maxwell distribution) by Basu and Grossbard (2011), nonextensive (Niyat et al., 2016)

Ohnuma et al. (1973) had shown the coupling between EIC and acoustic modes in 2 component laboratory plasma (argon plasma). They observed that coupling occurs near the second-harmonic ion cyclotron frequency and appears strongly with low ion temperature. This result was in accordance with the dispersion relation which they derived using kinetic theory. Also, the frequency at which coupling happens was found to be dependent on magnetic field. Using data from THEMIS satellite,Tang et al. (2015) showed that EIC waves can be a source for providing perpendicular ion heating at the Earth's magnetopause. They also suggested plasma density gradient within the low-latitude boundary layer can be a possible source of free energy for the EIC waves and also pointed out the possibility of coupling of EIC waves with ion acoustic waves. They observed that the magnetosheath particles were transported inward by resonating with the EIC waves. Thus, the presence of EIC waves in

the magnetopause boundary layer may contribute to maintaining the boundary layer itself.

Harmonics of EIC waves in the downward current auroral region of Saturn was reported by Menietti et al. (2011). Waves upto 3^{rd} harmonics were seen in the satellite data. Also, they have concluded that contribution of harmonics other-than fundamental towards the ion heating rates is minimal. Later on, Sharma et al. (2013) studied the generation of higher harmonics by a spiraling ion beam in a collisionless magnetized plasma containing K^+ light positive ions, electrons, and $C_7F_{14}^-$ heavy negative ions. The ion beams drives EIC waves to instability via cyclotron interactions. The fast magnetosonic waves, in the frequency range of ion cyclotron waves, was employed to heat the plasma in Aditya tokmak (Chattopadhyay et al., 2015). It is shown that the efficiency of ion heating critically depends on the temperature of ions. The heating capabilities of the EIC waves and presence of heavier ions in the various regions of the Earth's magnetosphere warrants study of the waves and its harmonics.

1.8 Scope and outline of the thesis

This thesis invokes energetic particles to explain various wave phenomena that is observed in space plasmas, with a special emphasis to electrostatic waves such as electron acoustic waves, ion acoustic wave and electrostatic ion cyclotron waves.

A wide variety of waves are supported by plasma such as ion-acoustic, electron acoustic, ion cyclotron waves etc. Each wave is unique and characterized by its own frequency and propagation with respect to ambient magnetic field. For example, ion and electron acoustic waves are prominent in unmagnetized plasmas and propagate almost parallel to ambient magnetic field whereas ion cyclotron waves observed in magnetized plasmas propagate nearly perpendicular. These waves are observed almost everywhere, be it Earth's magnetosphere, solar wind or lunar wake. Simultaneously more than one plasma mode can exist, thereby giving chance of coupling or merging with various other modes. The presence of electrostatic ion cyclotron waves and ion acoustic waves have been confirmed by many observation- both in laboratory as well as space plasma observation (Gurnett et al., 1979, 1993; Hess et al., 1998; Huttunen et al., 2007; Rehman et al., 2018b; D'Angelo and Motley, 1962; Dakin et al., 1976; Cattell, 1981; Cattell et al., 1991; Gavrishchaka et al., 1999). There have been numerous investigations which study these waves independently rather than

focusing on the coupling aspects on these waves, even though Ohnuma et al. (1973) have reported the coupling of these waves in laboratory plasma. The coupling of waves have also been reported in space plasma observation (Tang et al., 2015).

Lunar wake plasma has gathered renewed interest with the launch of new satellites. A variety of electrostatic and electromagnetic plasma waves are seen in this region (Farrell et al., 1996; Kellogg et al., 1996; Nakagawa et al., 2003; Rubia et al., 2017). Tao et al. (2012) has presented a detailed analysis of electrostatic plasma waves observed by ARTEMIS satellite. By performing 1-D Vlasov simulation of a four-component plasma comprising of protons, ions, suprathermal (κ distribution) electrons and an electron beam, they have shown that observed electrostatic waves falls in frequency range (0.1-0.4) f_{pe} (where f_{pe} stands for electron plasma frequency) in the higher frequency end and 0.01 f_{pe} in the low frequency end. A linear analysis of electrostatic waves will give the information as to what are the nature of the plasma modes present in the region. So far, there has not been any study in this direction.

Out of the different types of electrostatic instability that exist in a plasma, electrostatic ion cyclotron instability (EICI) has the lowest threshold among various current driven instabilities. Previous studies have concentrated on instability of harmonics of EIC with heavier ions (Kindel and Kennel, 1971; Kim et al., 2008; Rosenberg and Merlino, 2009; Kurian et al., 2009; Sharma et al., 2013). However, space plasma is also populated with He^{++} as shown by Sharp et al. (1974); Tang et al. (2015) which are of solar wind origin. In-order to have better understanding of the propagation characteristics of plasma waves, a realistic model of magnetized plasma has to be considered, which has not been discussed anywhere in the literature. Moreover, it is long known that the many regions of space plasma are far removed from thermal equilibrium and hence these plasmas cannot be treated with Maxwell-Boltzmann distribution function. A system under thermodynamic equilibrium arranges the particle in Maxwell-Boltzmann distribution. Maxwell-Boltzmann distribution is the most preferred way of arranging the particle of a system as this have the least entropy, which have a Gaussian type bell curved plot. The earlier studies on plasma waves mainly focused on the Maxwellian particle distribution. However, new high time resolution observations in space plasmas reveals that the particle distributions are characterized by power law decrease, rather than exponential decrease as dictated by Maxwell-Boltzmann distribution. This means most

of the space plasma reside in a state which is not in thermal equilibrium with surroundings. The distribution function that is used to describe this state is called non-thermal distribution function or Lorentzian distribution function or Kappa distribution function. The concept of Kappa distribution was introduced by Olbert (1968) which he used to account for the electric current produced by electrons in the magnetosheath. Later on, it was used by Vasyliunas (1968) to fit the electron number data in the magnetosphere by OGO 1 (Orbiting Geophysical Observatory) and OGO 3 satellite. Ever since there had been a numerous observations of this type of distribution function space plasmas [for an extensive review, see Livadiotis (2015)]. There has not been any comprehensive study looking into the coupling or merging aspect of plasma wave modes in nonthermal plasmas and neither harmonic studies of the ion cyclotron waves involving doubly charged helium ions which are essential part of solar wind and can be found other regions of the magnetosphere.In this thesis, low frequency waves such as electrostatic ion cyclotron waves, ion acoustic wave and electron-acoustic waves in multi component space plasmas are studied. Fluid as well as kinetic theory of plasma waves is used to study the coupling of ion-acoustic & ion cyclotron waves and their generation in Maxwellian and non-thermal plasmas. The harmonic generation of light and heavy ion cyclotron waves has also been studied by using kinetic theory. The relevance of the theoretical results has been brought out in sync with observations in solar wind/lunar wake and magnetospheric plasmas. The thesis is divided into six chapters and detailed description of subject matter discussed in each chapter is given below:

The thesis is organized as follows. Chap. 1 gives overall view of the subject of plasma physics including basic definitions and the fundamental principles. The brief description of natural sources of plasma is discussed along with theoretical approaches used to explore plasma. After giving a brief overview of different distribution functions used in plasma physics, the various types of waves related to the thesis work are also presented. In the following chapters, the original work done by the candidate is described. In Chap. 2, a theoretical investigation of plasma waves in lunar wake plasma is carried out which is modeled by fluid proton and doubly charged Helium ions along with beam electrons and kappa distributed electrons. It is seen that for particular value of beam velocity, the electron beam driven mode merges with slow ion acoustic mode and then with fast ion acoustic mode thereby generating electron beam driven slow-ion acoustic mode and electron beam- driven

fast ion acoustic mode, both having finite growth rate. Chap. 3 investigates the coupling of proton and Helium cyclotron modes with fast and slow ion acoustic modes in the 3 component magnetized plasma comprising of fluid kappa electron, fluid proton and doubly charged Helium ions in the solar wind. The effect of magnetic field in the model described in Chap. 2 is investigated in Chap. 4, where the coupling and merging of various modes can be seen. The generation of electrostatic ion cyclotron waves in auroral plasma is examined in Chap. 5, wherein the magnetized plasma consists of Maxwell-Boltzmann distributed proton, doubly charged Helium ions and electron beam. In Chap. 6, the results are summarized and scope for future work is discussed.

Chapter 2

Excitation of ion acoustic waves by electron beam in Lunar wake plasma

2.1 Introduction

Interaction of solar wind with moon has been studied in great detail due to the advent of new space technologies. The moon acts as an obstacle that intercepts and absorbs much of the streaming solar wind and energetic particles on its sunlit surface, creating a downstream plasma-void cavity left behind it for several lunar radii. This region is known as lunar wake region. Several studies had been undertaken to understand various processes in this region(Ness, 1965; Michel, 1968). WIND satellite, which was launched in November 1, 1994 significantly increased the understanding of Lunar wake (Bosqued et al., 1996). Initially it was thought that beyond 4 lunar radii, evidence of lunar wake will not be observable (Ness, 1972), however, WIND spacecraft observations (Owen et al., 1996; Ogilvie et al., 1996) have shown the presence of lunar wake at a distance of $\sim 6.8\, R_L$, where R_L stands for lunar radius. Simulation studies by Farrell et al. (1998) have shown the presence of counter streaming ion beams and rarefaction wave emanating outward from the wake which were consistent with the satellite observations (Ogilvie et al., 1996). The existence of ion and electron rarefaction waves and an increase in the temperature of the electrons were observed by Birch and Chapman (2001) in their simulations. Recently, Xie et al. (2013) studied the interaction between the Moon and the solar wind under three different IMF conditions using three-dimensional MHD simulation. They showed that an acceleration region may appear in the void when the

plasma temperature is enhanced. Also, they reported that fast magnetosonic waves propagate away from the limb as the plasma moves in the wake. In recent years, wave phenomena in the vicinity of Moon have gained considerable importance. Popel et al. (2013) showed that the relative motion of the solar wind with respect to the photoelectrons over the lunar surface can lead to the excitation of high-frequency oscillations such as Langmuir and electromagnetic waves on the lunar dayside and the dust-acoustic waves in the vicinity of the lunar terminator. Popel et al. (2015) have shown the possibility of the existence of a dusty plasma sheath-like structure with large electric fields of the order of 300 V/m in the lunar terminator region. Recently, Popel and Morozova (2017) have shown that interaction of the Earth's magnetotail with the dusty plasma near the Lunar surface can lead to the excitation of ion-acoustic and dust-acoustic waves. Because of the relatively long growth time of these instabilities, ion-acoustic as well as dust-acoustic plasma turbulence may develop. Planned future missions such as Luna-25 and Luna-27 lunar modules will have the potential to detect and unravel the manifestations of the low and high frequency wave motions near the lunar surface (Popel and Morozova, 2017).

The electrostatic and electromagnetic plasma waves such as ion-acoustic, Langmuir, whistler waves have been observed in the wake region which is a natural laboratory for observation of these waves (Kellogg et al., 1996; Nakagawa et al., 2003; Farrell et al., 1996; Bale et al., 1997). The simulation studies have predicted variety of instabilities, e.g., two-stream electron instabilities, bump-on-tail instabilities, ion acoustic-like beam instabilities, flute instabilities and low-frequency electromagnetic waves near local proton cyclotron frequency (Birch and Chapman, 2001, 2002; Farrell et al., 1998; Borisov and Mall, 2000; Trávníček et al., 2005).

A detailed analysis of the electrostatic waves observed by the ARTEMIS P1 spacecraft on the outbound side of the flyby has been presented by Tao et al. (2012). They also performed 1-D Vlasov simulation of a four-component plasma comprising of protons, ions, an electron beam and suprathermal (κ-distribution) electrons. They were able to explain the physical properties of the observed electrostatic waves in the frequency range of (0.1-0.4)f_{pe}; f_{pe} is the electron plasma frequency and concluded that the observed waves were most likely the electron beam mode. However, observations below $0.1 f_{pe}$ did not find any explanation. Recently, Rubia et al. (2017) performed a nonlinear analysis of 4 component

plasma comprising of hot protons, hot heavier ions (α-particles, He^{++}), electron beam and suprathermal electrons following kappa distribution. They have proposed an alternate generation mechanism for the electrostatic waves in terms of slow and fast ion-acoustic and electron-acoustic solitons. They could successfully explain the observed low and high frequency waves in the lunar wake.

It is important to mention here, that there has been a number of nonlinear studies on the slow and fast ion-acoustic solitons and double layers (Lakhina et al., 2008, 2014; Maharaj et al., 2015; Lakhina and Singh, 2015; Olivier et al., 2015; Rubia et al., 2016, 2017, 2018) but to the authors knowledge, none on the linear regime. Therefore, we undertake a linear dispersion analysis of electrostatic waves in lunar wake plasma with the model as taken up by Rubia et al. (2017). The purpose of the study is to understand how electron beam affects the various modes, e.g., low-frequency modes (slow and fast ion-acoustic) and high-frequency mode(electron-acoustic) modes.

The chapter is organized as follows: In Sect. 2.2, linear dispersion relation for the electrostatic waves is derived. In Sect. 2.3, numerical results are presented and in Sect. 2.4 discussions and conclusions are given.

2.2 Theoretical model

The lunar wake plasma is modeled by a homogeneous, collisionless, and magnetized four-component plasma comprising of fluid protons (N_{p0}, T_p), doubly charged fluid alpha particles, He^{++} (N_{i0}, T_i), electron beam streaming along ambient magnetic field (N_{b0}, T_b, U_b) and suprathermal electrons (N_{e0}, T_e). Here, N_{s0} and T_s represent the equilibrium values of the density and temperature of the species s, and s = p, i, b and e for protons, alpha particles, electron beam and suprathermal electrons, respectively, U_b is the drift speed of the beam electrons. We consider the electrostatic waves propagating parallel to the ambient magnetic field. In such a case the presence of magnetic field does not affect the propagation properties of the waves. The fluid equations which govern the propagation characteristic of plasma waves are:

$$\frac{\partial n_s}{\partial t} + \nabla.(n_s \mathbf{v}_s) = 0 \tag{2.1}$$

$$m_s n_s[\frac{\partial \mathbf{v}_s}{\partial t} + (\mathbf{v}_s.\nabla)\mathbf{v}_s] = q_s n_s(-\nabla\phi) - \nabla P_s \tag{2.2}$$

$$\nabla^2\phi = -\frac{e}{\varepsilon_0}(N_p + N_i z_i - N_e - N_b) \tag{2.3}$$

where m_s, $\mathbf{v}_s$, P_s, z_i, q_s represents respectively, mass, velocity, pressure, atomic number and charge of the individual species. The pressure term in this case becomes $\nabla P_s = \gamma_s T_s \nabla n_s$, where $\gamma_s = 3$ is the ratio of specific heats for specie "s".

The suprathermal electrons are assumed to have κ distribution which is given by Summers and Thorne (1991):

$$f_\kappa(v) = \frac{N_{e0}}{\pi^{\frac{3}{2}}}\frac{1}{\theta^3}\frac{\Gamma(\kappa+1)}{\kappa^{\frac{3}{2}}\Gamma(\kappa-\frac{1}{2})}\left(1+\frac{v^2}{\kappa\theta^2}\right)^{-(\kappa+1)} \tag{2.4}$$

where κ is the superthermality index; Γ is the gamma function; $\theta = [\frac{2\kappa-3}{\kappa}]^{\frac{1}{2}}(\frac{T_e}{m_e})^{\frac{1}{2}}$ is the effective thermal speed and N_{e0} is the equilibrium destiny of suprathermal electrons. It has to be emphasized that in order to have meaningful value for the thermal speed of suprathermal electrons, we need to have $\kappa > \frac{3}{2}$.

The number density of electrons in the presence of electrostatic waves having potential, ϕ can be obtained by replacing v^2/θ^2 by $v^2/\theta^2 - 2e\phi/m_e\theta^2$ in Eq. (3.4) and by integrating it over velocity space (Devanandhan et al., 2011b,a, 2015):

$$N_e = N_{e0}\left[1 - \frac{e\phi}{T_e(\kappa-\frac{3}{2})}\right]^{\frac{1}{2}-\kappa} \tag{2.5}$$

Linearization and simplification of Eqs. (2.1) to (2.3) and (2.5), yields the following general dispersion relation:

$$1 + \frac{\omega_{pe}^2}{k^2 v_{te}^2}\frac{2\kappa-1}{2\kappa-3} = \frac{\omega_{pb}^2}{(\omega-kU_b)^2 - 3k^2v_{te}^2} + \frac{\omega_{pp}^2}{\omega^2 - 3k^2v_{tp}^2} + \frac{z_i^2\omega_{pi}^2}{\omega^2 - 3k^2v_{ti}^2} \tag{2.6}$$

Here $\omega_{ps} = \sqrt{\frac{N_{0s}e^2}{\varepsilon_0 m_s}}$ is the plasma frequency of s^{th} species. This is similar to the expression which has been derived by Devanandhan et al. (2011a), where they have unmagnetized plasma having cold electrons and ions, superthermal hot electrons and an electron beam, but have studied electron acoustic waves.

2.3 Numerical Results

In this section, we carry out the numerical computations of the general dispersion relation (6) for the Lunar wake plasma parameters. The relevant lunar wake and solar wind plasma parameters for the computations are taken from Tao et al. (2012) and Mangeney et al. (1999). In order to facilitate the numerical analysis of Eq. (2.6), following normalizations are used: frequencies are normalized by effective proton plasma frequency, $\omega_{p0} = \sqrt{\frac{N_0 e^2}{\varepsilon_0 m_p}}$ where N_0 is the total equilibrium electron number density given by the expression $N_0 = N_{p0} + z_i N_{i0} = N_{e0} + N_{b0}$, wave number k with effective hot electron Debye length $\lambda_{De} = \sqrt{\frac{\varepsilon_0 k_B T_e}{N_0 e^2}}$ and the velocities are normalized with ion acoustic velocity C_s given by the expression $C_s = \sqrt{\frac{k_B T_e}{m_p}}$.

Before we proceed further, it is important to describe how the different electrostatic wave modes are identified. Initially, we put electron beam density to zero $(N_{b0} = 0)$, we obtain four modes: two with positive phase speed and two with negative phase speed which are symmetrical. The modes with lower phase speed are identified as slow ion- acoustic modes whereas those with higher phase speeds as fast ion-acoustic modes (Lakhina et al., 2008). Then, we introduce electron beam but neglect the streaming, now additional two modes (with positive and negative phase speeds) with highest phase speeds appear along with slow and fast ion-acoustic modes. The modes with highest phase speed are identified as electron-acoustic modes (Rubia et al., 2017). Thus, the six modes are identified as electron acoustic with positive phase speed (mode 1, dash-dot curve, pink color) & negative phase speed (mode 6, solid curve, black color), fast ion-acoustic mode with positive phase speed (mode 2, short dashed curve, blue color) & negative phase speed (mode 5, long dashed curve, green color) and slow ion-acoustic mode with positive phase speed (mode 3, dash-dot-dot-dot curve, red color) and negative phase speed (mode 4, medium dashed curve, magenta color). In figure 1 and subsequent figures these are clearly identified. Also, it must be noted that real frequencies and growth rates (wherever applicable) are plotted in upper and lower panels, respectively. In the next subsection, we present the effect of electron beam velocity on the instability.

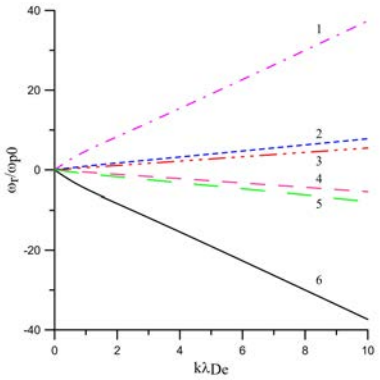

(a) $U_b/C_s = 0.0$

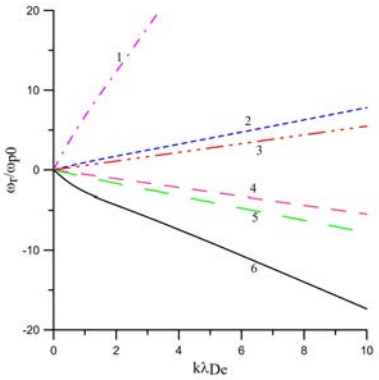

(b) $U_b/C_s = 2$

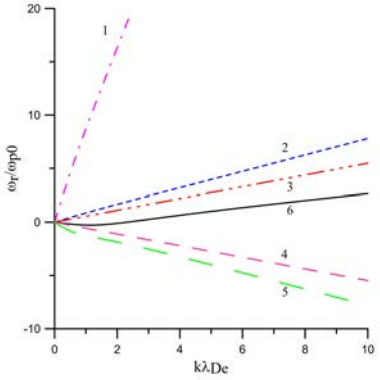

(c) $U_b/C_s = 4$

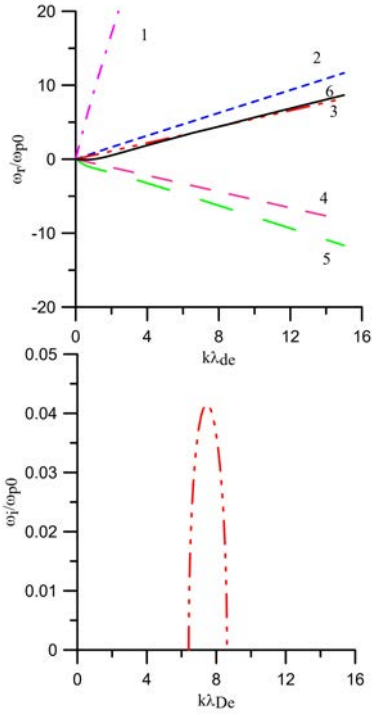

(d) $U_b/C_s = 4.3$

Figure 2.1: Plot of real frequency, ω_r/ω_{p0} and growth rate, ω_i/ω_{p0} versus $k\lambda_{de}$ for the fixed parameters $n_b/N_0 = 0.01$, $n_i/N_0 = 0.05$, $\kappa = 6$, $T_b/T_e = 0.0025$, $T_p/T_e = 0.2$, $T_i/T_e = 0.4$ and various values of normalized electron beam speed, U_b/C_s.

2.3.1 Effect of electron beam velocity

In Fig. 2.1, the characteristics of dispersion relation Eq. (2.6) are studied by taking into account the effect of electron beam variation. The Fig. 2.1a shows plot of ω_r/ω_{p0} versus $k\lambda_{de}$ for $U_b/C_s = 0$. The other fixed plasma parametersTao et al. (2012); Mangeney et al. (1999); Lakhina and Singh (2015) are $n_b/N_0 = 0.01$, $n_i/N_0 = 0.05$, $\kappa = 6$, $T_b/T_e = 0.0025$, $T_p/T_e = 0.2$, $T_i/T_e = 0.4$. With $U_b/C_s = 0$, six real roots are obtained, three positive and three negative which are shown by six curves in the Fig. 2.1a. These six modes are identified as: two electron acoustic modes (modes 1 and 6), two fast ion acoustic modes (modes 2 and 5) and two slow ion acoustic modes (modes 3 and 4). The modes 1, 2, 3 have positive phase speeds whereas modes 4, 5, 6 have negative phase speeds. All these curves are perfectly symmetrical about x-axis.

In Figs. 2.1b and 2.1c, the electron beam velocity is increased to $U_b/C_s = 2$ and $U_b/C_s = 4$ respectively. It can be seen that frequency of the modes 1 and and 6 are affected the most as compared to modes 2, 3, 4 and 5. The frequency of the modes 1 and 6 increases drastically for fixed value of $k\lambda_{de}$. In fact, phase speed of mode 6 turns positive from negative when U_b/C_s is increased from 0 to 4 whereas electron beam speed has insignificant effect on other modes, i.e., modes 2 to 5.

When the normalized electron beam velocity is increased further to a value of 4.3 (Fig. 2.1d), the dispersion curves for modes 1 and 6 change drastically. Here, it can be seen that mode 6 (electron acoustic mode) and mode 3 (slow ion acoustic mode) merges in the range $k\lambda_{de} \approx 6.4 - 8.6$, i.e., in this $k\lambda_{de}$ range the phase speeds of both the modes become the same and modes merges together and become unstable with finite growth rate as can be seen in the lower panel of Fig. 2.1d. This is a electron beam driven slow ion-acoustic mode. The maximum value of growth rate is, $\omega_i/\omega_{p0} \approx 0.041$ at $k\lambda_{de} = 7.45$ with corresponding real frequency, $\omega_r/\omega_{p0} \approx 4.1$.

For electron beam speed $U_B/C_s = 4.5$ the merging of modes occurs at two places: first at $k\lambda_{de} = 1.87 - 2.88$ where mode 6 merges with mode 3 (this is electron beam driven slow ion-acoustic mode) and then again mode 6 merges with mode 2 at $k\lambda_{de} = 6.83 - 19.98$ (this is electron beam driven fast ion-acoustic mode) (see Fig. 2.2a). First merging happens at smaller range of wavenumbers whereas second merging occurs over a broad range and at larger values of wavenumbers. In the first case i.e., the electron beam driven slow

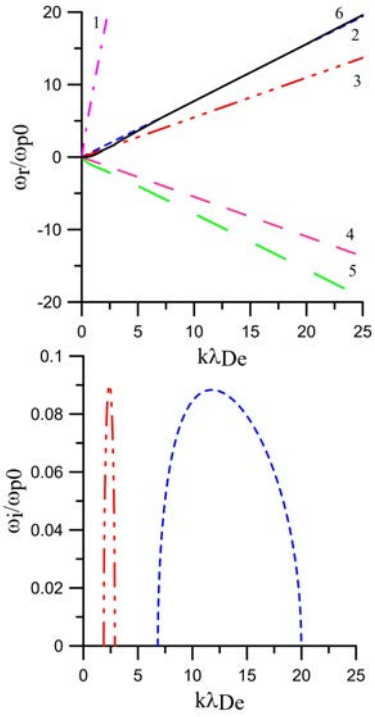

(a) $U_b/C_s = 4.5$

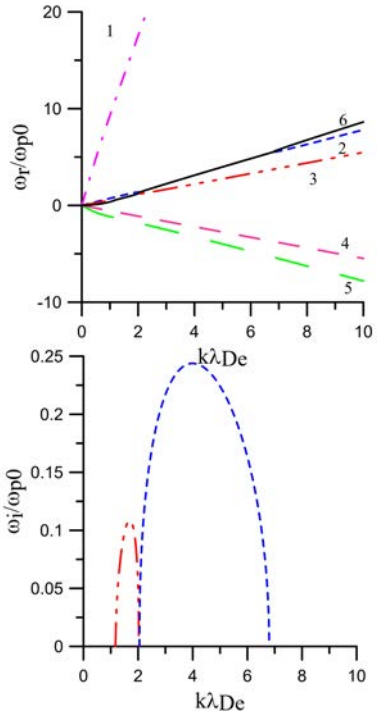

(b) $U_b/C_s = 4.6$

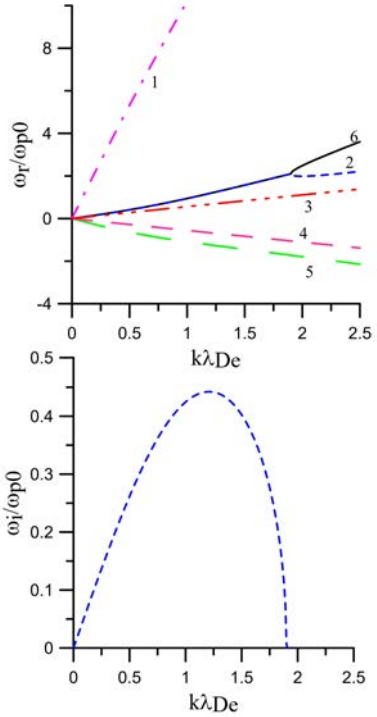

(c) $U_b/C_s = 5.5$

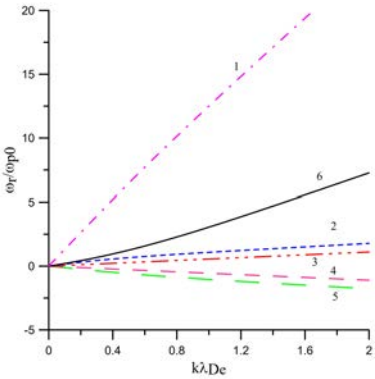

(d) $U_b/C_s = 7.8$

Figure 2.2: Plot of real frequency ω_r/ω_{p0} and growth rate, ω_i/ω_{p0} versus $k\lambda_{de}$. All other plasma parameters are the same as in Fig. 2.1

ion-acoustic mode, the maximum value of $\omega_i/\omega_{p0} \approx 0.09$ at $k\lambda_{de} = 2.38$ with corresponding real frequency, $\omega_r/\omega_{p0} \approx 1.31$ and for second case, i.e., electron beam driven fast ion-acoustic mode, $\omega_i/\omega_{p0} \approx 0.088$ at $k\lambda_{de} = 11.78$ with $\omega_r/\omega_{p0} \approx 9.12$. It is seen that the maximum growth rates in the two cases are comparable. Thereafter, when the value of U_B/C_s is increased to 4.6 (Fig. 2.2b), the merging of modes again occurs at two places, first at the $k\lambda_{de} \approx 1.18 - 2.02$ and second 2.06 to 6.79. The former merging represents the electron beam driven slow ion-acoustic mode whereas the latter represents the electron beam driven fast ion-acoustic mode. From Fig. 2.2b, it is also clear that the maximum value of ω_i/ω_{p0} for the electron beam driven slow ion-acoustic mode is ≈ 0.11 at $k\lambda_{de} = 1.69$ with $\omega_r/\omega_{p0} \approx 0.94$ and for the electron beam driven fast ion-acoustic mode is 0.24 at $k\lambda_{de} \approx 4$ with $\omega_r/\omega_{p0} = 3.11$. Interestingly, the peak growth rate for the electron beam driven fast ion-acoustic modes is nearly twice than that of the slow ion-acoustic mode. Similar trend continues as U_B/C_s increased to 5.4, fast ion-acoustic continues to grow with larger growth rate and slow ion-acoustic wave growth diminishes.

The dispersion plot for $U_b/C_s = 5.5$ is plotted in Fig. 2.2c. It is clear from the figure that there is no interaction between the electron beam (mode 6) and slow ion-acoustic (mode 3) and hence, the slow ion-acoustic mode become stable. In this case only the electron beam driven fast ion acoustic is unstable. The maximum value of the growth rate ω_i/ω_{p0} in this case is 0.44 at $k\lambda_{de} = 1.21$ with corresponding real frequency, $\omega_r/\omega_{p0} = 1.2$. The $k\lambda_{de}$ range in which the electron beam driven fast ion-acoustic mode is unstable is $k\lambda_{de} \approx 0 - 1.9$. The unstable region shifts towards lower wavenumber region with increase in U_b/C_s. The growth rate of fast ion-acoustic waves start to decrease at $U_b/C_s > 5.5$ and continue to decrease until U_b/C_s=7.7. The unstable region for these waves disappears at $U_b/C_s = 7.8$ and beyond as is clear from Fig. 2.2d which shows no interaction between the electron beam mode and other modes as all modes remain distinct. In the next subsection, we study the effect of density of electron beam on the dispersion of the waves.

2.3.2 Effect of electron beam density

Here we study the effect of variation of number density of beam electrons on the dispersion characteristics of the various wave modes. The fixed plasma parameters for this variations are $n_i/N_0 = 0.05$, $\kappa = 6$, $T_b/T_e = 0.0025$, $T_p/T_e = 0.2$, $T_i/T_e = 0.4$ and $U_b/C_s = 5$. It can

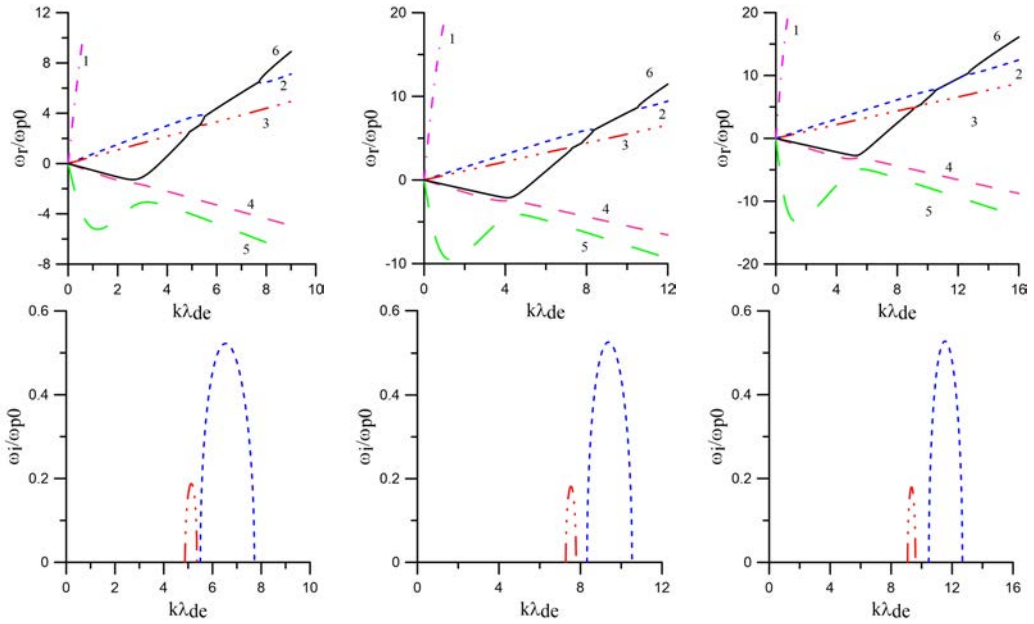

(a) $n_b/N_0 = 0.1$ (b) $n_b/N_0 = 0.2$ (c) $n_b/N_0 = 0.3$

Figure 2.3: Effect of n_b/N_0 variation on dispersion characteristics for $U_b/C_s = 5$. The other fixed plasma parameters are same as in Fig. 2.1

be seen from Fig. 2.3a that at $n_b/N_0 = 0.1$, both electron beam driven slow ion- acoustic mode (merging of mode 6 and 3) and fast ion-acoustic mode (merging of modes 6 and 2) are unstable with maximum growth rates of $\omega_i/\omega_{p0} \approx 0.19$ and 0.52 respectively. As we increase the value of n_b/N_0 to 0.2 (Fig. 2.3b) and 0.3 (Fig. 2.3c), the unstable regions for both the modes shift towards higher $k\lambda_{de}$ range. However, the growth rates marginally decreases for electron beam driven slow ion- acoustic mode and increases for electron beam driven fast ion- acoustic mode. Further, the separation between electron beam driven slow and fast ion-acoustic modes increases with increase in the value of electron beam density.

2.3.3 Effect of density of Helium ions

In this subsection, the effect of variation of number density of Helium ions is studied on the dispersion characteristic of the waves. The fixed plasma parameters for the Fig. 2.4 are $n_b/N_0 = 0.01$, $\kappa = 6$, $T_b/T_e = 0.0025$, $T_p/T_e = 0.2$, $T_i/T_e = 0.4$, $U_b/C_s = 5$. We have plotted real frequency (upper panel) and growth rates (lower panels) for n_i/N_0 from 0.1 (Fig. 2.4a), 0.15(Fig. 2.4b) and 0.2 (Fig. 2.4c). Though, it is not clearly visible from real frequency

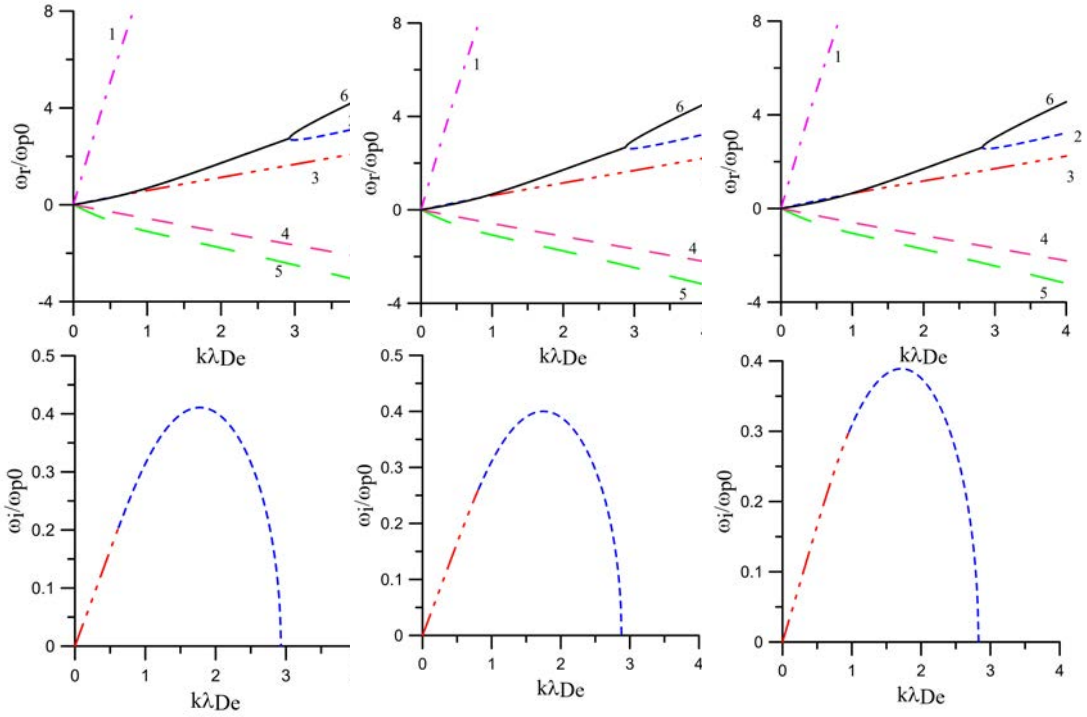

(a) $n_i/N_0 = 0.10$ (b) $n_i/N_0 = 0.15$ (c) $n_i/N_0 = 0.20$

Figure 2.4: Effect of n_i/N_0 variations on dispersion characteristics for $U_b/C_s = 5$. The other fixed plasma parameters are same as in Fig. 2.1

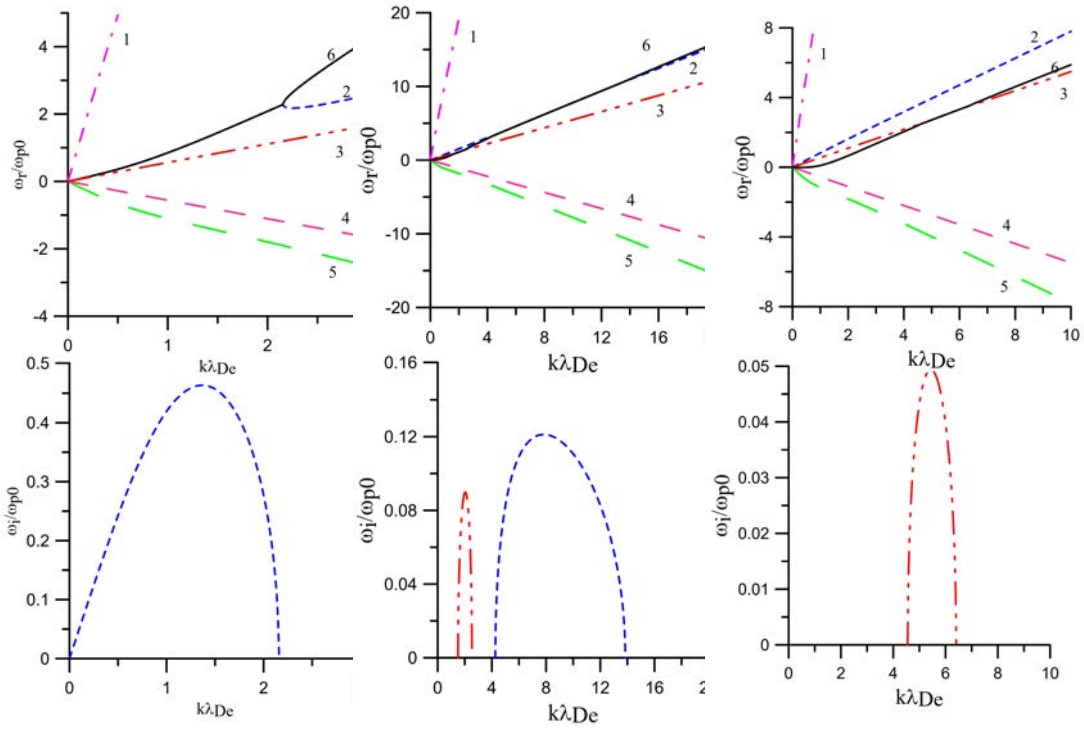

(a) $T_b/T_e = 0.002$ (b) $T_b/T_e = 0.0032$ (c) $T_b/T_e = 0.0035$

Figure 2.5: Effect of T_b/T_e variations on characteristics of the waves for $U_b/C_s = 5$. The other fixed plasma parameters are the same as in Fig. 2.1

curves, but from the growth rate curves, it is evident that the merging of electron beam mode occurs with slow (red, dash-dot-dot-dot curve) and fast (blue, dashed curve) ion-acoustic modes. The $k\lambda_{de}$ range in which electron beam driven fast ion-acoustic mode (merging of mode 6 and 2) is unstable decreases slightly whereas it increases for electron beam driven slow ion-acoustic modes. For instance, the $k\lambda_{de}$ ranges over which electron beam driven fast ion-acoustic mode is unstable for $n_i/N_0 = 0.10$, $n_i/N_0 = 0.15$ and $n_i/N_0 = 0.20$, respectively are 0.62-2.92, 0.81-2.87 and 0.96-2.80.

2.3.4 Effect of electron beam temperature

In this section, we study the effect of the variation of temperature of electron beam on the growth of the electrostatic waves. The plasma parameters fixed for this variation are $n_i/N_0 = 0.05$, $n_b/N_0 = 0.01$, $\kappa = 6$, $T_p/T_e = 0.2$, $T_i/T_e = 0.4$, $U_b/C_s = 5$. One of the most prominent feature of this variation is the behavior of mode 6. In Fig. 2.5a, the electron beam

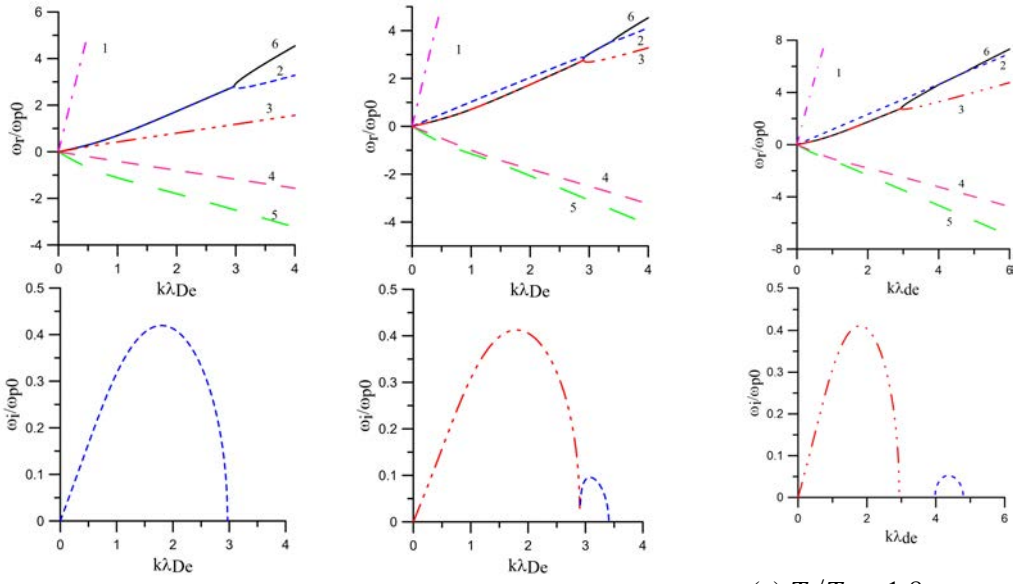

(a) $T_i/T_e = 0.2$ (b) $T_i/T_e = 1.4$ (c) $T_i/T_e = 1.8$

Figure 2.6: Effect of T_i/T_e variations on the characteristics of the waves for $U_b/C_s = 5$. The other fixed plasma parameters are the same as in Fig. 2.1

driven fast ion-acoustic mode becomes unstable in the range $k\lambda_{de} \approx$ 0-2.15 for T_b/T_e=0.002. The electron beam driven slow ion-acoustic mode along with fast ion-acoustic mode start to appear as the electron beam temperature is increased further and slow and fast ion-acoustic modes are clearly distinguishable at T_b/T_e=0.0032 (Fig. 2.5b). In Fig. 2.5b, the electron beam driven slow ion-acoustic mode is unstable in the range, $k\lambda_{de} \approx$ 1.5-2.5 whereas for higher range of $k\lambda_{de} \approx$ 4.3-13.9 fast ion-acoustic mode is unstable. When the value of T_b/T_e is further increased, the growth rate of electron beam driven fast ion-acoustic mode becomes less than that of electron beam driven slow ion-acoustic mode (not shown here). It is interesting to note that the electron beam driven fast ion-acoustic mode ceases to exist when the value of T_b/T_e reaches 0.00324. When T_b/T_e is increased to 0.0035, electron beam driven slow ion-acoustic mode is the only unstable mode for large value of $k\lambda_{de}(\approx$ 4.6- 6.4). The electron beam driven slow ion-acoustic mode also disappear at T_b/T_e=0.004. Overall, growth rates of both the modes, i.e., fast and slow ion-acoustic modes decrease substantially with the increase in the T_b/T_e values.

2.3.5 Effect of temperature of Helium ions

The effect of variation of temperature of ions is displayed in Fig. 2.6. For $T_i/T_e = 0.2$, the electron beam driven fast ion-acoustic mode is unstable in the range $k\lambda_{de} \approx$ 0-3 whereas slow ion-acoustic mode is stable. With subsequent increase in T_i/T_e, the electron beam driven slow ion-acoustic mode become more unstable with larger growth rate whereas growth of fast ion-acoustic mode decreases significantly. At $T_i/T_e = 1.4$ slow and fast ion-acoustic modes almost start to separate from each other and eventually separate as shown in Fig. 2.6c at $T_i/T_e = 1.8$. Initially, electron beam driven fast ion-acoustic mode is excited for large range of wavenumbers, however, as the ion temperature increases its range diminishes and also shifts to higher wavenumbers. The range of wavenumbers for which slow ion-acoustic mode is excited also diminishes with the increase in ion temperature. It is also observed (not shown here) that beyond $T_i/T_e = 2.3$, mode 6 interacts with mode 3 only, i.e., electron beam can drive only slow ion-acoustic mode unstable.

2.3.6 Effect of temperature of protons

The effect of temperature of protons on the dispersion of the waves has been plotted in Fig. 2.7. The ratio of temperature of protons to electrons, T_p/T_e has been increased from 0.4 to 0.8. For T_p/T_e=0.4, initially mode 6 merges with mode 3 with maximum growth rate of electron beam driven slow ion-acoustic mode, ω_i/ω_{p0}=0.11 and later on mode 6 merges with mode 2 and drives the fast ion-acoustic mode unstable with a maximum growth rate, ω_i/ω_{p0}= 0.26. With subsequent increase in T_p/T_e upto 0.553, both slow and fast ion-acoustic modes are unstable with growth rate of electron beam driven fast ion-acoustic mode becoming lesser than that of the slow ion-acoustic mode. Beyond $T_p/T_e >$0.553, there is no interaction between modes 6 and 2, but mode 6 interacts with mode 3 and drives the slow ion-acoustic waves unstable. In general, as the temperature of the protons increases there is slight increase in the maximum growth rate of electron beam driven slow ion-acoustic waves, whereas growth rate of fast ion-acoustic mode decreases substantially and eventually fast ion-acoustic mode vanishes.

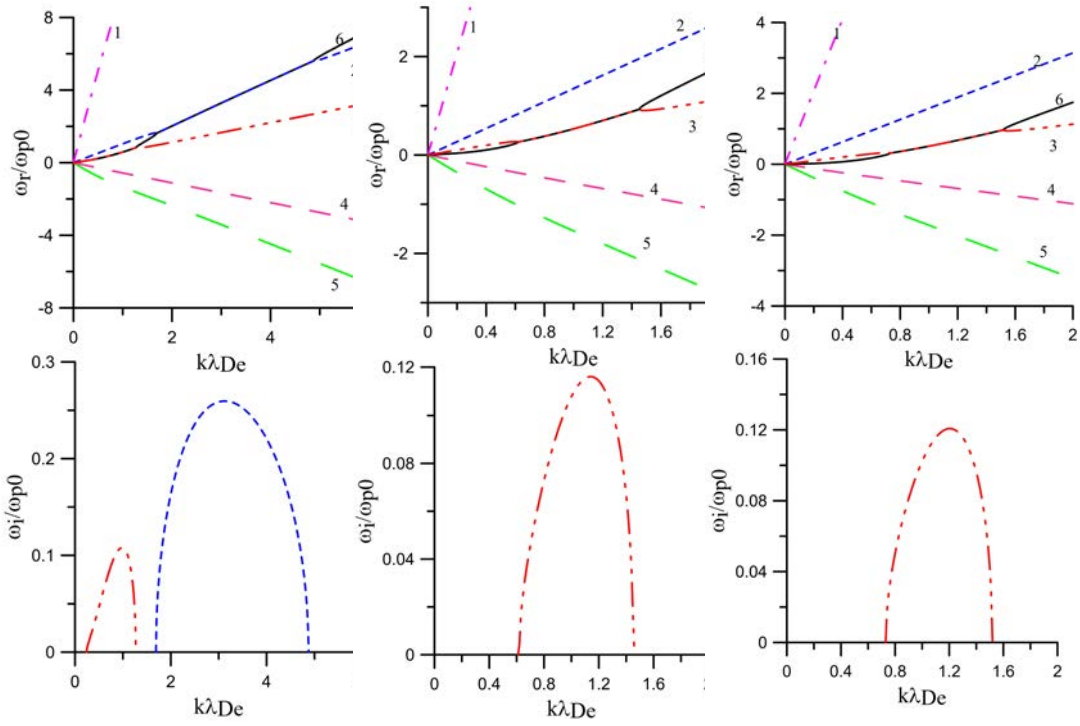

(a) $T_p/T_e = 0.4$ (b) $T_p/T_e = 0.6$ (c) $T_p/T_e = 0.8$

Figure 2.7: Effect of T_p/T_e variations on characteristics of the waves for $U_b/C_s = 5$. The other fixed plasma parameters are same as in Fig. 2.1

2.4 Conclusions

Recently, Tao et al. (2012) have reported observation of electrostatic waves in the lunar wake during the first flyby of the Acceleration, Reconnection, Turbulence and Electrodynamics of the Moon's Interaction with the Sun (ARTEMIS) and performed 1-D Vlasov simulation on a four-component lunar wake plasma concluded that the observed electrostatic waves, in the frequency range (0.1-0.4)f_{pe} (WB2/WB3), were most likely the electron beam mode in the wave bursts WB2 and WB3, whereas wave burst WB1 has a low-frequency component which can reach as low as $0.01 f_{pe}$. The frequency of the wave burst in WB1 is closer to ion plasma frequency, therefore, ion dynamics becomes important. We have carried out a linear analysis of parallel propagating electrostatic waves in a four component magnetized plasma comprising of fluid protons, fluid He^{++}, electron beam and suprathermal electrons following kappa distribution. This theoretical plasma model is relevant to the lunar wake plasma. It is found that as the electron beam velocity is increased, mode 6 gets affected the most and start to merge with mode 3 (slow ion-acoustic mode) and mode 2 (fast ion-acoustic mode) to form an unstable region with finite wave growth. It is observed that merging of modes 6 & 3 occurs at smaller value of wavenumbers as compared to the merging of modes 6 & 2. Actually, the merging denotes a complex double root, where phase velocities of the electron acoustic and slow (fast) ion-acoustic modes become the same. This interaction results in one mode growing (positive imaginary part, unstable) and the other as damped (equal negative imaginary part). Here, we have shown only the unstable electron beam driven slow and fast ion-acoustic modes. The increase in number density and temperature of electron beam has adverse effect on the electron beam driven slow ion-acoustic mode. On the other-hand, the growth rate of electron beam driven slow ion-acoustic mode increases with increase in number density of ions and temperatures of ions & protons. In the case of electron beam driven fast ion-acoustic mode, the growth rate increases with increase in electron beam density and decreases with increase in ion number density, temperatures of electron beam, ions and protons. We have carried out numerical computation for typical case of Fig. 2.2a where mode 6 merges first with slow mode and thereafter with fast mode. The frequency corresponding to the maximum growth rate of the electron beam driven slow ion-acoustic mode is $\omega_r = 0.03\omega_{pe}$ and for the electron beam driven fast ion-acoustic mode is $\omega_r = 0.2\omega_{pe}$. These frequency estimates agree very well with the observed low-frequency waves $\omega \approx 0.01\omega_{pe}$(WB1) and high

frequency waves $\omega \approx$0.1 -0.4ω_{pe}(WB2/WB3) in the Lunar wake by Tao et al. (2012)

Chapter 3

Electrostatic ion cyclotron and ion acoustic waves coupling in solar wind plasma

3.1 Introduction

The electrostatic ion cyclotron (EIC) waves are the low-frequency (frequency near ion gyrofrequency) waves which propagate nearly perpendicular to the ambient magnetic field and have a small wavenumber along the magnetic field. In a multi-ion plasma, EIC wave can have frequencies near the respective ion gyrofrequencies. These waves were first observed by D'Angelo and Motley (1962) & Motley and D'Angelo (1963) in laboratory plasmas and subsequently have been observed in high latitude ionosphere by Mosier and Gurnett (1969). EIC waves have been investigated in variety of laboratory plasma conditions (Barkan et al., 1995; Lang and Boehmer, 1983; Song et al., 1989; Kim et al., 2008). Based on the observation that disruption of electron flux occurred in concordance with EIC wave frequency, it was concluded that large amplitude EIC waves can trap electrons (Lang and Boehmer, 1983).

In the auroral region, EIC waves have been observed frequently by various satellites, e.g., S3-3(Kintner et al., 1978, 1979; Temerin et al., 1979), ISEE-1 (Cattell et al., 1991), Viking (André et al., 1987), Polar (Mozer et al., 1997) and FAST (Cattell et al., 1998). First observations of large amplitude EIC waves near the Earth's dayside magnetopause were pre-

sented by Tang et al. (2015) by using the data from Time History of Events and Macroscale Interactions during Substorms (THEMIS) satellites. These EIC waves were observed in a boundary layer in the magnetosphere adjacent to the magnetopause where reconnection occurred. Further, plasma density gradient was identified as a possible source of free energy for these EIC waves. EIC waves have also been observed at low altitudes in diffuse aurora (Bering, 1984) and topside ionosphere (Ungstrup et al., 1979). The possible free sources of energy to generate EIC waves are field aligned currents, ion beams, velocity shear and relative streaming between ions, electron drifts and density gradients (Kindel and Kennel, 1971; Hauck et al., 1978; Kintner et al., 1979; Cattell, 1981; Bergmann, 1984; Kaufmann et al., 1986; Lakhina, 1987; Bergmann et al., 1988; Dusenbery et al., 1988; Ganguli et al., 1988; Cattell et al., 1991; Tang et al., 2015). Kindel and Kennel (1971) showed that the field aligned current can drive the EIC waves in the auroral arc. Cattell et al. (1998) showed that electron drift, i.e., field aligned current can act as source of EIC waves from the analysis of data from FAST satellite. Satellite measurements also showed observation of EIC waves even though the field aligned currents were below the critical threshold for their generation. Later on, it was shown (Ganguli et al., 2002) that if perpendicular velocity shear in the ion flow along the magnetic field lines were taken into account, then EIC waves could grow even in the absence of field aligned current. The study of EIC waves is important from the point of view that they can provide perpendicular heating of the ions in the Earth's magnetosphere and are of importance in understanding and maintaining the boundary layers (Tang et al., 2015). Tsurutani and Thorne (1982) suggested that the He^{++} in the magnetosheath may be transported inward by resonating with the EIC waves as they are capable of inducing the required rapid inward diffusion of typical magnetosheath ions. Further, H^{+} ions may also be heated and diffused by EIC waves.

EIC waves in multi-component plasmas have also attracted great deal of interest from theoretical plasma physicists and have been studied in variety of plasmas. Using kinetic theory, Chow and Rosenberg (1996) showed that for the excitation of both the positive ion and negative ion modes, the critical electron drift velocity decreased with increase in the relative density of the negative ions. On the other hand, the frequencies and growth rates of both the unstable modes increase with the relative density of negative ions. EIC wave excitation in a plasma containing negatively charged dust particles has been investigated

both experimentally and theoretically by Barkan et al. (1995), and Chow and Rosenberg (1995). Sharma and Sharma (2010) studied the excitation of EIC waves by an ion beam in a two-component collisionless plasma which was extended by Sharma et al. (2015) to include collisions. Sharma et al. (2013) developed a theoretical model to study the excitation of higher harmonics of ion-cyclotron waves in a plasma cylinder with heavy negative ions. The propagation characteristics of electrostatic ion cyclotron waves have been studied in a homogeneous pair-ion plasma in a cylindrical system Kono and Batool (2014). Using the kinetic theory, the observed waves are identified to be ion cyclotron harmonic waves in the intermediate frequency range whereas in the low-frequency range a coupled wave of ion cyclotron mode and ion thermal mode is identified. Using a fluid theory, Merlino (2002) showed that electrostatic ion cyclotron waves propagating at large angles to the ambient magnetic field can be excited in a magnetized plasma by perpendicular shear in the magnetic field aligned plasma flow. In a uniform plasma, the resonant excitation of EIC modes by the electron drift relative to the ions has been studied by Drummond and Rosenbluth (1962). Lakhina (1987); Gavrishchaka et al. (1999, 2000); Ganguli et al. (2002) investigated the effect of parallel velocity shear on the excitation of current-driven ion acoustic and EIC modes. In some of the cases, it was found that the presence of shear can drastically reduce the necessary critical drift velocities for the excitation of these modes. It was also shown that even in the absence of relative electron drift, perpendicular shear in the parallel ion flow could lead to the excitation of multiple ion-cyclotron harmonics.

The low-frequency ion acoustic waves have been observed in the solar wind and various regions of the Earth's magnetosphere (Gurnett and Frank, 1978; Gurnett et al., 1979; Lin et al., 2001; Backrud et al., 2005a).These waves have been extensively studied theoretically (Hellberg and Mace, 2002; Sultana et al., 2010; Kadijani et al., 2010). The electrostatic ion cyclotron and ion acoustic waves (IAWs) have been studied independently rather than the focus on coupling of these waves in magnetized plasmas. The study on the coupling between the electrostatic ion cyclotron and ion acoustic waves was carried out in laboratory plasma by Ohnuma et al. (1973), where they observed the coupling between EIC and ion acoustic waves near the second harmonic frequency in a QP machine. The recent observations from THEMIS (Tang et al., 2015) also indicated the possible occurrence of a coupling between EIC and ion acoustic waves.

Solar wind is a stream of charged particles ejected from the Sun and consists of protons, electrons along with an admixture of alpha particles and much less abundant heavier ions. As it turns out, there are two different class of solar wind- namely fast solar wind and slow solar wind. The properties and composition of both these types of solar wind varies considerably. In fast solar wind ($V_{sw} \sim 650$ km/s), ions tend to be hotter than both protons and electrons, the protons are hotter than the electrons as well, the α particles move faster than the protons. Also, in fast solar wind, proton temperature are anisotropic with $\frac{T_{p\perp}}{T_{p\parallel}} > 1$. On the other hand, for the slow solar wind ($V_{sw} \sim 350$ km/s), electrons are much hotter than ions and the proton temperature anisotropy is opposite to that of fast solar wind (Bruno and Carbone, 2005; Marsch, 2006; Marsch et al., 1982).

In the solar wind, two different kinds of charged particles: a low energy thermal core and a suprathermal halo which are isotropically distributed at all pitch angles are found (Montgomery et al., 1968; Maksimovic et al., 2005). In the fast solar wind, the halo distribution can carry a highly energetic and antisunward moving magnetic field aligned strahl population (Pilipp et al., 1987; Marsch, 2006). Both electrons and ion species such as H^+, He^{++} and other heavier ions present in the solar wind can have suprathermal particle distributions (Collier et al., 1996; Chotoo et al., 2000). These suprathermal particle distributions can be modelled by kappa distribution. In order to fit the experimentally observed data from OGO-1 and OGO-3 satellite for the observation made in magnetosphere, it was Vasyliunas (1968) in 1968 who first postulated this kind of distribution function for the electrons. Thereafter, kappa distribution function has been observed and used in various regions of magnetosphere and beyond: like solar wind Maksimovic et al. (1997), magnetosheath Ogasawara et al. (2013), ring current Pisarenko et al. (2002), plasma sheet Kletzing et al. (2003), magnetosphere of other planets , e.g., Saturn Schippers et al. (2008) and also on planetary nebulae Nicholls et al. (2012). Theoretically, linear ion-acoustic and ion-cyclotron waves in magnetized electron-proton plasma have been studied with electrons having kappa distribution Hellberg and Mace (2002); Sultana et al. (2010); Kadijani et al. (2010). The current driven, electrostatic ion-cyclotron instability has been studied in electron-proton plasma with kappa-Maxwellian distributions for electrons and ions (Basu and Grossbard, 2011). In these articles, coupling between the electrostatic ion cyclotron and ion acoustic waves has not been discussed.

In this chapter, electrostatic low-frequency waves are studied in a three-component, magnetized plasma composed of electrons, protons and alpha particles. The electrons are assumed to have superthermal distribution characterised by kappa distribution. Protons and alpha particles are assumed to follow fluid dynamical equations. Our focus is on the coupling process of ion acoustic and ion cyclotron waves. The parameters from slow solar wind are used for the numerical computation of the dispersion relation characteristics.

The chapter is organized as follows: In Sect. 3.2, theoretical model to study the low-frequency electrostatic waves in magnetized plasma is presented and dispersion relation is analyzed for special cases of short and long wavelength limits for two-component (electron-proton) magnetized plasma and general dispersion relation is analyzed for parallel and perpendicular propagation. In the Sect. 3.3, numerical results are presented and conclusion and discussion are given in Sect. 3.4.

3.2 Theoretical model

The solar wind plasma is modeled by a homogeneous, collisionless, and magnetized three component plasma comprising of fluid protons (n_p, T_p), fluid heavier ions (n_i, T_i) and suprathermal electrons (n_e, T_e) having κ distribution. Here n_s and T_s, respectively are the number density and temperature of the species s, where $s = p,\ i,$ and e stands for protons, heavier ions and suprathermal electrons, respectively. The heavier ions are considered to be doubly charged helium (He^{++}, z_i=2) ions, i.e., alpha particles. The ambient magnetic field is considered to be in the z-direction, i.e., $\mathbf{B}_0 \parallel \mathbf{z}$. For simplicity, we take the propagation vector, $\mathbf{k}$ to be in $x-z$ plane making an angle α to the B_0 (see Fig. 3.1). For the linear, electrostatic waves propagating obliquely to the ambient magnetic field, the dynamics of both protons and the heavy ions are described by the multi-fluid equations of continuity, momentum, and the Poisson equation. Thus, the set of governing equations is given by:

$$\frac{\partial n_s}{\partial t} + \nabla.(n_s \mathbf{v}_s) = 0 \tag{3.1}$$

$$m_s n_s [\frac{\partial \mathbf{v}_s}{\partial t} + (\mathbf{v}_s.\nabla)\mathbf{v}_s] = q_s n_s(-\nabla\phi + \mathbf{v}_s \times \mathbf{B}_0) - \nabla P_s \tag{3.2}$$

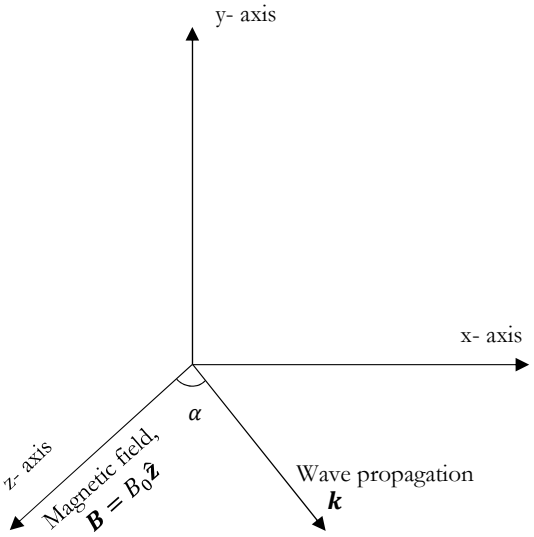

Figure 3.1: Geometry of the model

$$\nabla^2\phi = -\frac{e}{\varepsilon_0}(n_p + n_i z_i - n_e) \tag{3.3}$$

where m_s, $\mathbf{v}_s$, P_s, q_s represents respectively, mass, velocity, pressure and charge of the the species $s = p$ and i. The pressure term in our case amounts to $\nabla P_s = \gamma k_B T_s \nabla n_s$, where γ is the ratio of specific heats and k_B represents the Boltzmann constant.

The suprathermal electrons are assumed to have κ distribution which is given by (Summers and Thorne, 1991):

$$f_\kappa(v) = \frac{n_{e0}}{\pi^{\frac{3}{2}}}\frac{1}{\theta^3}\frac{\Gamma(\kappa+1)}{\kappa^{\frac{3}{2}}\Gamma(\kappa-\frac{1}{2})}(1+\frac{v^2}{\kappa\theta^2})^{-(\kappa+1)} \tag{3.4}$$

where κ is the superthermality index; $\Gamma(\kappa)$ is the gamma function with the argument κ; θ is the effective thermal speed of electron given by the expression $\theta = [\frac{2\kappa-3}{\kappa}]^{\frac{1}{2}}(\frac{k_B T_e}{m_e})^{\frac{1}{2}}$, and n_{e0} is the equilibrium density of energetic electrons. From this definition it's clear that in order to have meaningful value for the thermal speed, we need to have $\kappa > \frac{3}{2}$.

Zeroth moment of this distribution in the presence of wave potential ϕ gives the number density of electron, which is:

$$n_e = n_{e0}\left[1 - \frac{e\phi}{k_B T_e(\kappa-\frac{3}{2})}\right]^{\frac{1}{2}-\kappa} \tag{3.5}$$

Linearization and simplification of Eqs. (3.1) to (3.3) and (3.5), yields the following general

dispersion relation for the low frequency, coupled electrostatic cyclotron (proton and helium) and acoustic (fast and slow) modes:

$$1+\frac{\omega_{pe}^2}{k^2v_{te}^2}\frac{2\kappa-1}{2\kappa-3}-\frac{\omega_{pp}^2(\omega^2-\Omega_p^2\cos^2\alpha)}{\omega^4-\omega^2\Omega_p^2-\gamma k^2v_{tp}^2(\omega^2-\Omega_p^2\cos^2\alpha)} -\frac{z_i^2\omega_{pi}^2(\omega^2-z_i^2\Omega_i^2\cos^2\alpha)}{\omega^4-\omega^2z_i^2\Omega_i^2-\gamma k^2v_{ti}^2(\omega^2-z_i^2\Omega_i^2\cos^2\alpha)}=0 \tag{3.6}$$

Here $\omega_{ps}=\sqrt{\frac{n_{s0}e^2}{\varepsilon_0 m_s}}$ is the plasma frequency, $\Omega_s=\frac{eB_0}{m_s}$ is the cyclotron frequency and $v_{\rm ts}=\sqrt{\frac{k_BT_s}{m_s}}$ is the thermal speed of the s$^{\rm th}$ species, respectively. In the dispersion relation Eq. (3.6), the second term is due to the electrons having kappa distribution, third term represents the protons and the last term is due to the heavier ions.

3.2.1 Two component plasma

It is interesting to note that in the absence of the ions, the dispersion relation given below describes the coupling of ion-acoustic and ion cyclotron modes in pure electron-proton plasma,

$$1+\frac{\omega_{pe}^2}{k^2v_{the}^2}\frac{2\kappa-1}{2\kappa-3}=\frac{\omega_{pp}^2(\omega^2-\Omega_p^2\cos^2\alpha)}{\omega^4-\omega^2\Omega_p^2-\gamma k^2v_{thp}^2(\omega^2-\Omega_p^2\cos^2\alpha)} \tag{3.7}$$

Eq. (3.7) is a quadratic in ω^2 and the solution of this can be given as:

$$\omega_\pm^2=\frac{1}{2}[B\pm\sqrt{B^2-4C}] \tag{3.8a}$$

$$B=\Omega_p^2+\gamma k^2v_{tp}^2+\frac{\omega_{pp}^2k^2\lambda_{de}^2(2\kappa-3)}{k^2\lambda_{de}^2(2\kappa-3)+(2\kappa-1)} \tag{3.8b}$$

$$C=\Omega_p^2cos^2\alpha\left(\gamma k^2v_{tp}^2+\frac{\omega_{pp}^2k^2\lambda_{de}^2(2\kappa-3)}{k^2\lambda_{de}^2(2\kappa-3)+(2\kappa-1)}\right) \tag{3.8c}$$

Here, $\lambda_{de}=v_{the}/\omega_{pe}$ is the electron Debye length. The Eq. (3.8) is similar to the equation that has been obtained by Hellberg and Mace (2002); Sultana et al. (2010); Kadijani et al. (2010) for a two component plasma model of cold protons and superthermal electrons described by kappa distribution. The Eq. (3.8) describes the coupling of ion-acoustic and ion-cyclotron waves in two component plasma. Further, we would like to discuss propagation characteristics of the low-frequency waves by analysing the dispersion relation for special

cases, e.g., parallel and perpendicular wave propagation, and large and short wavelength limits.

Parallel propagation:

For parallel propagation ($\alpha = 0^0$, i.e., cos $\alpha = 1$), Eq. (3.8) reduces to

$$\omega_+^2 = \Omega_p^2 \tag{3.9}$$

$$\omega_-^2 = \gamma k^2 v_{thp}^2 + \frac{\omega_{pp}^2 k^2 \lambda_{de}^2 (2\kappa - 3)}{k^2 \lambda_{de}^2 (2\kappa - 3) + (2\kappa - 1)}, \tag{3.10}$$

where the decoupling of ion cyclotron and ion-acoustic mode occurs. The Eq. (3.9) refers to non propagating ion-cyclotron mode which is the fluctuation at the proton cyclotron frequency and Eq. Eq. (3.10) refers to ion-acoustic mode.

Perpendicular propagation:

For perpendicular propagation ($\alpha = 90^0$, i.e., cos $\alpha = 0$), the only surviving root is

$$\omega_+^2 = \Omega_p^2 + \gamma k^2 v_{thp}^2 + \frac{\omega_{pp}^2 k^2 \lambda_{de}^2 (2\kappa - 3)}{k^2 \lambda_{de}^2 (2\kappa - 3) + (2\kappa - 1)} \tag{3.11}$$

This equation corresponds to the ion cyclotron wave with the thermal corrections. The acoustic mode completely disappears. Next we analyse the dispersion relation given by Eq. (3.7) in the large and short wavelength limits.

Large wavelength limit:

In the large wavelength limit, i.e., $\Omega_p^2 >> \gamma k^2 v_{thp}^2 + \frac{\omega_{pp}^2 k^2 \lambda_{de}^2 (2\kappa - 3)}{k^2 \lambda_{de}^2 (2\kappa - 3) + (2\kappa - 1)}$, the two roots of the Eq. (3.7) can be written as

$$\omega_+ = \Omega_p + \frac{sin^2 \alpha}{2\Omega_p} [\gamma k^2 v_{thp}^2 + \frac{\omega_{pp}^2 k^2 \lambda_{de}^2 (2\kappa - 3)}{k^2 \lambda_{de}^2 (2\kappa - 3) + (2\kappa - 1)}] \tag{3.12}$$

$$\omega_- = cos\alpha \sqrt{\gamma k^2 v_{thp}^2 + \frac{\omega_{pp}^2 k^2 \lambda_{de}^2 (2\kappa - 3)}{k^2 \lambda_{de}^2 (2\kappa - 3) + (2\kappa - 1)}} \tag{3.13}$$

The Eq. (3.12) refers to proton cyclotron mode and Eq. (3.13) describes the obliquely propagating ion acoustic mode in a magnetized electron-ion plasma. These results are identical to Hellberg and Mace (2002); Sultana et al. (2010); Kadijani et al. (2010).

Short wavelength limit:

In the short wavelength limit, i.e., $\Omega_p^2 << \gamma k^2 v_{thp}^2 + \frac{\omega_{pp}^2 k^2 \lambda_{de}^2 (2\kappa-3)}{k^2\lambda_{de}^2(2\kappa-3)+(2\kappa-1)}$, the two roots of the Eq. (3.7) can be written as

$$\omega_+ = \sqrt{\gamma k^2 v_{thp}^2 + \frac{\omega_{pp}^2 k^2 \lambda_{de}^2 (2\kappa-3)}{k^2\lambda_{de}^2(2\kappa-3)+(2\kappa-1)}} \tag{3.14}$$

$$\omega_- = \Omega_p cos\alpha \tag{3.15}$$

In the short wavelength limit, the mode given by Eq. (3.14) behaves like ion-acoustic mode in unmagnetized plasma and the other mode described by Eq. (3.15) is the oblique ion cyclotron fluctuation.

We now numerically investigate Eq. (3.7). For this purpose, we have normalised the frequencies by cyclotron frequency of proton, Ω_p, wavenumber by Larmor radius of proton, ρ_p given by the expression $\rho_p = \frac{v_{thp}}{\Omega_p}$. The parameters chosen are $\frac{T_e}{T_p} = 5$, $\gamma = 3$ and $\kappa = 2$. Ratio of plasma frequency to cyclotron frequency of proton is taken to be 5000 (Mangeney et al., 1999; Borovsky and Gary, 2014). The results of the finding are presented in Fig. 3.2. As mentioned in the text earlier, for parallel wave propagation, i.e. $\alpha = 0^0$, the two different modes viz. ion cyclotron (solid curve parallel to x- axis, branch 1) and ion acoustic (solid straight line passing through origin, branch 2) modes decouple. These two modes are represented by Eq. (3.9) and Eq. (3.10), respectively. The effect of obliqueness is also examined on the dispersion characteristics of ion-cyclotron and ion-acoustic waves in two component plasma. First, we have analysed Eq. (3.7) for the case of $\alpha = 15^0$, for which the dispersion relation curve gets modified as shown by short dashed curves in Fig. 3.2. It is seen that the coupling between the ion cyclotron and ion acoustic modes occur as the wave propagates at an angle to the ambient magnetic field. The short-dashed curve starting at ω/Ω_p =1.0 is the ion cyclotron mode which is modified by acoustic mode (given by Eq. (3.12)). The obliquely propagating ion-acoustic mode (given by Eq. (3.13)) is represented by short-dashed curve starting at from ω/Ω_p =0.0. Further increase in the angle of propagation (as shown by long dashed curves in the Fig. 3.2 with $\alpha = 30^0$), weakens the coupling as the gap between the two modes widens and continues to weaken for $\alpha = 45^0$ and $\alpha = 60^0$ (not shown here). The

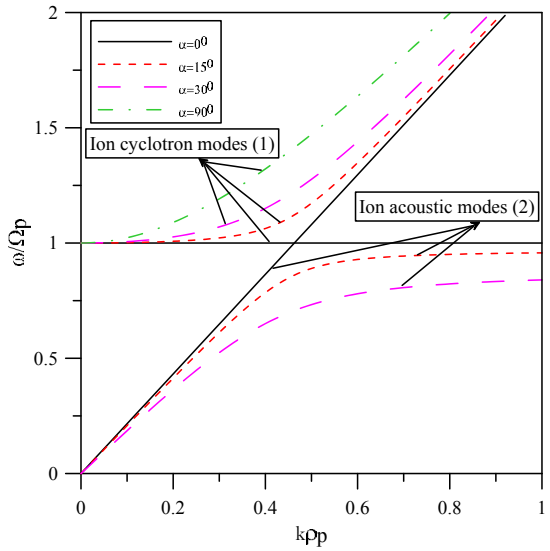

Figure 3.2: Dispersion characteristics of the electrostatic ion cyclotron and ion acoustic modes in electron-ion plasma for various angles of propagation. Other parameters are $\frac{T_e}{T_p} = 5$, $\gamma = 3$ and $\kappa = 2$

coupling completely vanishes at $\alpha = 90^0$ (dash dot curve) as only ion-cyclotron wave remain and ion-acoustic mode disappear which is in agreement with the Eq. (3.11).

3.2.2 Three component plasma

The analysis carried out above help us in identifying the various modes of plasma given by the general dispersion relation Eq. (3.6) in a three-component plasma which can not be solved analytically. However, we would like to discuss further, the special cases where analytical expressions are tractable and various modes can be identified.

Parallel wave propagation:

For the case of parallel propagation ($\alpha = 0^0$, i.e., $\cos\alpha = 1$) of the various modes, the general dispersion relation Eq. (3.6) reduces to the following:

$$(\omega^2 - \Omega_p^2)(\omega^2 - z_i^2\Omega_i^2)\left[1 - \frac{\omega_{pp}^2}{(1 + \frac{\omega_{pe}^2}{k^2 v_{the}^2}\frac{2\kappa-1}{2\kappa-3})(\omega^2 - \gamma k^2 v_{thp}^2)} - \frac{z_i^2\omega_{pi}^2}{(1 + \frac{\omega_{pe}^2}{k^2 v_{the}^2}\frac{2\kappa-1}{2\kappa-3})(\omega^2 - \gamma k^2 v_{thi}^2)}\right] = 0 \tag{3.16}$$

It is obvious from the the above equation (Eq. (3.16)) that the proton- ($\omega = \pm\Omega_p$) and helium- ($\omega = \pm\Omega_i$)cyclotron modes (as shown by the first and second terms respectively) decouple from the acoustic modes given by third term in the square bracket. It has to be pointed out that for parallel propagation of the electrostatic waves, the two cyclotron modes are non-propagating, i.e, they represent fluctuations at the proton and Helium cyclotron frequency, respectively. Therefore, third term inside the square brackets of Eq. (3.16) is further analyzed which is quadratic equation in ω^2 and can be solved analytically. The two roots of the equations are given by the expressions:

$$\omega_{\pm}^2 = \tfrac{1}{2}[B_1 \pm \sqrt{B_1^2 - 4C_1}] \tag{3.17a}$$

with

$$B_1 = \gamma k^2 v_{tp}^2 + \gamma k^2 v_{ti}^2 + \frac{(\omega_{pp}^2 + z_i^2\omega_{pi}^2)k^2\lambda_{de}^2(2\kappa-3)}{k^2\lambda_{de}^2(2\kappa-3)+(2\kappa-1)} \tag{3.17b}$$

and

$$C_1 = \gamma^2 k^4 v_{tp}^2 v_{ti}^2 + \frac{\gamma(v_{ti}^2\omega_{pp}^2 + v_{tp}^2 z_i^2\omega_{pi}^2)k^4\lambda_{de}^2(2\kappa-3)}{k^2\lambda_{de}^2(2\kappa-3)+(2\kappa-1)} \tag{3.17c}$$

The $\omega_{\pm}$ refers to the fast and slow acoustic modes, respectively. There is no effect of magnetic field on the fast and slow acoustic modes for the case of parallel propagation. Next, we consider the case of perpendicular propagation of the waves.

Perpendicular wave propagation:

For wave propagation perpendicular to the ambient magnetic field, i.e., for $\alpha = 90^0$ i.e. cos $\alpha = 0$, the general dispersion relation Eq. (3.6) reduces to the following:

$$1 - \frac{\omega_{pp}^2}{(1 + \frac{\omega_{pe}^2}{k^2 v_{the}^2}\frac{2\kappa-1}{2\kappa-3})(\omega^2 - \Omega_p^2 - \gamma k^2 v_{thp}^2)} - \frac{z_i^2\omega_{pi}^2}{(1 + \frac{\omega_{pe}^2}{k^2 v_{the}^2}\frac{2\kappa-1}{2\kappa-3})(\omega^2 - z_i^2\Omega_i^2 - \gamma k^2 v_{thi}^2)} = 0 \tag{3.18}$$

The above equation is quadratic in ω^2 which has four roots. The algebraic manipulation leads to the following roots of the Eq. (3.18).

$$\omega_{\pm}^2 = \tfrac{1}{2}[B_2 \pm \sqrt{B_2^2 - 4C_2}] \tag{3.19a}$$

where

$$B_2 = \Omega_p^2 + z_i^2\Omega_i^2 + \gamma k^2 v_{thp}^2 + \gamma k^2 v_{thi}^2 + \frac{(\omega_{pp}^2 + z_i^2\omega_{pi}^2)k^2\lambda_{de}^2(2\kappa-3)}{k^2\lambda_{de}^2(2\kappa-3)+(2\kappa-1)} \tag{3.19b}$$

and

$$C_2 = (\Omega_p^2 + \gamma k^2 v_{thp}^2)(z_i^2\Omega_i^2 + \gamma k^2 v_{thi}^2) + \frac{(z_i^2\Omega_i^2 + \gamma k^2 v_{thi}^2)\omega_{pp}^2 k^2\lambda_{de}^2(2\kappa-3)}{k^2\lambda_{de}^2(2\kappa-3)+(2\kappa-1)} + \frac{(\Omega_p^2 + \gamma k^2 v_{thp}^2)z_i^2\omega_{pi}^2 k^2\lambda_{de}^2(2\kappa-3)}{k^2\lambda_{de}^2(2\kappa-3)+(2\kappa-1)} \tag{3.19c}$$

The $\omega_{\pm}$ in Eq. (3.19) gives the relation for cyclotron modes for protons and Helium ions, respectively which are modified by the acoustic contribution. In the next section, the general dispersion relation Eq. (3.6) is analyzed numerically.

3.3 Numerical results

In this section, the numerical results are presented on the coupling of various modes and effect of nonthermality, density and temperature of ions on the dispersive properties of the modes. For numerical analysis, we have normalised the general dispersion relation by following parameters: frequencies by cyclotron frequency of proton, Ω_p, wavenumber by Larmor radius of proton, ρ_p given by the expression $\rho_p = \frac{v_{thp}}{\Omega_p}$. For the fast solar wind, $\frac{T_p}{T_e} \geq 1$, $\frac{T_i}{T_p} \geq 1$ and for the slow solar wind: $\frac{T_p}{T_e} \leq 1$, $\frac{T_i}{T_p} \geq 1$ (Bruno and Carbone, 2005). It was shown by Maksimovic et al. (1997) that κ can take the value from 2 to 6. The recent survey for the value of kappa index undertaken by Livadiotis (2015) for various space plasmas has shown that kappa value for solar wind can vary from $\sim$1.5 to 7. From, the satellite observations it can be deduced that the ratio of plasma to cyclotron frequencies of proton is nearly 5000 (Mangeney et al., 1999; Borovsky and Gary, 2014). For numerical computations of the dispersion relation (Eq. (3.6)), we have taken slow solar wind parameters at 1AU which are specified for each figure. For parallel propagation of waves in electron-ion magnetized plasmas, it is relatively easier to analyze a dispersion relation. However, multi-components and oblique propagation of waves in magnetized plasmas make the dispersion relation complex

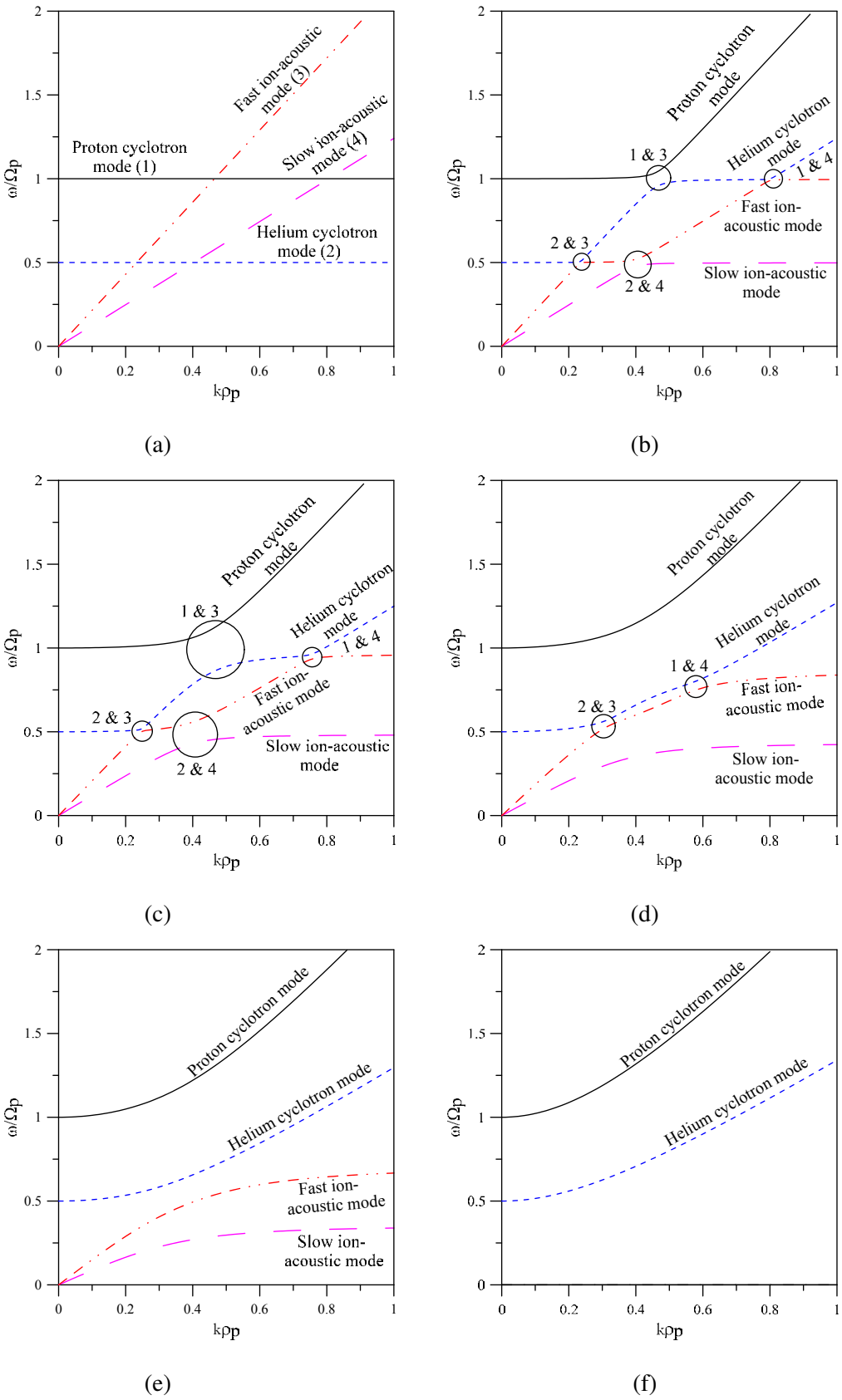

Figure 3.3: Dispersion characteristics of the electrostatic ion cyclotron and ion acoustic modes at different angle of propagation, α= 0^0(a), 5^0(b), 15^0(c), 30^0(d), 45^0(e), 90^0(f) for the slow solar wind parameters $\frac{n_i}{n_e}$=0.05, $\frac{T_e}{T_p} = 5$, $\frac{T_i}{T_p} = 2$, $\gamma = 3$ and $\kappa = 2$

and difficult to analyze analytically. Therefore, it is necessary to do the numerical analysis of the dispersion relation and bring out the characteristics of the various wave modes. We undertake a parametric investigation of the dispersion relation Eq. (3.6) which is analyzed for effect of obliqueness, ion concentration, superthermality index and temperature of ions on the characteristics of the various modes. To start with, the dispersion relation Eq. (3.6) is analysed for parallel propagation, i.e., $\alpha = 0^0$ and results are presented in Fig. 3.3a. The typical chosen parameters corresponding to the slow solar wind are: n_i/n_e=0.05, T_e/T_p=5, T_i/T_p=2, γ=3, and κ=2. It is clearly seen in the Fig. 3.3a that the four modes namely, proton-cyclotron (solid curve, branch 1)and helium-cyclotron (short dash curve, branch 2) modes, fast ion-acoustic (dash-dash dot dot curve, branch 3) and slow ion-acoustic (long dash curve, branch 4) modes decouple at parallel propagation. We have purposely named various wave modes as branches 1-4 for the case of parallel propagation as they come in handy for oblique propagation cases where coupling of the modes occur. It has to be pointed out here that only physically acceptable solution for parallel propagation are fast and slow acoustic modes. Since we have normalised the frequency with respect to proton cyclotron frequency, parallel lines at ω/Ω_p=1 and at ω/Ω_p=0.5 (m_{He}/m_p=4) represent proton (solid line) and helium cyclotron (dashed line) nonpropagating modes, respectively. The above results are in sync with the Eq. (3.16) as first two terms on the left hand side describe the proton and helium cyclotron modes, respectively. The fast and slow ion-acoustic modes are the solutions ($\omega_\pm$) of the third term and are given by Eq. (3.17), respectively.

In Fig. 3.3b, the effect of obliqueness is examined on the dispersion relation Eq. (3.6). It must be emphasized here that we start with small angle of propagation, $\alpha = 5^0$ so that intricate coupling process between the acoustic (fast and slow) and cyclotron (proton and helium) modes can be delineated properly. Here the plasma parameters are the same as for Fig. 3.3a. It is obvious from the figure that as the wave propagates oblique to the ambient magnetic field, the coupling between cyclotron and acoustic modes occur. Further, the proton cyclotron (branch 1) mode couples with two modes, i.e., fast ion-acoustic ((branch 3) mode at $k\rho_p \approx 0.45$ and slow ion-acoustic (branch 4) mode at $k\rho_p \approx 0.8$. These two couplings are marked in this and subsequent figures by circles with labels 1 & 3 and 1 & 4, respectively. On the other hand, helium cyclotron mode (branch 2) couples with fast ion-acoustic (branch 3) mode at $k\rho_p \approx 0.24$ and with slow ion-acoustic (branch 4) mode at $k\rho_p \approx 0.41$. The

couplings are marked in this and subsequent figures by circles with a labels 2 & 3 and 2 & 4, respectively. Further, proton cyclotron mode couples with the two acoustic modes at larger value of $k\rho_p$ as compared to helium cyclotron mode.

In Fig. 3.3c, we have shown the results for propagation angle, $\alpha = 15^0$ for the same values of parameters as in Fig. 3.3a. It is observed that coupling between proton-cyclotron (branch 1) and fast ion acoustic (branch 3) modes weakens as gap between the two widens (labelled 1& 3). Similarly, coupling weakens between helium (branch 2) and slow-ion-acoustic (branch 4) modes (labelled 2& 4), however, gap is smaller as compared to branches 1 and 3. On the other hand, stronger coupling exists between branches 1 & 4 and 2 & 3. The coupling between branches 1 & 3 and 2 & 4 further weakens at an angle of propagation, $\alpha = 30^0$ (Fig. 3.3d) but coupling is still strong between branches 2 & 3 and 1 & 4. Increase in angle of propagation, $\alpha = 45^0$ further weakens the coupling as can be gauged by the widening gaps (Fig. 3.3e). There is no coupling between the various branches at an angle of propagation, $\alpha = 60^0$ (not shown here). Finally, at exactly perpendicular propagation,($\alpha = 90^0$) both the acoustic (slow and fast) modes disappear and only proton and helium cyclotron modes exist (Fig. 3.3f) which can be corroborated with the Eq. (3.19). Here $\omega_{\pm}$ refers to proton and helium cyclotron modes.

The effect of number density of helium ions is studied in Fig. 3.4 for the parameters of Fig. 3.3a and angle of propagation, $\alpha = 30^0$. The normalized helium ion density is varied from $n_i/n_e = 0.05 - 0.3$. It is observed that frequency and phase speed of proton cyclotron, fast and slow ion acoustic modes do not change significantly with the increase in the concentration of helium ions. However, for fixed value of the wavenumber, the frequency and phase speed of the proton cyclotron and fast ion acoustic modes decreases slightly whereas there is increase in frequency and phase speed of the slow ion acoustic mode with the increase in helium ion concentration. For helium cyclotron mode, there is insignificant effect on the frequency for $k\rho_p \leq 0.3$ whereas frequency increases beyond $k\rho_p \geq 0.3$. The coupling of various modes remains similar to the one described in Fig. 3.3d.

In Fig. 3.5, the effect of superthermality index, κ on the various modes is studied. The fixed parameters in this case are $\frac{n_i}{n_e} = 0.05$, $\alpha = 15^0$, $\gamma = 3$, $\frac{T_e}{T_p} = 5$ and $\frac{T_i}{T_p} = 2$. The frequency of the proton cyclotron mode is not affected initially (for $k\rho_p \leq 0.2$) with an increase in the superthermality (decrease in κ values), however, for $k\rho_p \geq 0.2$, it decreases

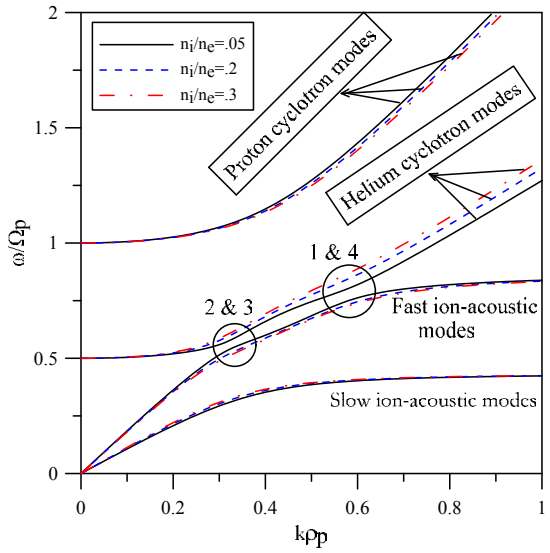

Figure 3.4: Dispersion relation curves for variations in number density of Helium ions to protons for propagation angle $\alpha = 30^0$. The other parameters are the same as in the Fig. 3.3

for fixed values of $k\rho_p$. Similarly, for helium cyclotron mode, there is no effect of variation of κ on the frequency of the mode for the wavenumber ranges $k\rho_p \leq 0.2$ and $k\rho_p \geq 0.75$. On the other hand, frequency of the helium cyclotron mode increases with increase in κ values for the wavenumber ranges $0.2 \leq k\rho_p \leq 0.75$. Further, frequency of the fast-ion acoustic mode increases with increase in κ values for $k\rho_p \leq 0.25$ and it remains unchanged beyond $k\rho_p \geq 0.25$. The variation of κ does not show any effect on the frequency of the slow-ion acoustic mode. The highest frequency for both proton and helium cyclotron modes and fast ion-acoustic modes occurs at larger κ values, i.e., for Maxwellian distribution of electrons. These results are consistent with Sultana et al. (2010) though they have studied ion-acoustic and ion cyclotron waves in two-component, electron-ion magnetized plasma with electrons having κ distribution.

In Fig. 3.6, the general dispersion relation Eq. (3.6) is analyzed for the effect of variation of temperature of ions. The fixed parameters are $\frac{n_i}{n_e} = 0.05$, $\alpha = 15^0$, $\gamma = 3$, $\kappa = 2$ and $\frac{T_e}{T_p} = 5$. The ratio of the ion to proton temperature, T_i/T_p is varied from 2-5 as shown by the legends in the figure. The frequency of the proton cyclotron mode is not affected significantly by the variation of helium ion temperature. There is appreciable increase in the frequency of the helium cyclotron mode with increase in helium ion temperature for $k\rho_p \geq 0.45$ whereas it is slightly affected for $k\rho_p \leq 0.45$. For fast-ion acoustic mode, the frequency increases with

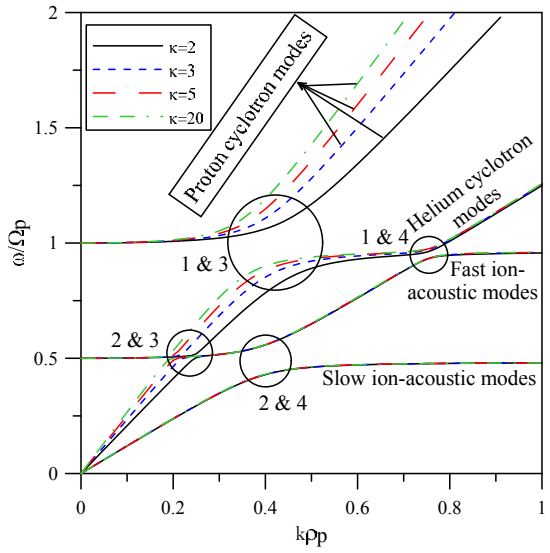

Figure 3.5: Dispersion relation curves for varying value of superthermality index, κ, for propagation angle $\alpha = 15^0$. The other parameters are the same as in the Fig. 3.3

increase in helium ion temperature for $0.25 \leq k\rho_p \leq 0.75$, otherwise it remain unchanged. Similarly, for there is increase in frequency of the slow-ion acoustic mode for $k\rho_p \leq 0.5$, whereas it is not affected for other values of wavenumbers.

3.4 Conclusions

Electrostatic ion cyclotron and ion acoustic waves which are observed in solar wind and various regions of the Earth's magnetosphere have been studied in three-component plasma. The plasma model consists of electrons with kappa distributions, protons and alpha particles. For parallel propagation of the waves slow and fast ion-acoustic modes and proton and helium-cyclotron modes are decoupled. The proton and helium cyclotron modes are non-propagating modes whereas other two modes, i.e., slow and fast ion-acoustic modes are propagating modes. It is interesting to note that for oblique propagation of the electrostatic waves, the coupling between acoustic and cyclotron modes occurs. For small angle of propagation, there is stronger coupling between proton cyclotron and fast ion acoustic modes, proton cyclotron and slow ion acoustic modes as well as between helium cyclotron and fast ion acoustic modes and helium cyclotron and slow ion acoustic modes. However, coupling between proton cyclotron and slow ion acoustic modes and helium cyclotron and fast ion

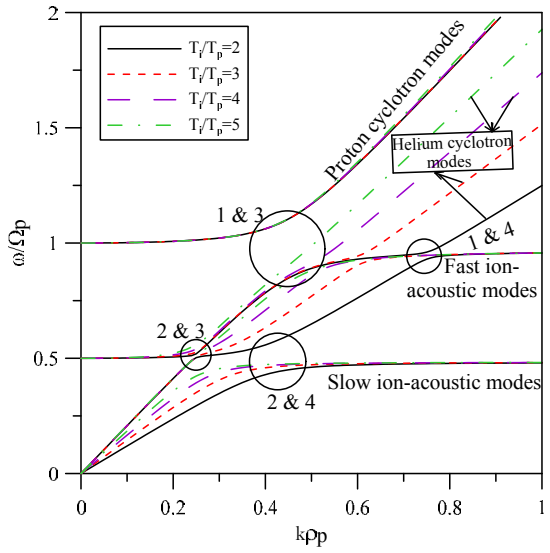

Figure 3.6: Effect of $\frac{T_i}{T_p}$ on the dispersion curves for propagation angle $\alpha = 15^0$. The other parameters are the same as in the Fig. 3.3

acoustic modes is much stronger than between proton cyclotron and fast ion acoustic modes and helium cyclotron and slow ion acoustic modes. Further, for more oblique cases the coupling between the various modes weakens as the separation between them increases and for the case of perpendicular propagation of the waves, acoustic (both fast and slow) modes disappear and only proton and helium cyclotron modes remain.

The effect of helium ion concentration is not significant on the frequency of the other modes except for helium cyclotron mode, where its frequency increases beyond $k\rho_p \geq 0.3$ with the increase in helium ion concentration. The frequencies of all modes decrease for certain wave numbers regimes with an increase in the superthermality (decrease in κ values), except for slow ion acoustic mode for which there is insignificant effect of superthermality. The effect of helium ion temperature is significant on the frequency of helium cyclotron mode and it increases with increase in temperature. It must be pointed out here that the coupling between the various branches occur for $k\rho_p < 1$.

We have focussed our attention on the coupling of EIC and ion-acoustic waves which is important in the case of multi-component plasmas in space and laboratory plasmas. Earlier theoretical studies did not consider the coupling of these modes either in two component or multi-component plasmas. Though we have taken solar wind parameters in this study, however, our results can be generalised and applied to recent observations of coupling of

electrostatic ion cyclotron and ion acoustic wave by THEMIS (Tang et al., 2015) near the magnetopause. The EIC waves are important from the point of view that they can resonantly heat and efficiently transfer energy to the ions in perpendicular direction.

Chapter 4

Excitation of electrostatic ion cyclotron waves and ion acoustic waves by electron beam in solar wind/Lunar wake plasma

4.1 Introduction

The wake region of moon, commonly called as lunar wake, is an interesting natural area to view various type of plasma waves and related phenomenon. This wake region is formed by the interaction of moon with solar wind impinging on its surface with solar wind plasma refilling these regions (Ogilvie et al., 1996; Futaana et al., 2010; Dhanya et al., 2018). The study of lunar wake picked up gradual pace with launching of satellites. Early studies of about moon using satellites was conducted by Dolginov et al. (1961, 1963) using Luna 1 and Luna 2 satellites launched by USSR. They had concluded that either the magnetic field of the moon is too weak to observe, else it is not present at all. IMP-1 (Explorer 18) has added another dimension to the knowledge of lunar wake. Ness (1965) has shown that the approximate length of this wake region can go up-to 150 lunar radii. Michel (1968) corrected this idea by using the data from IMP-2 (Explorer 35), who has claimed that what Ness (1965) has interpreted was a disturbance already in the solar wind.

Wind satellite significantly provided great insights into understanding of lunar wake. Bosqued et al. (1996) have reported that a structured lunar plasma umbra (or plasma cavity)

can be seen in the downstream of the moon at ~ 6 R_m, where $R_m = 1720$ km, is the lunar radius. Electron and ion densities decrease to a value of 0.5 cm^{-3} near to the center of the optical umbra. Bale et al. (1997) have reported the presence of ion acoustic waves, Langmuir waves and beam modes in the wake regions of the moon using the data from Wind satellite. Farrell et al. (1997) have demonstrated that ion beam drives the electrostatic waves unstable and thereby generating broadband electrostatic noise which was reported by Kellogg et al. (1996) and are associated with density discontinuity and velocity shear at the boundary of the wake. Hashimoto et al. (2010) have shown that intense waves in frequency range 10-20 kHz, which are Langmuir waves enhanced at local plasma frequency.

Refilling of lunar wake plasma is a typical example of expansion of plasma into vacuum (Halekas et al., 2014) and has been subject of study by many researchers (Farrell et al., 1998; Birch and Chapman, 2002; Kimura and Nakagawa, 2008; Dhanya et al., 2018). Lunar wake is refilled by the charged particles along the magnetic field lines. Due to the higher thermal speed of the electrons a charge-separation electric field is set up that slows down the electron expansion and accelerates the ions into the wake thereby maintaining the quasi-neutrality. Theoretical studies and simulations have shown that this leads to a rarefaction wave propagating back into the plasma. The particle expands with a velocity related to the ion sound speed, and an exponentially decreasing density into the vacuum (Halekas et al., 2011). These conclusions are also in line with the observations made by Ogilvie et al. (1996). The simulation studies by Xie et al. (2013) showed that as the plasma moves into the wake region, some rarefaction waves propagate away from the limb via the fast magnetosonic mode. Recently, Dhanya et al. (2018) have shown that near wake filling is done primarily by solar wind protons.

With the help of data from spacecraft P1 of the new ARTEMIS (Acceleration, Reconnection, Turbulence, and Electrodynamics of the Moon's Interaction with the Sun) mission, Wiehle et al. (2011) showed the presence of basic MHD modes, i.e., fast, Alfvén and slow modes in the wake region. P1 satellite from ARTEMIS also measured the electrostatic oscillations closely correlated with counter streaming electron beams in the wake (Halekas et al., 2011). Halekas et al. (2011) showed that wake potential driven by the refilling process filters and accelerates both ions and electrons thereby generating numerous instabilities. In a comprehensive study, Tao et al. (2012) reported the existence of electrostatic waves. Further-

more, by 1-D Vlasov simulation, they have speculated that observed electrostatic waves are the electron beam mode branch, which falls in the frequency range (0.1-0.4)f_{pe}, where f_{pe} is the electron plasma frequency. Through a nonlinear analysis of four component plasma modeled by hot protons, hot heavier ions (α-particles, He^{++}), electron beam, and suprathermal electrons following kappa distribution, Rubia et al. (2017) have explained the low frequency part ($< 0.1f_{pe}$) of the observed spectrum. Sreeraj et al. (2018) have undertaken linear analysis of the model proposed by Rubia et al. (2017) and have shown that fast and slow ion acoustic modes are driven unstable when a finite electron beam is introduced into the system. These are electron beam driven fast and slow ion-acoustic modes. The frequency corresponding to the maximum growth rate of these modes agree with the observed high and low frequency waves reported by Tao et al. (2012).

In this chapter, we extend the theoretical model discussed in Chap. 2 to include the effects of magnetic field. In Sect. 4.2, the theoretical model to describe the solar wind/Lunar wake plasma is discussed and general dispersion relation is derived. The effect of variation of electron beam and propagation angle on the dispersion characteristics of the waves is analyzed numerically in Sect. 4.3. The results are discussed and concluded in Sect. 4.4.

4.2 Theoretical model

We consider homogeneous, collision-less, and magnetized four-component plasma comprising of fluid protons (n_p, T_p), doubly charged fluid alpha particles, He^{++} (n_i, T_i), electron beam (n_b, T_b, U_b) streaming along ambient magnetic field and suprathermal electrons (n_e, T_e) following kappa distribution to model solar wind/Lunar wake plasma. The ambient magnetic field, $\mathbf{B}_0$ is considered to be in z direction. The dispersion relation for the waves in the plasma is dictated by the fluid equations, which are:

$$\frac{\partial n_s}{\partial t} + \nabla.(n_s \mathbf{v}_s) = 0 \tag{4.1}$$

$$m_s n_s [\frac{\partial \mathbf{v}_s}{\partial t} + (\mathbf{v}_s.\nabla)\mathbf{v}_s] = q_s n_s (\mathbf{E} + \mathbf{v}_s \times \mathbf{B}_0) - \nabla P_s \tag{4.2}$$

Here, n_s and T_s represent the values of the density and temperature of the species 's' which stands for protons (p), doubly charged Helium ions (i), beam electrons (b) and kappa-

electrons (e). U_b, m_s, $\mathbf{v}_s$, P_s, q_s represents respectively, drift speed of the beam electrons, mass, velocity, pressure and charge of the individual species. The pressure term in this case becomes $\nabla P_s = \gamma k_B T_s \nabla n_s$, where γ is the ratio of specific heats and k_B represents the Boltzmann constant.

The electrons, which are suprathermal, are assumed to follow kappa distribution:

$$f_\kappa(v) = \frac{n_e}{\pi^{\frac{3}{2}}} \frac{1}{\theta^3} \frac{\Gamma(\kappa+1)}{\kappa^{\frac{3}{2}}\Gamma(\kappa-\frac{1}{2})} \left(1+\frac{v^2}{\kappa\theta^2}\right)^{-(\kappa+1)} \tag{4.3}$$

The κ is the suprathermal index, which is a measure of how much the system deviates from Maxwell-Boltzmann distribution function and Γ is the gamma function and $\theta = \sqrt{[\frac{2\kappa-3}{\kappa}](\frac{T_e}{m_e})}$ is the effective thermal speed. As one can see from this expression, for thermal velocity to have a meaningful value, one needs to have value of κ more than $3/2$.

The number density of the kappa distributed electron is found by integrating the Eq. (4.3) in presence of electrostatic waves with potential ϕ and can be obtained by replacing v^2/θ^2 by $v^2/\theta^2 - 2e\phi/m_e\theta^2$ (Devanandhan et al., 2011b, 2012):

$$n_e = n_{e0}\left[1-\frac{e\phi}{T_e(\kappa-\frac{3}{2})}\right]^{\frac{1}{2}-\kappa} \tag{4.4}$$

By linearizing the Eqs. (4.1), (4.2) and (4.4), the perturbed number density of each individual fluid component ($n_{p1}, n_{i1}, n_{b1}, n_{e1}$) can be found and clubbed with Poisson's equation

$$\nabla^2\phi = -\frac{e}{\varepsilon_0}(n_{p1} + z_i n_{i1} - n_{b1} - n_{e1}) \tag{4.5}$$

one can arrive at the dispersion relation:

$$\begin{aligned} 1+\frac{\omega_{pe}^2}{k^2v_{te}^2}\frac{2\kappa-1}{2\kappa-3} =& \frac{\omega_{pb}^2[(\omega-\mathbf{k}.\mathbf{U}_b)^2-\Omega_b^2\cos^2\theta]}{(\omega-kU_b)^4-(\omega-kU_b)^2\Omega_b^2-\gamma k^2v_{te}^2[(\omega-kU_b)^2-\Omega_b^2\cos^2\theta]} \\ &+\frac{\omega_{pp}^2[\omega^2-\Omega_p^2\cos^2\theta]}{\omega^4-\omega^2\Omega_p^2-\gamma k^2v_{tp}^2[\omega^2-\Omega_p^2\cos^2\theta]} + \frac{\omega_{pi}^2[\omega^2-\Omega_i^2\cos^2\theta]}{\omega^4-\omega^2\Omega_i^2-\gamma k^2v_{ti}^2[\omega^2-\Omega_i^2\cos^2\theta]} \end{aligned} \tag{4.6}$$

Here, $\omega_{ps} = \sqrt{\frac{n_{s0}z_s^2q_s^2}{\varepsilon_0 m_s}}$, $\Omega_s = \sqrt{\frac{z_s q_s B_0}{m_s}}$ and $v_{ts} = \sqrt{\frac{k_B T_s}{m_s}}$ are, respectively, the plasma frequency, cyclotron frequency and thermal velocity of s^{th} species with z_s being the multiplicity. Except for Helium ions, all other plasma species has multiplicity value ($z_{p,b,e}$) of 1 and for Helium, it will be 2. In Sect. 4.3, we numerically analyze the dispersion relation (Eq. (4.6)) for various modes for relevant plasma parameters.

4.3 Numerical Analysis

The numerical analysis of dispersion relation Eq. (4.6) is undertaken in this section. The relevant solar wind/Lunar wake plasma parameters are taken from Tao et al. (2012) and Mangeney et al. (1999). The various parameters are normalized as follows: the frequencies are normalized with electron plasma frequency, $\omega_{pe} = \sqrt{\frac{n_{0e}k_B e^2}{\varepsilon_0 m_e}}$; wave vector k by Debye length of electron, $\lambda_{De} = \sqrt{\frac{\varepsilon_0 T_e}{n_{0e}e^2}} = \frac{v_{te}}{\omega_{pe}}$. The number densities of the species is bound by the quasi neutrality condition, $n_{p0} + z_i n_{i0} = n_{b0} + n_{e0}$. The ratio of proton plasma frequency to that of proton cyclotron frequency is found to be 1620 (Tao et al., 2012).

4.3.1 Effect of electron beam variation

In Fig. 4.1a, dispersion curve corresponding to Eq. (4.6) is plotted with $k\lambda_{De}$ on x axis and $\frac{\omega_r}{\omega_{pe}}$ on y axis. The number densities are normalized with respect to total number density of electrons and temperature by temperature of kappa electron. The total number density is given by the expression $N_0 = n_{e0} + n_{b0} = n_{p0} + z_i n_{i0}$. The parameters fixed for this set of variation are $n_{b0}/N_0 = 0.010$, $n_{i0}/N_0 = 0.05$, $\kappa = 6$, $T_b/T_e = 0.0025$, $T_p/T_e = 0.2$, $T_i/T_e = 0.4$, $\gamma = 3$ and $\theta = 0^\circ$. Numerical analysis of the dispersion relation shows the presence of 12 modes in the plasma. These are electron cyclotron modes (1 (green colored line) & 12 (baby blue colored line)), electron acoustic modes (2 (black colored line) & 11 (blue colored line)), fast ion acoustic modes (3 (red colored line) & 10 (majestic purple colored line)) and slow ion acoustic modes (4 (magenta colored line) & 9 (cyan colored line)) (see Fig. 4.1). Though not shown, there are proton cyclotron mode (5 (sea green colored line) & 8 (yellow colored line)) and Helium cyclotron mode (6 (spring green colored line) & 7 (pink colored line)) (see Fig. 4.4). Modes 1, 2, 3, 4, 5 and 6 have positive phase speed, whereas modes 12, 11, 10, 9, 8 and 7 have negative phase speed. For angle of propagation $\theta = 0^\circ$, the modes 5, 6, 7 & 8 are non propagating and do not show any variation and hence, these modes are omitted in for the figures shown in this section. All the acoustic mode start with frequency $\frac{\omega_r}{\omega_{pe}} = 0$ at $k\lambda_{De} = 0$, on the other hand, electron, proton and Helium cyclotron modes start at 0.026475, 0.000014 and 0.000007 respectively. This figure is similar to what one can see in Fig. 2.1a, except for the fact that there are non-propagating electron cyclotron modes.

With the increase in the beam velocity, phase velocity of mode 11 becomes less and

less negative. This also means that for some value of $\frac{U_b}{c_s}$ the mode 11 has greater phase speed than that of mode 10 and 9. When the beam velocity is increased to $\frac{U_b}{c_s} = 4$ (Fig. 4.1b), the electron acoustic mode (mode 11), which had a negative phase speed, starts to become positive after $k\lambda_{De} \approx 2.33$ (for variations in between, kindly see Sect. 2.3.1). The striking feature that differentiates this figure from Fig. 2.1c is the behavior of modes 1 and 12 (electron cyclotron modes). For the parallel propagation the electron, proton and Helium cyclotron mode will have a constant frequency for all the values of $k\lambda_{De}$. However, the introduction of beam in electron term introduces kU_b term, which modifies these modes significantly. Also, one can see that the electron acoustic mode (mode 11) has come above modes 10 and 9.

When the beam velocity reaches the value of 4.3, the phase velocity of electron acoustic mode goes positive starting from $k\lambda_{De} \approx 1.01$, and merges with the slow ion acoustic mode and forms electron beam driven slow ion acoustic mode in the $k\lambda_{De}$ range 6.38 - 8.57 (see Fig. 4.1c). In this region phase velocity of mode 11 (electron acoustic mode) and mode 4 (slow ion acoustic mode) are the same with finite imaginary part which corresponds to finite growth rate and is shown in the lower panel of Fig. 4.1c. The maximum growth has a value of $\frac{\omega_i}{\omega_{pe}} = 0.00103$ which occurs at $k\lambda_{De} = 7.41$ and has a real value of $\frac{\omega_r}{\omega_{pe}} = 0.09945$. These results are the same as reported in Chap. 2. For the sake of completeness and better readability, we are reporting it here as well.

With further increase in the beam velocity to $\frac{U_b}{c_s} = 4.5$, the merging of acoustic modes happens at two different places: in the lower $k\lambda_{De}$ range (between 1.87 - 2.89), electron acoustic mode merges with slow ion acoustic mode to form electron beam driven slow ion acoustic mode and in the higher $k\lambda_{De}$ range between (6.66 -19.51) forms electron beam driven fast ion acoustic mode Fig. 4.1d. Electron beam driven slow ion acoustic mode exists in shorter $k\lambda_{De}$ range compared to electron beam driven fast ion acoustic mode. There exist a small $k\lambda_{De}$ range wherein mode 11 does not interacts with any other modes. The growth rates of beam driven slow ion acoustic mode and fast ion acoustic mode is almost the same ($\frac{\omega_i}{\omega_{pe}} \approx 0.00223$ & 0.00224 respectively).

With subsequent increase in $\frac{U_b}{c_s}$, the merging of electron acoustic modes first with slow ion acoustic mode and then with fast ion acrostic mode still occurs, but in the lower $k\lambda_{De}$ range. The growth rate of electron beam driven slow ion acoustic mode decreases subsequently and that of electron beam driven fast ion acoustic mode increase.

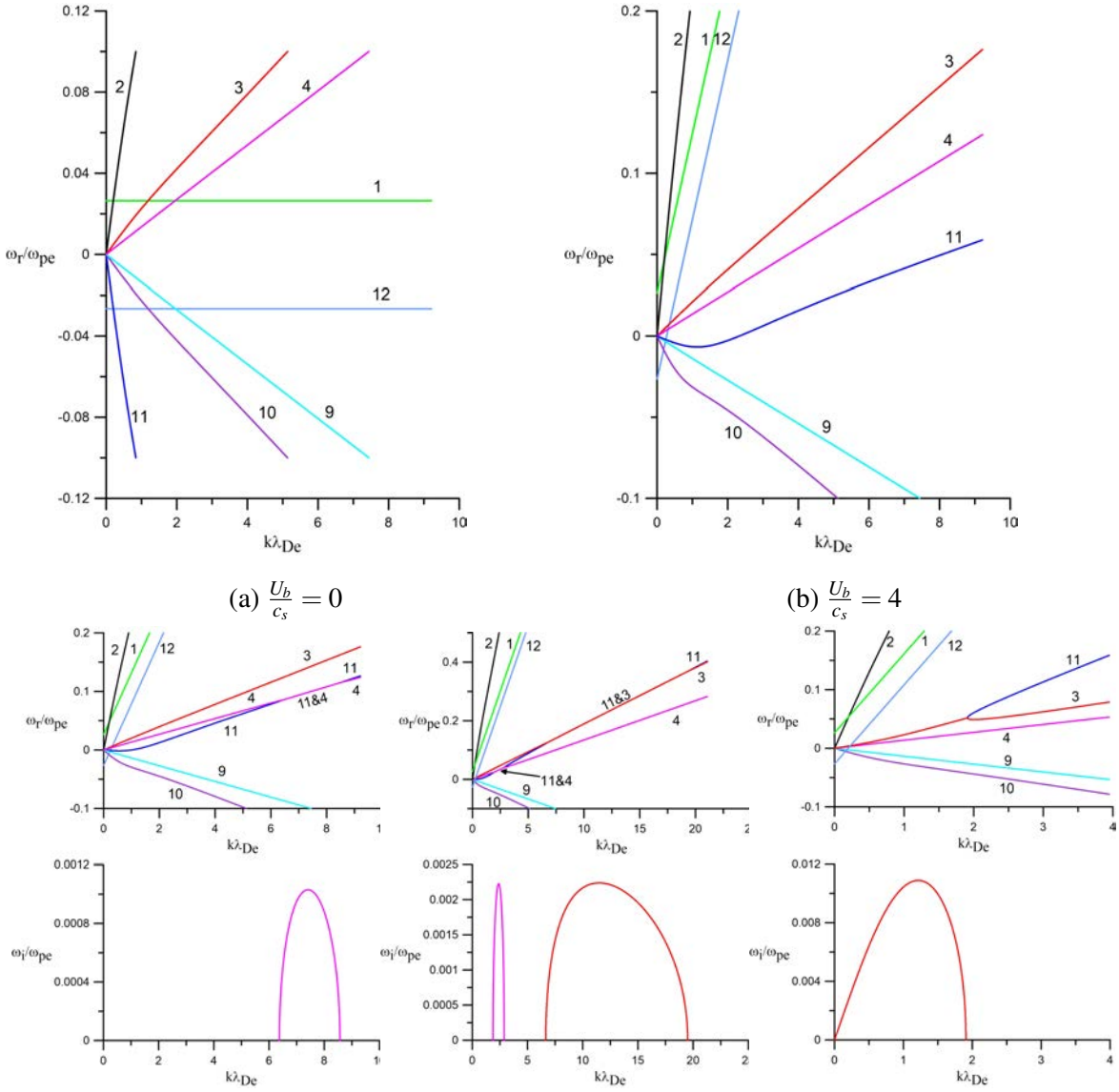

(a) $\frac{U_b}{c_s} = 0$ (b) $\frac{U_b}{c_s} = 4$

(c) $\frac{U_b}{c_s} = 4.3$. (d) $\frac{U_b}{c_S} = 4.5$ (e) $\frac{U_b}{c_S} = 5.5$

Figure 4.1: Plot of real frequency, ω_r/ω_{pe} and growth rate, ω_i/ω_{pe} versus $k\lambda_{De}$ for various values of $\frac{U_b}{c_s}$. The fixed parameters are $\theta = 0$, $n_{b0}/N_0 = 0.010$, $n_{i0}/N_0 = 0.05$, $\kappa = 6$, $T_b/T_e = 0.0025$, $T_p/T_e = 0.2$, $T_i/T_e = 0.4$. The colored lined indicates various modes in plasma: green color (mode 1- electron cyclotron mode with positive phase speed), black color (mode 2- electron acoustic mode with positive phase speed), red color (mode 3- fast ion acoustic mode with positive phase speed), magenta color (mode 4- slow ion acoustic mode with positive phase speed), cyan color (mode 9- slow ion acoustic mode with negative phase speed), majestic purple color (mode 10- fast ion acoustic mode with negative phase speed), blue color (mode 11- electron acoustic mode with negative phase speed), baby blue color (mode 12- electron cyclotron mode with negative phase speed). Due to scale size, sea green color (mode 5- proton cyclotron mode with positive phase speed), spring green color (mode 6- Helium cyclotron mode with positive phase speed), pink color (mode 7- Helium cyclotron mode with negative phase speed) and yellow color (mode 8- proton cyclotron mode with negative phase speed) are shown in Fig. 4.4.

The beam velocity is increased further to $\frac{U_b}{c_s} = 5.5$ and results are shown in Fig. 4.1e. Here, the electron acoustic modes merges with only fast ion acoustic wave and slow ion acoustic mode is not excited. The $k\lambda_{De}$ range in which the unstable region appears shifts to lower values of $k\lambda_{De} < 1.91$. The growth rate increases to $\frac{\omega_i}{\omega_{pe}} \approx 0.01$.

Further increase in the beam velocity, decreases the growth rate and with beam velocity reaching a value of 7.8, there are no unstable modes. These results are consistent with Chap. 2.

4.3.2 Effect of variation of angle of propagation without electron beam streaming

In the earlier section, we have presented results for parallel propagation with finite streaming of the electrons and shown that these results are in agreement of the results presented in Chap. 2. This is expected as for parallel propagation the magnetic field does not affect the wave propagation or its excitation. The effect of obliqueness on the dispersion relation Eq. (4.6) without electron beam streaming are discussed in this section. This is an extension of theoretical analysis carried out in Chap. 3 for the case of coupling of electrostatic ion cyclotron mode and acoustic mode in the context of solar wind plasma, wherein the magnetized plasma comprised of kappa electron, fluid proton and doubly charged Helium ions. For this set of variation, we keep the beam velocity to be zero (i.e. $\frac{U_b}{c_s} = 0$) and other parameters remain same as in Fig. 4.1. Since there is no change in the dispersion characteristic of electron cyclotron mode in the $k\lambda_{De}$ range considered (it stays parallel to x-axis all the time as $\frac{U_b}{c_s} = 0$), we have omitted it in the dispersion relation graph to represent other modes clearly.

For $\theta = 0^\circ$, all the modes are decoupled as shown in Fig. 4.2a. Modes 5 and 6 represent the proton cyclotron mode and Helium cyclotron mode, respectively. In the case of parallel propagation, these modes are non-propagating modes and the only physically acceptable solution are that of acoustic modes.

When finite angle of propagation is introduced ($\theta = 5^\circ$), the coupling of different modes can be seen clearly as in Fig. 4.2b. The various coupling is indicated by circles. The mode 2 couples with modes 6 and 5 at $k\lambda_{De}$ value of 0.00013 and 0.00006 respectively. In a similar fashion, mode 3 couples with mode 6 at $k\lambda_{De} \approx 0.00031$. Rest of the coupling hap-

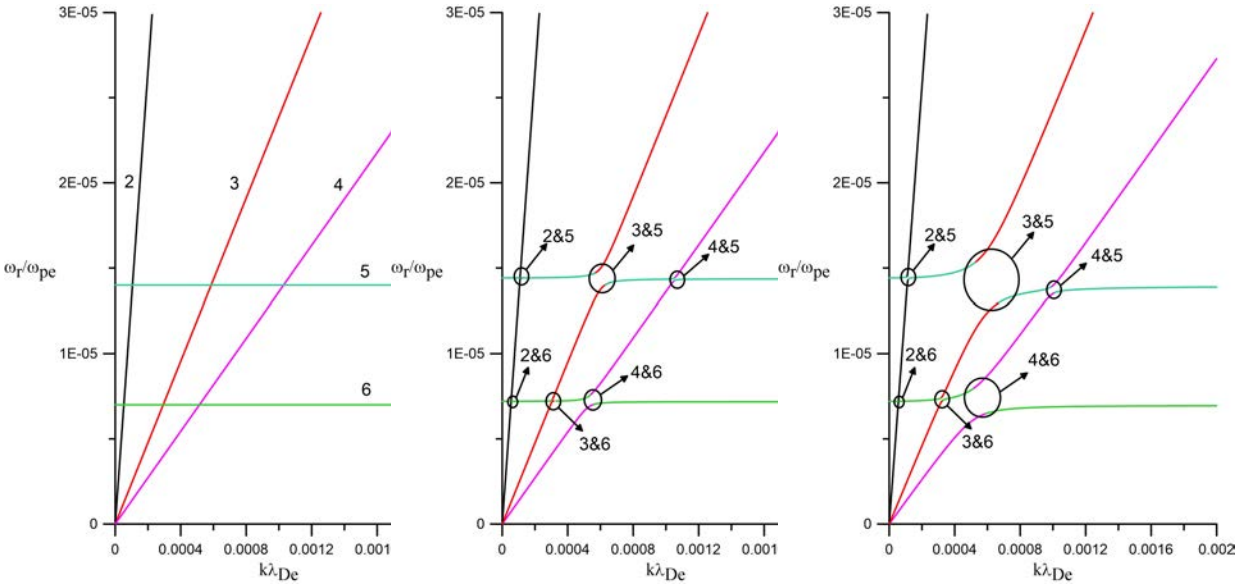

(a) $\theta = 0^\circ$ (b) $\theta = 5^\circ$ (c) $\theta = 15^\circ$

Figure 4.2: Plot of real frequency, ω_r/ω_{pe} versus $k\lambda_{De}$ for various values of θ with $\frac{U_b}{c_s} = 0$. Other parameters are the same as in Fig. 4.1

pens at certain $k\lambda_{De}$ range. Mode 4 couples with mode 6 in the $k\lambda_{De}$ range 0.00050-0.00060, mode 3 couples with mode 5 in the $k\lambda_{De}$ range 0.00055-0.00068 and mode 4 couples with mode 5 in the $k\lambda_{De}$ range 0.00103-0.00107. It has to be emphasized that similar kind of coupling will happen in the negative y-axis also, in-order to show the dispersion relation clearly, we have not indicated that. So, in total the coupling happens at 12 different places, which is in sharp contrast to what is shown in Chap. 3, where coupling occurred at 8 different places.

In Fig. 4.2c, the angle of propagation is increased to 15°. It is clear from dispersion curve that the coupling of mode 3 and mode 5 is very much weaker compared to that in case of Fig. 4.2b, which is indicated by gap between the modes. The coupling between mode 2 and mode 6 remains the strongest one which is happening at $k\lambda_{De} \approx 0.00006$. There exist a certain $k\lambda_{De}$ in which other modes couple: mode 4 couples with mode 6 in the range 0.0005-0.00065; mode 4 couples with mode 5 in 0.000965-0.00104; mode 3 couples with mode 6 in 0.00029-0.00035;mode 3 couples with mode 5 in 0.00053-0.00075; mode 2 and mode 5 in 0.000090-0.00014.

With the increase in the angle of propagation to 30° (see Fig. 4.3a), the coupling between mode 3 & mode 5, 4 & 5 and 4 & 6 vanishes. In this case mode 3 couples with mode 6 in two different $k\lambda_{De}$ regime: first in 0.00038-0.00044 and then at 0.00076-0.00084.

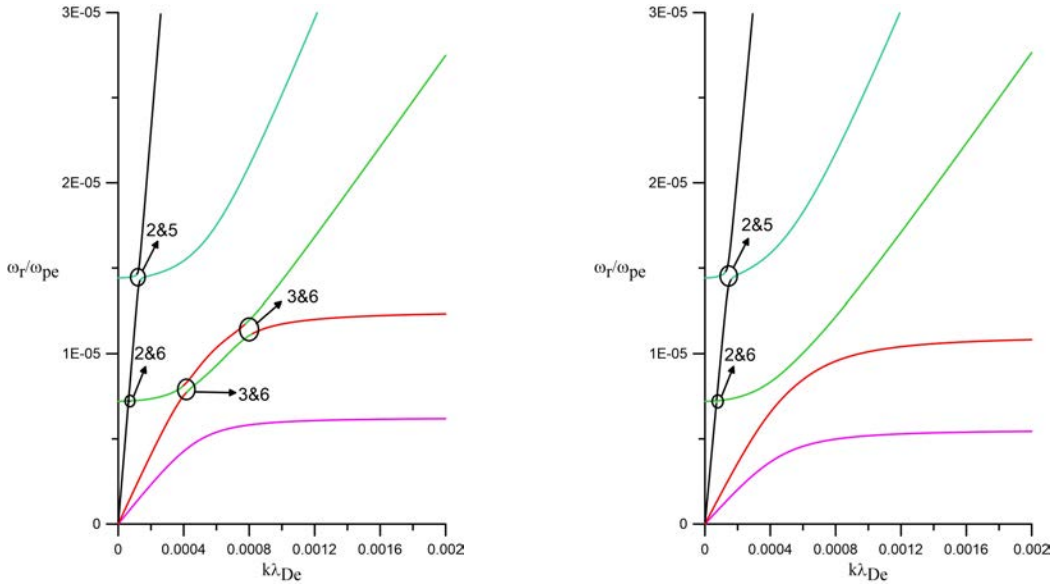

(a) $\theta = 30^\circ$ (b) $\theta = 40^\circ$

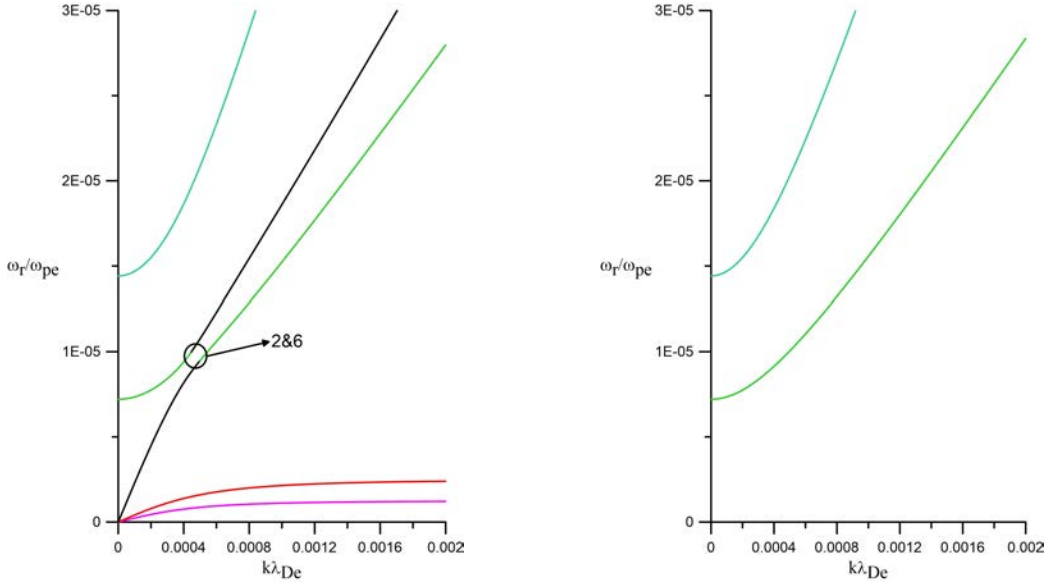

(c) $\theta = 80^\circ$ (d) $\theta = 90^\circ$

Figure 4.3: Plot of real frequency, ω_r/ω_{pe} versus $k\lambda_{De}$ for various values of θ with $\frac{U_b}{c_s} = 0$. Other parameters are the same as in Fig. 4.1

Furthermore, the coupling between mode 2 and mode 6 still remains intact and happens at 0.00007. However, the coupling between modes 2 and 5 is weak as compared to that in case of $\theta = 15^\circ$ (see Fig. 4.2c) and happens in the $k\lambda_{De}$ range 0.00009-0.00015. The slow ion acoustic mode (mode 4) completely decouples from the rest of the modes.

In Fig. 4.3b, the dispersion relation curve is plotted for $\theta = 40^\circ$ and $\frac{U_b}{c_s} = 0$. It is seen that the mode 3 (fast ion acoustic) and mode 4 (slow ion acoustic) do not couple with any of the cyclotron modes. The only coupling is between mode 2 and mode 6 at $k\lambda_{De}$ 0.000070 and then between mode 2 and mode 5 in the $k\lambda_{De}$ range 0.0001-0.000180. Further increasing the angle of propagation weakens the coupling between mode 2 and mode 5 (this has been tested for $\theta = 60^\circ$, but not shown here).

With further increase in angle of propagation to 80°, the coupling between mode 2 and mode 5 also vanishes with only coupling existing between mode 2 and mode 6. A notable thing to mention here is that the frequencies of slow and fast ion acoustic mode decreases substantially compared with that of Fig. 4.3b.

Finally for $\theta = 90^\circ$, the only cyclotron mode exist in the system as seen in Fig. 4.3d.

4.3.3 Effect of variation of angle of propagation with finite electron beam streaming

In this section, we analyze Eq. (4.6) for various angles of propagation with beam velocity fixed to 4.5.

The Fig. 4.4 shows the dispersion plot for $\frac{U_b}{c_s} = 4.5$ and $\theta = 0^\circ$. This is the same plot as shown in Fig. 4.1d, but here it is shown in different scale. It may seem that the mode 11 merge with mode 5 and mode 6 in Fig. 4.4, but it is just a crossover as there is no imaginary part associated with it. The two electron cyclotron modes neither couple nor merge with any other modes in the $k\lambda_{De}$ range that is considered, so these modes are not shown here to represent other modes clearly. Also, since the coupling happening on both sides of x-axis are different, compared to what is seen at Sect. 4.3.2, we have shown the negative axis too in all figures in this section.

When angle of propagation is increased to 5° dispersion relation curve becomes complicated with coupling as well as merging as seen in Fig. 4.5. We have separated the graphs

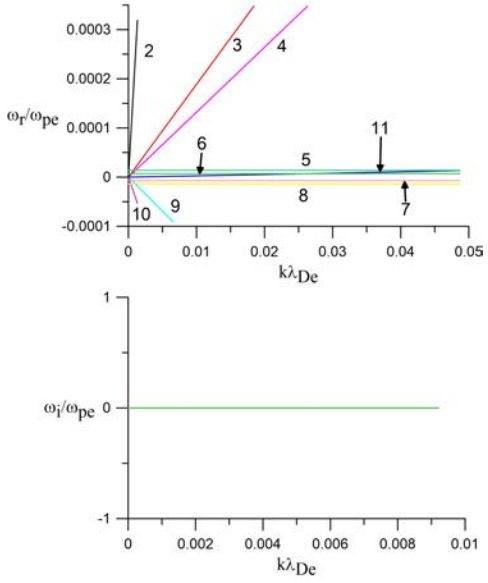

Figure 4.4: Plot of real frequency, ω_r/ω_{pe} and growth rate, ω_i/ω_{pe} versus $k\lambda_{De}$ for $\theta = 0^\circ$ and $\frac{U_b}{c_s} = 4.5$. Other parameters are the same as in Fig. 4.1

in two different panels because the merging and coupling of modes which is happening occurs at different $k\lambda_{De}$ scale and it is not be possible to show both coupling and merging in same graph. In Fig. 4.5a, it can be seen that the coupling happening at 6 different places in the positive y-axis region and 4 different places in negative y-axis region. This is in sharp contrast to what was reported for in Sect. 4.3.2, where coupling was same in both the axis. Fig. 4.5b shows the same dispersion plot as in Fig. 4.5a, but in the higher $k\lambda_{De}$ range. Here, one can clearly see the merging of mode 11 with mode 6 thereby generating a unstable region first in the $k\lambda_{De}$ range 0.0264-0.0267 with maximum growth rate 1.740e-08 and then in 0.0485-0.0493 with maximum growth rate 7.670e-08. The first merging happens between mode 11 and mode 6 and then with mode 5. Thus, the proton and helium cyclotron modes are excited by an electron beam.

With further increase in angle of propagation to 10° (not shown here), mode 11 still merges with mode 6 in $k\lambda_{De}$ range 0.0251-0.0255 with maximum growth rate 3.514e-08 and then with mode 5 in the $k\lambda_{De}$ range 0.0429-0.0443 with maximum growth rate 16.062e-08.

The dispersion relation curves for $\theta = 30^\circ$ is shown in Fig. 4.6. As one can see from Fig. 4.6a, the mode 4 does not couple with any other modes. Also, in the negative y-axis, all the coupling regions comes closer to each other. Here, the mode 11 first merges with

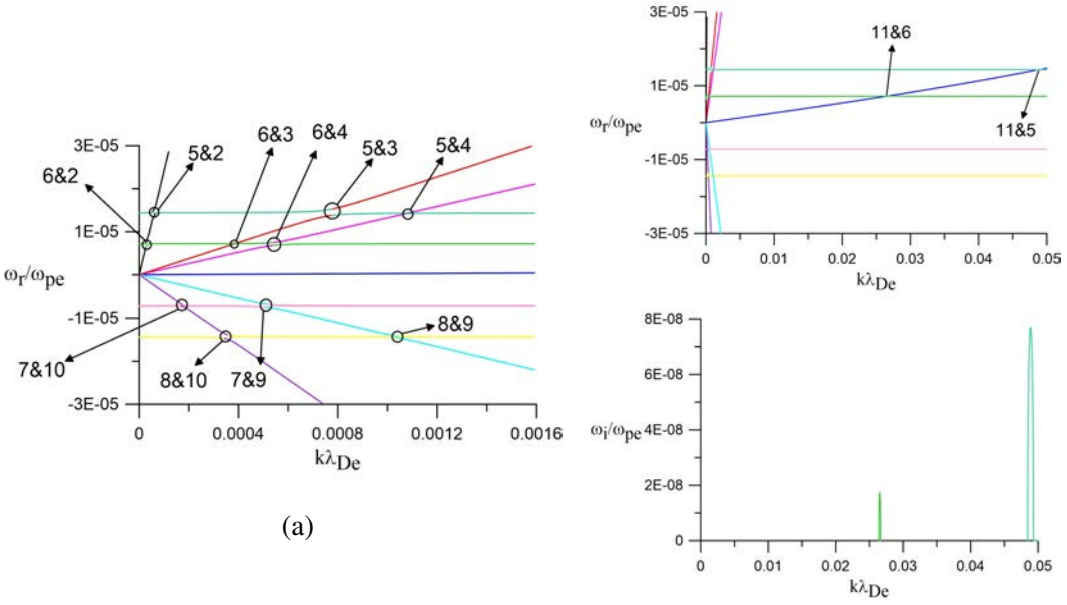

(a)

(b)

Figure 4.5: Plots showing coupling (Fig. 4.5a) and merging (Fig. 4.5b) of different modes for $\theta = 5^\circ$ and $\frac{U_b}{c_s} = 4.5$. Other parameters are the same as in Fig. 4.1

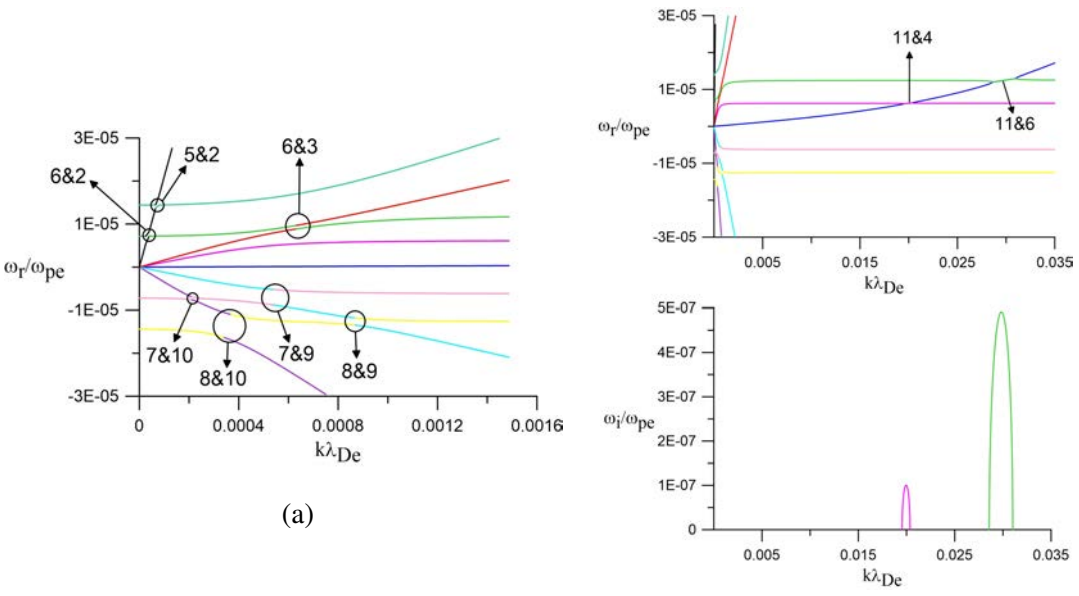

(a)

(b)

Figure 4.6: Plots showing coupling (Fig. 4.6a) and merging (Fig. 4.6b) of different modes for $\theta = 30^\circ$ and $\frac{U_b}{c_s} = 4.5$. Other parameters are the same as in Fig. 4.1

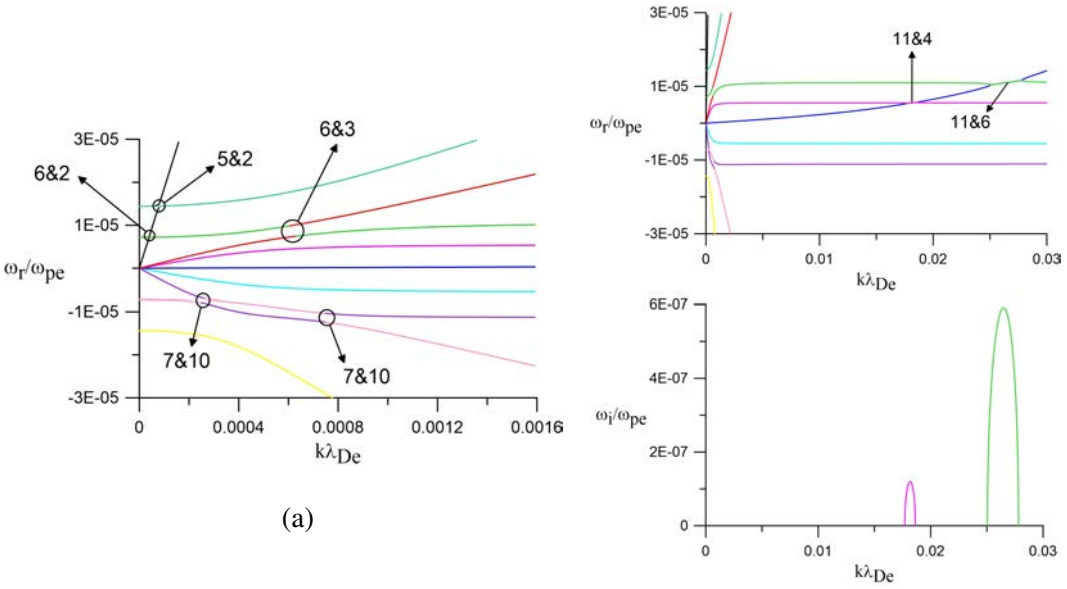

Figure 4.7: Plots showing coupling (Fig. 4.7a) and merging (Fig. 4.7b) of different modes for $\theta = 40^\circ$ and $\frac{U_b}{c_s} = 4.5$. Other parameters are the same as in Fig. 4.1

mode 4 in the $k\lambda_{De}$ range 0.0195-0.0204 with maximum growth rate 1.0045e-07 and then with mode 6 in the $k\lambda_{De}$ range 0.0286-0.0310 with maximum growth rate of 4.912e-07 as shown in Fig. 4.6b. The growth rate of merged mode of 11 and 6 increases as compared to that of $\theta = 5^\circ$ (as shown in Fig. 4.5b) and those of 10° (not shown here) and 40° (see Fig. 4.7b). Also, for $\theta = 40^\circ$, in negative y-axis, the only coupling happens is between mode 7 and mode 10, which occurs at two different $k\lambda_{De}$ range- the coupling between mode 8 & 10, mode 7 & mode 9 and mode 8 & 9 vanishes.

When the angle of propagation is increased to 50°, the only coupling that exists is between mode 5 & 2 and mode 6 & 2 in the positive y-axis. In the negative y-axis mode 7 couples with mode 10 as shown in Fig. 4.8a. The modes that now merges with mode 11 are mode 4 in $k\lambda_{De}$ range 0.0164-0.0174 with maximum growth rate to be 12.447e-08 and mode 3 in the $k\lambda_{De}$ range 0.0227-0.0257 with maximum growth rate to be 61.572e-08. With further increase in the angle of propagation, mode 11 merges with mode 4 and then with 3 with decrease in growth rate and unstable regions shifting to lower $k\lambda_{De}$ range. These are electron beam driven slow and fast ion acoustic modes, respectively.

Angle of propagation is increased to $\theta = 80^\circ$ and results are shown in Fig. 4.9. Here,

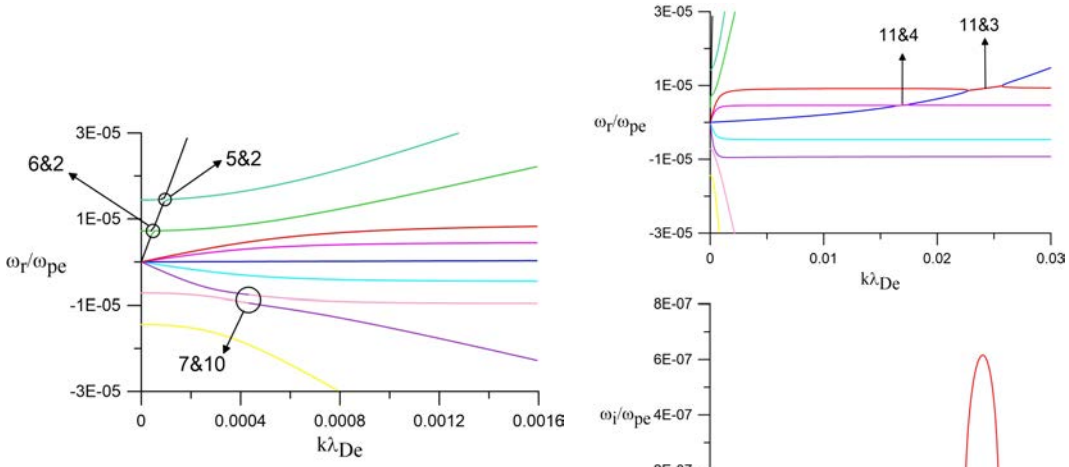

(a)

(b)

Figure 4.8: Plots showing coupling (Fig. 4.8a) and merging (Fig. 4.8b) of different modes for $\theta = 50^\circ$ and $\frac{U_b}{c_s} = 4.5$. Other parameters are the same as in Fig. 4.1

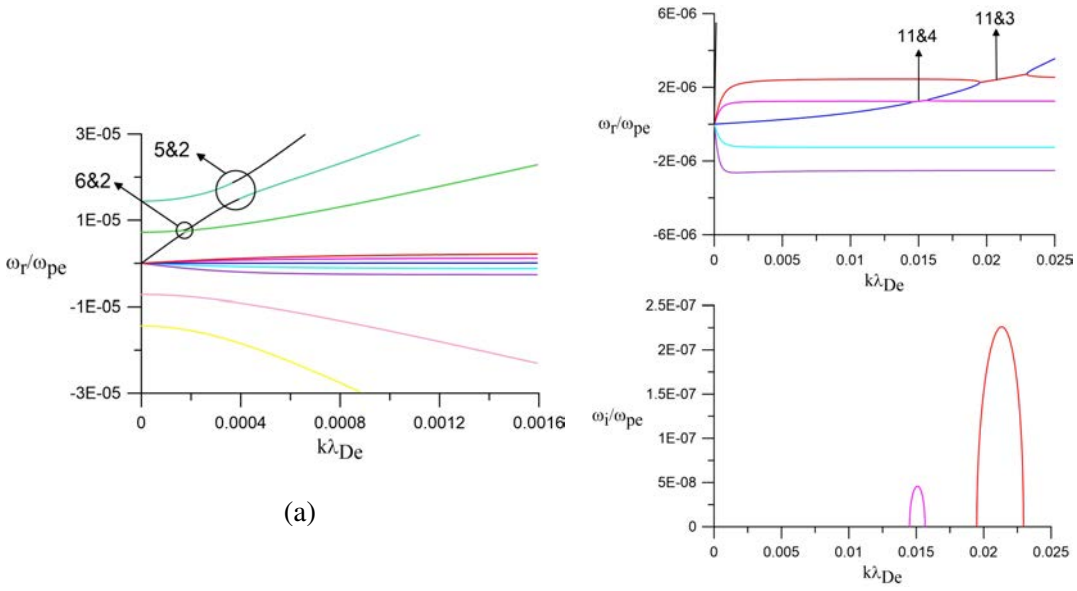

(a)

(b)

Figure 4.9: Plots showing coupling (Fig. 4.9a) and merging (Fig. 4.9b) of different modes for $\theta = 80^\circ$ and $\frac{U_b}{c_s} = 4.5$. Other parameters are the same as in Fig. 4.1

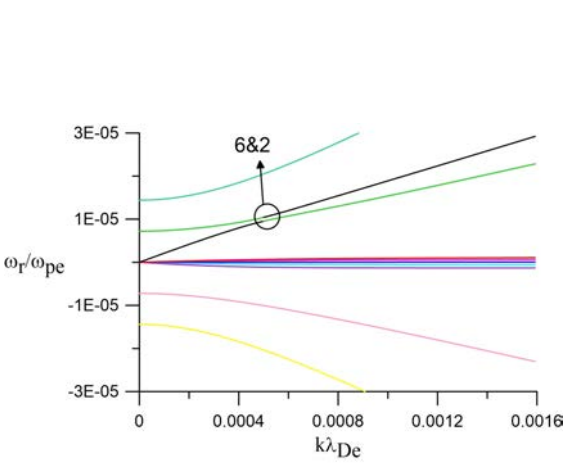

(a)

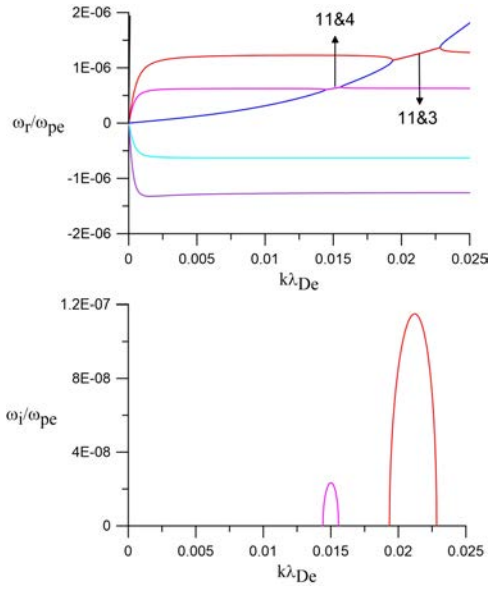

(b)

Figure 4.10: Plots showing coupling (Fig. 4.10a) and merging (Fig. 4.10b) of different modes for $\theta = 85^\circ$ and $\frac{U_b}{c_s} = 4.5$. Other parameters are the same as in Fig. 4.1

it can be seen that there is no coupling between mode 7 and mode 10 (Fig. 4.9a). The growth rate of first merging (mode 11 & 4) and second merging (mode 11 & 3) decreases to 4.588e-08 and 22.6e-08 respectively (Fig. 4.9b).

When the angle of propagation is further increased to $\theta = 85^\circ$, the coupling between mode 5 and mode 2 also vanishes leaving out the coupling between mode 6 & mode 2 as shown in Fig. 4.10. The merging between modes 11 and 3 and 11 and 4 continue to occur with lower growth rate as compared to $\theta = 80^\circ$.

When the angle of propagation is further increased to $\theta = 87^\circ$, all the modes decouple with mode 11 merging with mode 4 first and then with mode 3 (see Fig. 4.11).

For perpendicular propagation, the acoustic mode vanishes and there exist only proton and Helium cyclotron mode only. At perpendicular propagation there is will not be any unstable region. This is shown in Fig. 4.12.

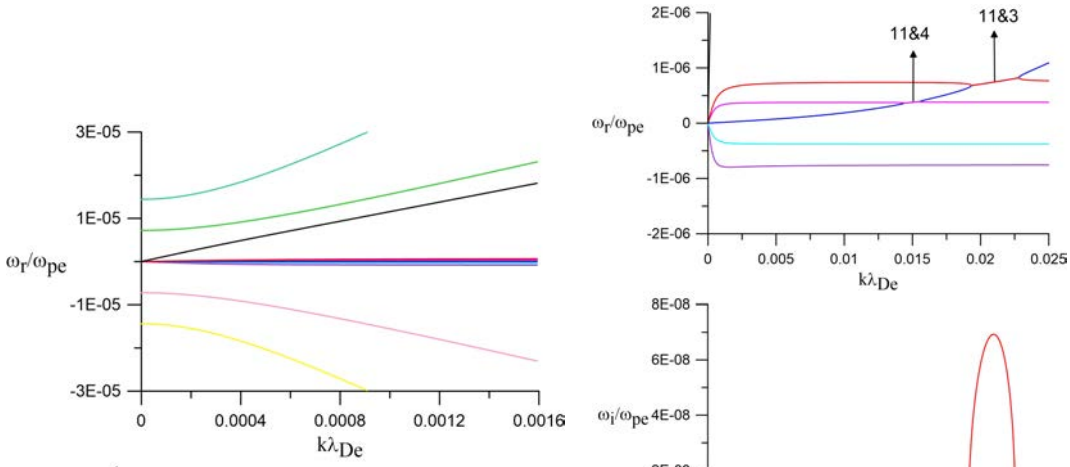

(a)

(b)

Figure 4.11: Plots showing coupling (Fig. 4.11a) and merging (Fig. 4.11b) of different modes for $\theta = 87^\circ$ and $\frac{U_b}{c_s} = 4.5$. Other parameters are the same as in Fig. 4.1

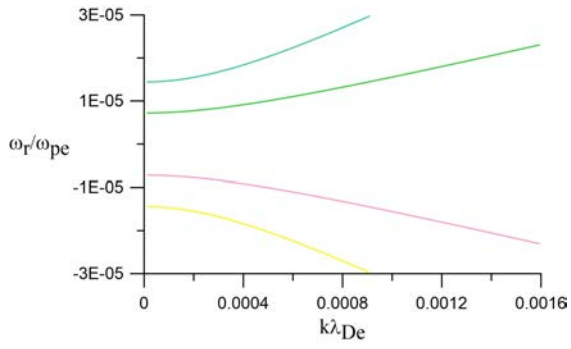

Figure 4.12: Plot of real frequency, ω_r/ω_{pe} versus $k\lambda_{De}$ for $\theta = 90^\circ$ with $\frac{U_b}{c_s} = 4.5$. Other parameters are the same as in Fig. 4.1

4.4 Conclusion

In this chapter, we present a linear study of propagation of electrostatic ion cyclotron waves and ion acoustic waves in four-component magnetized plasma comprising of fluid protons, doubly charged fluid Helium ions, beam electron streaming along ambient magnetic field and electron in kappa distribution. From the numerical analysis of dispersion relation, the presence of electron, proton and Helium cyclotron modes and slow, fast and electron acoustic modes is seen. For parallel propagation without electron streaming, the dispersion relation curves are perfectly symmetrical about x-axis.

With increase in the beam velocity for parallel propagation, phase speed of electron acoustic mode turns to positive from negative. This mode further merges with the slow ion acoustic to form beam-driven slow ion acoustic wave in the lower wave-number regime and merges with fast ion acoustic wave to form beam-driven fast ion acoustic wave in the higher wave-number regime. The merging of the modes makes it unstable with finite growth rate. All these results are consistent with Chap. 2.

The dispersion relation is further analysed for non- parallel propagation by keeping velocity of beam electron to zero revealing coupling of various modes in the plasma. Here coupling occurs at 12 different places- 6 in positive y-axis and 6 in negative y-axis. On the other hand, the coupling described in Chap. 3, occurs at 8 different places- 6 in positive y-axis and 6 in negative y-axis. With increase in the angle of propagation, the coupling between mode 3 and 5 is the first one to vanish followed by mode 4 & 6 and then mode 4 & 5. The mode 3 couples with mode 6 at two different places at $\theta = 30^{\circ}$ after which mode 3 does not couple with any other mode. Further increase in the angle of propagation decreases the strength of coupling between mode 2 and mode 5 compared to mode 2 and mode 6. At perpendicular propagation, only cyclotron modes exist.

When the dispersion relation is numerically analysed for different angles of propagation with finite electron beam velocity, the coupling and merging of various modes can be seen. For oblique propagation, the mode 11 merges with mode 6 in the lower $k\lambda_{De}$ range and then with mode 5. When the angle of propagation is increased to 30°, the mode 4 does not couple with any mode and mode 11 merges first with mode 4 and then with mode 6 (see Fig. 4.6). With further increase in the angle of propagation, mode 3 does not couples with

any other mode and the merging happens with mode 4 and mode 3 in the lower and higher $k\lambda_{De}$ range, respectively (see Fig. 4.8). After this, the mode 11 merges only with mode 4 and 3. At perpendicular propagation, the mode 11 vanishes as it is an acoustic mode and hence there will not be any merging of modes. These results are at fixed value of electron beam velocity. Initially, for $\theta = 50^{\circ}$ proton and helium cyclotron modes are excited by and later for more oblique angles acoustic modes are generated with diminishing growth rate as angle of propagation reaches closer to 90°.

Chapter 5

Higher harmonic instability of electrostatic ion cyclotron waves in auroral plasma

5.1 Introduction

Electrostatic ion cyclotron (EIC) waves are among the important waves that have been observed in the magnetized plasma. EIC waves propagate nearly perpendicular to the ambient magnetic field, with a small finite wave number along the ambient magnetic field. EIC waves were first observed in laboratory plasma comprising of cesium and potassium by D'Angelo and Motley (1962) and Motley and D'Angelo (1963). Motley and D'Angelo (1963) explained the electrostatic oscillations near ion cyclotron frequency by using fluid theory. With the help of kinetic theory, Drummond and Rosenbluth (1962) studied the stability of EIC waves in plasma containing drifting electrons and ions. Their observations were in line with the experimental observations reported by D'Angelo and Motley (1962). Ever since Mosier and Gurnett (1969) have observed these waves in high latitude ionosphere, there have been numerous instances of EIC wave observations by many spacecraft, for example, S3-3 (Kintner et al., 1978, 1979; Temerin et al., 1979),ISEE-1 (Cattell et al., 1991), Viking (André et al., 1987),Polar (Mozer et al., 1997), FAST (Cattell et al., 1998) and GEOS 1 & 2 satellite(Young et al., 1981; Roux et al., 1982). EIC waves serve as a main source for ion heating in magne-

tosphere and for this reason, they are of great interest to the space plasma community. Dakin et al. (1976) demonstrated that significant ion heating can occur by EIC modes excited by electron current. Soon after, Ungstrup et al. (1979) found that EIC waves heats up the ions to super-thermal energies transverse to the earth's magnetic field, which subsequently are accelerated away from Earth by Earth's magnetic field. Roux et al. (1982) also observed heating of He^+ ions associated with EIC waves in the magnetospheric region. Song et al. (1989) observed EIC waves in plasma containing K^+ ions, SF_6^- ions and electrons. They observed low frequency K^+ and high frequency SF_6^- EIC modes, with their frequencies increasing with the increase in percentage of negative ions, while the critical electron drift velocities for excitation of either mode decreases with increases in percentage of negative ions. This in turn means that in a multi-component plasma, there can be EIC waves associated with each component (See also Chow and Rosenberg (1996)). Chow and Rosenberg (1996) studied the effect of negative ions on EIC instability in three-component plasma comprising of electrons and two singly charged species of ions- one which is heavy ion and other is lighter ion. They found that critical drifts for the excitation of both the light and heavy ion EIC modes decrease as the relative density of negative ions increases.

Electrostatic ion cyclotron instability (EICI) has gained much attention owing to the fact that it has lowest threshold among the various current driven instabilities (Kindel and Kennel, 1971). EIC instability in the ionosphere and magnetosphere can arise from different free energy sources like field aligned currents, ion beams; velocity shear, relative streaming between ions, electron drifts, and density gradients. The ion beam driven EIC instability destabilizes the waves by resonant and non resonant interactions (Weibel, 1970; Perkins, 1976; Yamada et al., 1977), whereas the current driven instability is driven by inverse Landau damping of electrons(Kindel and Kennel, 1971; Drummond and Rosenbluth, 1962). The current driven EICI has been studied by many workers. The work of Drummond and Rosenbluth (1962) was a starting point for this. This work was later on extended by others like Kindel and Kennel (1971) and in the nonlinear regime by Lysak et al. (1980), Okuda et al. (1981a) and Okuda and Ashour-Abdalla (1981). Ion and electron beams have become strong contender as a source of free energy for EIC instability (Kintner et al., 1979; Cattell, 1981; Okuda and Nishikawa, 1984). Sometimes, even if the field aligned currents were shown to be below the critical value, EIC waves were observed. Lakhina (1987) and Ganguli et al. (2002)

have shown that EIC waves could grow unstable even in the absence of field aligned current if perpendicular velocity shear in the ion flow along the magnetic field lines was taken into account.

In the dusty plasma experiment, it was shown that the presence of negatively charged dust enhances the instability growth rate of EIC waves (Barkan et al., 1995). The effect of temperature anisotropy on EIC instability has been carried out by Lee (1972) in a two component magnetized plasma comprising of electrons drifting relative to ions in the direction of the magnetic field. They found that the critical drift velocity decreases and the growth rate increases with decrease in perpendicular ion temperature. In four component magnetized plasma comprising of electrons, hydrogen (H^+), positively charged oxygen (O^+) and negatively charged oxygen (O^-), it was shown that temperature anisotropy of the oxygen ions only slightly enhance the growth rates (Kurian et al., 2009). Recently, Niyat et al. (2016) have derived dispersion relation for EIC waves that has nonextensive electrons drifting with respect to stationary ions. They found that minimum value of the critical drift velocity decreases with decrease in the non-extensivity parameter of electrons, whereas larger temperature anisotropy of ions weakens the instability and increases the minimum value of the critical drift velocity.

Study of higher harmonics of EIC waves has been undertaken by a few researchers. Kim et al. (2008) experimentally verified the excitation of EIC waves in plasma comprising of K^+ ions, electrons, and $C_7F_{14}^-$ negative ions. They showed that as the presence of negative ions increased, both the number of harmonic modes excited and the intensity of all modes increases. Rosenberg and Merlino (2009) studied the generation of higher harmonics of EIC waves in plasma containing positive ions, electrons, and negative ions that are much more massive than the positive ions. They had found that it is easier to excite the fundamental and higher harmonic EIC modes of both ion species in the presence of a large density of negative ions. Later on, Sharma et al. (2013) studied the generation of higher harmonics by a spiraling ion beam in a collisionless magnetized plasma containing K^+ light positive ions, electrons, and $C_7F_{14}^-$ heavy negative ions. The ion beams drives EIC waves to instability via cyclotron interactions. The presence of heavy ions is not restricted to laboratory plasmas, they can be found in space plasmas as well. For example, presence of alpha (He^{++}) particles precipitating into the night side auroral zone on a satellite pass over the southern hemisphere

on May 16, 1972 has been found during a magnetic storm (Sharp et al., 1974). These alpha particles are of solar wind origin whereas O^+ which were also reported are of ionospheric origin. The typical alpha to proton ratio was found to be 4%. Recently, Tang et al. (2015) observed electrostatic ion cyclotron waves at fundamental and second harmonic of proton and at doubly charged Helium cyclotron frequencies which establish the presence of He^{++} ions in the magnetopause. Helium and oxygen are often seen inside the magnetopause and adjacent to it, however, the THEMIS mission does not make ion composition measurements to distinguish different ion species. The doubly charged Helium is of solar wind origin and hence density will be low ($<$5% or so).

So far, theoretical or experimental studies on EIC instabilities have been conducted keeping in mind the heavier ions (Kim et al., 2008; Rosenberg and Merlino, 2009)(K^+ ions, and $C_7F_{14}^-$) or Oxygen ions(Kindel and Kennel, 1971; Kurian et al., 2009). Therefore, it is important to study EIC instabilities involving He^{++} ions which are of solar wind origin and are found in various regions of the Earth's magnetosphere and can impact the growth of EIC waves. In this chapter, instability of higher harmonic of electrostatic proton cyclotron and Helium cyclotron waves are studied using kinetic theory in three component magnetized plasma comprising of drifting electrons, Maxwellian protons and doubly charged Helium ions. The results obtained will be useful in understanding EIC instabilities in laboratory and space plasmas where field aligned currents exist.

5.2 Theoretical Model

We consider three component magnetized plasma composed of electrons, protons and doubly charged Helium ions. The electrons are assumed to stream with speed U_b along the ambient magnetic field, B_0, which is in the z-direction. In this work, the collisions are neglected and protons and Helium follow Maxwell distribution whereas electrons are having a drifting Maxwellian distribution. The low-frequency electrostatic waves are considered to be propagating in the x - z plane $\mathbf{k} = k_\perp \hat{x} + k_\parallel \hat{z}$. In the equilibrium state, the quasi- neutrality condition demands:

$$n_{0e} \approx n_{0p} + z_\alpha n_{0\alpha} \tag{5.1}$$

where z_α is the charge of Helium. n_{0e}, n_{0p} and $n_{0\alpha}$ are the unperturbed number densities of electrons, protons and Helium ions respectively. The dispersion relation for the electrostatic waves in magnetized plasma can be written as (Swanson, 2003; Rosenberg and Merlino, 2009):

$$D(\omega,k) = 1+\sum_s \chi_s \tag{5.2}$$

where χ_s indicates the susceptibility of individual species with subscript s indicating electron (e), proton (p) and doubly charged Helium ions (α):

$$\chi_s = \frac{1}{k^2\lambda_{Ds}^2}\left[1+\sum_{n=-\infty}^{\infty}\frac{\omega-k_\parallel U_{bs}}{\sqrt{2}k_\parallel v_{ts}}\Gamma_n(b_s)Z(\xi_{ns})\right] \tag{5.3}$$

In the above equation, $\lambda_{Ds} = v_{ts}/\omega_{ps}$ is the Debye length, $\omega_{ps} = \sqrt{z_s^2 n_{0s} q_s^2/\varepsilon_0 m_s}$ is the plasma frequency; ε_0 is the permittivity of the free space, m_s, z_s and q_s are respectively the mass, atomic number and charge of the s^{th} species, $v_{ts} = \sqrt{k_B T_s/m_s}$ is the thermal velocity of species 's', ω is the wave frequency, $k = \sqrt{k_\parallel^2 + k_\perp^2}$, is the wavenumber, $\Gamma_n(b_s) = I_n(b_s)\exp(-b_s)$, where $I_n(b_s)$ is the modified Bessel function of order 'n' with its argument $b_s = k_\perp^2 v_{ts}^2/\Omega_s^2$ and Z is the plasma dispersion function with argument ξ_{ns}. Also, $\Omega_s = z_s q_s B_0/m_s$ is the cyclotron frequency of s^{th} species. Here $k_\parallel$ and $k_\perp$ are the wave number parallel and perpendicular to the ambient magnetic field, respectively. U_{bs} stands for the beam-velocity of s^{th} species. As we consider only electron to have a beam component, we denote $U_{bs} \equiv U_b$.

For wave frequency ω much less than electron cyclotron frequency, the the susceptibility for electrons can be written as (Rosenberg and Merlino, 2009; Stix, 1992):

$$\chi_e \approx \frac{1}{k^2\lambda_{De}^2}\left[1+\frac{\omega-k_\parallel U_b}{\sqrt{2}k_\parallel v_{te}}\Gamma_0(b_e)Z(\xi_{0e})\right] \tag{5.4}$$

To arrive at Eq. (5.4), we have used the fact that Larmor radius of the electron is small with $b_e << 1$. Since $b_e << 1$, we retain only $n = 0$ term as $\Gamma_0(0) = 1$ and $\Gamma_n(0) = 0$ for all $n \neq 0$. As we have considered electrons to be drifting- Maxwellian and protons and doubly charged Helium ions to be Maxwellian, the argument of plasma dispersion function $\xi_{p,\alpha}$ becomes:

$$\xi_{0e} = \frac{\omega-k_\parallel U_b}{\sqrt{2}k_\parallel v_{te}} \tag{5.5a}$$

$$\xi_{np,n\alpha} = \frac{\omega-n\Omega_{p,\alpha}}{\sqrt{2}k_\parallel v_{tp,\alpha}} \tag{5.5b}$$

Assuming $\omega = \omega_r + i\gamma$ where $\gamma << \omega_r$, the dispersion relation given by Eq. (5.2) can be written as

$$D_r(\omega_r, k) + iD_i(\omega_r, k) = 0 \tag{5.6}$$

where D_r and D_i are the real and imaginary parts of the dispersion relation Eq. (5.4) and the real frequency, i.e., ω_r is given by:

$$D_r(\omega_r, k) = 0 \tag{5.7}$$

The growth or damping of the low-frequency wave is given by:

$$\gamma = -\frac{D_i(\omega_r, k)}{\partial D_r(\omega_r, k)/\partial \omega_r} \tag{5.8}$$

In the following subsections, analytical results on proton and helium cyclotron harmonics are presented.

5.2.1 Proton cyclotron Harmonics

In this subsection, we study instability associated with proton cyclotron harmonics. To simplify the electron term in Eq. (5.4), we assume argument of the plasma dispersion function (Z) to be smaller than unity, i.e., $\xi_{0e} < 1$. Thus, the susceptibility for electron (Eq. (5.4)) becomes:

$$\chi_e \approx \frac{1}{k^2\lambda_{De}^2}\left[1 + i\sqrt{\frac{\pi}{2}}\frac{(\omega - k_\parallel U_b)}{k_\parallel v_{te}} e^{-\xi_{0e}^2}\right] \tag{5.9}$$

For the protons and doubly charged Helium ions, we consider $\xi_{np,n\alpha} >> 1$, hence, Eq. (5.3) can be written as,

$$\chi_{p,\alpha} \approx \frac{1}{k^2\lambda_{Dp,\alpha}^2}\left[1 - \sum_{n=-\infty}^{\infty}\frac{\omega\Gamma_n(b_{p,\alpha})}{\omega - n\Omega_{p,\alpha}} + i\sqrt{\frac{\pi}{2}}\sum_{n=-\infty}^{\infty}\frac{\omega\Gamma_n(b_{p,\alpha})e^{-\xi_{np,\alpha}^2}}{k_\parallel v_{tp,\alpha}}\right] \tag{5.10}$$

Since, proton cyclotron harmonics are being studied here, it is appropriate to assume $\omega \sim n\Omega_p$. Thus, the susceptibility for protons can be written as:

$$\chi_p \approx \frac{1}{k^2\lambda_{Dp}^2}\left[1 - \frac{\omega\Gamma_n(b_p)}{\omega - n\Omega_p} - G(b_p) + i\sqrt{\frac{\pi}{2}}\sum_{n=-\infty}^{\infty}\frac{\omega\Gamma_n(b_p)e^{-\xi_{np}^2}}{k_\parallel v_{tp}}\right] \tag{5.11}$$

where the function $G(b_p)$ is given by

$$G(b_p) = \sum_{m\neq n}\frac{\omega\Gamma_m(b_p)}{\omega - m\Omega_p} \tag{5.12}$$

The analytical expressions for $G(b_p)$ for n=1 and 2, as given by Eq. (5.12), have been derived by Kindel and Kennel (1971). For higher values of "n", the analytical expression for Eq. (5.12) is not easily tractable. Therefore, $G(b_p)$ has to be evaluated numerically to study the higher harmonics. A computer program has been developed to evaluate Eq. (5.12) in MATLAB. The numerical results have been verified with the results obtained from the analytical expression obtained for fundamental mode. After the verification, it has been applied to obtain the results for other harmonics studied here.

With the assumption that $\omega \sim n\Omega_p$, susceptibility for helium (α) component in Eq. (5.10) becomes

$$\chi_\alpha \approx \frac{1}{k^2\lambda_{D\alpha}^2}\left[1-2\sum_{n=-\infty}^{\infty}\Gamma_n(b_\alpha)+i\sqrt{\frac{\pi}{2}}\sum_{n=-\infty}^{\infty}\frac{\omega\Gamma_n(b_\alpha)e^{-\xi_{n\alpha}^2}}{k_\parallel v_{t\alpha}}\right] \tag{5.13}$$

Here we have used the fact that $\Omega_\alpha = \frac{\Omega_p}{2}$.

Since, $\sum_{n=-\infty}^{\infty}\Gamma_n(b_\alpha)=1$, therefore, $1-2\sum_{n=-\infty}^{\infty}\Gamma_n(b_\alpha)=-1$, and hence Eq. (5.13) can be approximated to:

$$\chi_\alpha \approx \frac{1}{k^2\lambda_{D\alpha}^2}\left[-1+i\sqrt{\frac{\pi}{2}}\sum_{n=-\infty}^{\infty}\frac{\omega\Gamma_n(b_\alpha)e^{-\xi_{n\alpha}^2}}{k_\parallel v_{t\alpha}}\right] \tag{5.14}$$

The dispersion relation for proton cyclotron mode can be obtained by combining the Eq. (5.9), Eq. (5.11) and Eq. (5.14) and can be written as:

$$\begin{aligned}1+\frac{1}{k^2\lambda_{De}^2}\left[1+i\sqrt{\frac{\pi}{2}}\frac{(\omega-k_\parallel U_b)e^{-\xi_{0e}^2}}{k_\parallel v_{te}}\right]+\\ \frac{1}{k^2\lambda_{Dp}^2}\left[1-\frac{\omega\Gamma_n(b_p)}{\omega-n\Omega_p}-G(b_p)+i\sqrt{\frac{\pi}{2}}\sum_{n=-\infty}^{\infty}\frac{\omega\Gamma_n(b_p)e^{-\xi_{np}^2}}{k_\parallel v_{tp}}\right]\\ +\frac{1}{k^2\lambda_{D\alpha}^2}\left[-1+i\sqrt{\frac{\pi}{2}}\sum_{n=-\infty}^{\infty}\frac{\omega\Gamma_n(b_\alpha)e^{-\xi_{n\alpha}^2}}{k_\parallel v_{t\alpha}}\right]=0\end{aligned} \tag{5.15}$$

The dispersion relation Eq. (5.15) contains real and imaginary parts as has been described earlier (refer to Eq. (5.6))and can be separated out. The real part, D_r, is given by:

$$D_r = 1+\frac{1}{k^2\lambda_{De}^2}-\frac{1}{k^2\lambda_{D\alpha}^2}+\frac{1-G(b_p)}{k^2\lambda_{Dp}^2}-\frac{\Gamma_n(b_p)}{k^2\lambda_{Dp}^2}-\frac{n\Omega_p}{\omega_r-n\Omega_p}\frac{\Gamma_n(b_p)}{k^2\lambda_{Dp}^2} \tag{5.16}$$

and imaginary part, D_i, is given by:

$$D_i = \sqrt{\frac{\pi}{2}}\frac{1}{k^2\lambda_{De}^2}\frac{(\omega_r - k_\parallel U_b)e^{-\xi_{0e}^2}}{k_\parallel v_{te}} + \sqrt{\frac{\pi}{2}}\frac{1}{k^2\lambda_{Dp}^2}\sum_{n=-\infty}^{\infty}\frac{\omega_r\Gamma_n(b_p)e^{-\xi_{np}^2}}{k_\parallel v_{tp}} + \sqrt{\frac{\pi}{2}}\frac{1}{k^2\lambda_{D\alpha}^2}\sum_{n=-\infty}^{\infty}\frac{\omega_r\Gamma_n(b_\alpha)e^{-\xi_{n\alpha}^2}}{k_\parallel v_{t\alpha}} \tag{5.17}$$

Assuming that $\omega_r \sim n\Omega_p$, the real frequency can be obtained from Eq. (5.16) and written in the following form:

$$\omega_r = n\Omega_p[1+\Delta_p] \tag{5.18}$$

where

$$\Delta_p = \frac{\Gamma_n(b_p)}{1+k^2\lambda_{Dp}^2 - \Gamma_n(b_p) - G(b_p) + \frac{T_p n_{0e}}{T_e n_{0p}}(1 - \frac{T_e z_\alpha^2 n_{0\alpha}}{T_\alpha n_{0e}})} \tag{5.19}$$

The assumption of $\omega_r \sim n\Omega_p$ is justified provided Δ_p is much smaller than 1. The growth/damping rates for proton cyclotron harmonics can be obtained by using the definition given by Eq. (5.8), and be written in a simple form as under:

$$\frac{\gamma}{\Omega_p} = -n\Delta_p^2\frac{k^2\lambda_{Dp}^2}{\Gamma_n(b_p)}D_i \tag{5.20}$$

For any instability to grow, there is a certain threshold required. In the present case, it is apparent from Eq. (5.20) that for proton cyclotron harmonic instability to occur, a condition $D_i < 0$ has to be satisfied. In the next subsection, analytical results on the helium cyclotron harmonics is presented.

5.2.2 Helium cyclotron harmonics

In the previous section, it has been shown how proton cyclotron harmonics and its instability is studied analytically under the approximation $\omega \sim n\Omega_p$. In this subsection, similar method is adopted to study the instability associated with helium cyclotron harmonics. Therefore, at the outset, it is assumed that frequency $\omega \sim n\Omega_\alpha$. Thus, using the fact that $\Omega_p = 2\Omega_\alpha$ from Eq. (5.10), the contribution of protons can be written as

$$\chi_p \approx \frac{1}{k^2\lambda_{Dp}^2}\left[1 + \sum_{n=-\infty}^{\infty}\Gamma_n(b_p) + i\sqrt{\frac{\pi}{2}}\sum_{n=-\infty}^{\infty}\frac{\omega\Gamma_n(b_{p,\alpha})e^{-\xi_{np,\alpha}^2}}{k_\parallel v_{tp,\alpha}}\right] \tag{5.21}$$

Consequently, the contribution of the protons is approximated by using the Bessel function identities used to derive Eq. (5.14) and can be written as:

$$\chi_p = \frac{1}{k^2\lambda_{Dp}^2}\left[2 + i\sqrt{\frac{\pi}{2}}\sum_{n=-\infty}^{\infty}\frac{\omega\Gamma_n(b_p)}{k_\parallel v_{tp}}e^{-\xi_{np}^2}\right] \tag{5.22}$$

Further, the corresponding term for helium ions is obtained as under:

$$\chi_\alpha \approx \frac{1}{k^2\lambda_{D\alpha}^2}\left[1 - \frac{\omega\Gamma_n(b_\alpha)}{\omega - n\Omega_\alpha} - G(b_\alpha) + i\sqrt{\frac{\pi}{2}}\sum_{n=-\infty}^{\infty}\frac{\omega\Gamma_n(b_\alpha)}{k_\parallel v_{t\alpha}}e^{-\xi_{n\alpha}^2}\right] \tag{5.23}$$

The dispersion relation for Helium cyclotron harmonics is obtained by combining the Eq. (5.9),Eq. (5.22), Eq. (5.23) and can be expressed as:

$$\begin{aligned}1 + \frac{1}{k^2\lambda_{De}^2}\left[1 + i\sqrt{\frac{\pi}{2}}\frac{(\omega - k_\parallel U_b)}{k_\parallel v_{te}}e^{-\xi_{0e}^2}\right] + \frac{1}{k^2\lambda_{Dp}^2}\left[2 + i\sqrt{\frac{\pi}{2}}\sum_{n=-\infty}^{\infty}\frac{\omega\Gamma_n(b_p)}{k_\parallel v_{tp}}e^{-\xi_{np}^2}\right] \\ + \frac{1}{k^2\lambda_{D\alpha}^2}\left[1 - \frac{\omega\Gamma_n(b_\alpha)}{\omega - n\Omega_\alpha} - G(b_\alpha) + i\sqrt{\frac{\pi}{2}}\sum_{n=-\infty}^{\infty}\frac{\omega\Gamma_n(b_\alpha)}{k_\parallel v_{t\alpha}}e^{-\xi_{n\alpha}^2}\right] = 0\end{aligned} \tag{5.24}$$

Here, the function $G(b_\alpha)$ can be written as,

$$G(b_\alpha) = \sum_{m\neq n}\frac{\omega\Gamma_m(b_\alpha)}{\omega - m\Omega_\alpha} \tag{5.25}$$

Following the same procedure as adopted in the derivation of Eqs. (5.18) to (5.20), real frequency from Eq. (5.24) is obtained as,

$$\omega_r = n\Omega_\alpha[1 + \Delta_\alpha] \tag{5.26}$$

where

$$\Delta_\alpha = \frac{\Gamma_n(b_\alpha)}{1 + k^2\lambda_{D\alpha}^2 - \Gamma_n(b_\alpha) - G(b_\alpha) + \frac{T_\alpha n_{0e}}{z_\alpha^2 T_e n_{0\alpha}}(1 + 2\frac{T_e n_{0p}}{T_p n_{0e}})} \tag{5.27}$$

The assumption of $\omega_r \sim n\Omega_\alpha$ is justified provided Δ_α is much smaller than 1. The growth/damping rate for helium cyclotron modes can be written as,

$$\frac{\gamma}{\Omega_\alpha} = -n\Delta_\alpha^2\frac{k^2\lambda_{D\alpha}^2}{\Gamma_n(b_\alpha)}D_i \tag{5.28}$$

The threshold required for helium cyclotron harmonic instability is similar to proton cyclotron instability, i.e., $D_i < 0$. The theoretical results obtained in this section are general in nature and can be applied to laboratory or space plasmas.

It must be pointed out that due to the assumptions $\omega \sim n\Omega_p$ and $\omega \sim n\Omega_\alpha$, $\xi_{np,n\alpha} >> 1$, both protons and doubly charged Helium ions are non-resonant. This means that our analysis is not valid when $\omega = n\Omega_p$ or $\omega = n\Omega_\alpha$ as then both ξ_{np} and $\xi_{n\alpha}$ would be $<<1$. Hence, the present analytical method avoids exact proton and Helium cyclotron resonances. A different analytical approach is needed to deal with exact resonances

5.3 Numerical analysis

In this section, numerical results are shown pertaining to the proton and Helium cyclotron instabilities. Numerical results are obtained by solving Eqs. (5.18) and (5.20) for real frequency and growth rate, respectively for proton cyclotron harmonics and for Helium cyclotron harmonics, the real frequency and growth rate, respectively are solution of Eqs. (5.26) and (5.28). We must mention here that, in the numerical results shown in the Sects. 5.3.1 and 5.3.2, all the assumptions made in deriving the Eqs. (5.18), (5.20), (5.26) and (5.28) are satisfied. Further, using plasma parameters from Okuda et al. (1981b) (cf. their Fig. 2) and Rosenberg and Merlino (2009) (cf. their Fig. 1) and by putting Helium ion density to zero, we are able to confirm that the growth rate for fundamental mode peaks near $k\rho_p \sim 1$ in both the cases. However, with increase in angle of propagation, the growth rate peaks at $k\rho_p > 1$, hence, we would like to emphasize that the peak growth rate is parameter dependent and does not necessarily always peaks at $k\rho_p \sim 1$. It is important to mention here that while carrying out the numerical computations of the growth rate/damping for proton and Helium harmonics, the damping arising due to proton and Helium ions has been taken into account.

5.3.1 Proton cyclotron instability

For proton cyclotron harmonics, we have normalized the various physical parameters in the following manner: frequencies are normalized with cyclotron frequency of proton, wavenumber with Larmor radius of proton $\rho_p = \frac{v_{thp}}{\Omega_p}$. The electron beam speed has been normalized with the thermal velocity of electron. The densities are normalized with total electron density at equilibrium. For numerical computations to study the proton cyclotron instability, the following fixed plasma parameters are used: $z_\alpha = 2$, $\frac{\omega_p}{\Omega_p} = 60$, $\frac{U_b}{v_{te}} = 0.80$, $\frac{n_{0\alpha}}{n_{0e}} = 0.05$, $\frac{m_p}{m_\alpha} = 0.25$, $\frac{m_p}{m_e} = 1837$, $\frac{T_e}{T_p} = 2$, $\frac{T_\alpha}{T_p} = 2$. In Fig. 5.1, the normalized frequency and normal-

ized growth rates of proton cyclotron instability are shown with $k_\perp \rho_p$ for two different values of angle of propagation, θ. The results in the panels Fig. 5.1a and Fig. 5.1b are shown for $\theta = 88.5^0$ and $\theta = 89^0$, respectively. Top and bottom panels of all the figures presented here, respectively show the real frequency and corresponding growth rates for each harmonic. The number 'n' mentioned on the curves refer to respective harmonic. In the top left panel, 5 harmonics are plotted for which all the relevant conditions on electron, proton and ions are satisfied. Though several other harmonics also satisfy the assumptions, we have omitted those as they are damped modes. From the fundamental harmonic to 3$^{\text{rd}}$ harmonic, the peak growth rate decreases gradually and for the 4$^{\text{th}}$ and the 5$^{\text{th}}$ harmonic, it decreases rapidly. In this figure and all subsequent figures, curves are restricted to wave number ranges where growth rates are positive. The peak growth for fundamental harmonic occurs at $k_\perp \rho_p \approx 1.5$ with $\omega_r \approx 1.2\Omega_p$ and the absolute value of the argument of plasma dispersion function for protons, i.e., $\frac{\omega - \Omega_p}{\sqrt{2} k_\parallel v_{tp}} \approx 3.8$ and it is larger for lower wavenumbers and decreases with increasing wavenumbers. This pattern is seen for all the harmonics. For an angle of propagation $\theta = 89.0^0$ (Fig. 5.1b), though the plasma assumptions are satisfied for large number of harmonics, however, growth is observed only upto 3$^{\text{rd}}$ harmonic. Also, the wave number for which these waves are excited shifts towards higher side with each higher harmonic. It is observed that growth rate decreases with each harmonic and the peak growth rate for the fundamental harmonic is the largest for both the angle of propagations. The peak growth rate for fundamental harmonics is larger for $\theta = 88.5^0 (\gamma/\Omega_p \approx 0.048)$ in comparison to $\theta = 89.0^0 (\gamma/\Omega_p = 0.027)$.

Fig. 5.2 shows the effect of variations of $\frac{n_{0\alpha}}{n_{0e}}$ on proton cyclotron real frequency and growth rate. With the increase in $\frac{n_{0\alpha}}{n_{0e}}$, the trend in the extent of range in wave number is similar to as shown in Fig. 5.1 for the chosen parameters of Fig. 5.1a. The growth rate increases slightly with increase in $\frac{n_{0\alpha}}{n_{0e}}$ value. For instance, the maximum value of $\frac{\gamma}{\Omega_p}$ for the first harmonic for $\frac{n_{0\alpha}}{n_{0e}} = 0.03$ is 0.044 (Fig. 5.2a)with maximum number of excited harmonics to be 5 and the corresponding value for $\frac{n_{0\alpha}}{n_{0e}} = 0.07$ is 0.052 (Fig. 5.2b) and it has already been shown in Fig. 5.1a, that for $\frac{n_{0\alpha}}{n_{0e}} = 0.05$, the value of $\frac{\gamma}{\Omega_p}$ peaks at 0.048 with maximum number of excited harmonics to be 5. The numerical computations show that for proton harmonics, the contribution of the helium damping (third term in Eq. (5.17)) is negligible. However, damping due to protons (second term in Eq. (5.17)) reduces with the increase in the number

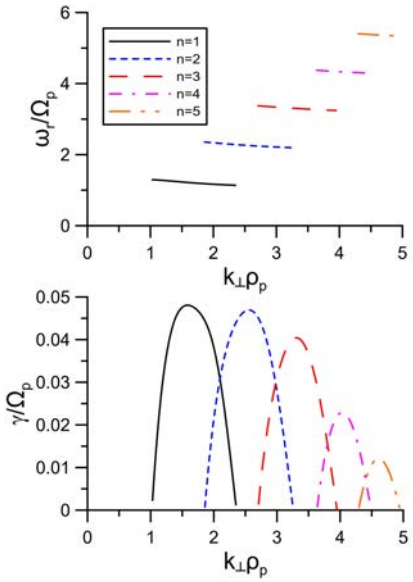

(a) $\theta = 88.5^0$

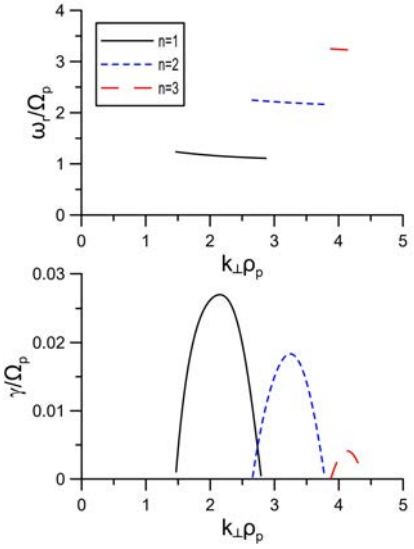

(b) $\theta = 89.0^0$

Figure 5.1: Normalized real frequency ω_r/Ω_p and growth rate γ/Ω_p for electrostatic proton cyclotron instability with respect to $k_\perp \rho_p$ for $\theta = 88.5^0$ [panel (a)] and $\theta = 89.0^0$ [panel (b)]. Other fixed plasma parameters are $z_\alpha = 2$, $\frac{\omega_p}{\Omega_p} = 60$, $\frac{U_b}{v_{te}} = 0.80$, $\frac{n_{0\alpha}}{n_{0e}} = 0.05$, $\frac{m_p}{m_\alpha} = 0.25$, $\frac{m_p}{m_e} = 1837$, $\frac{T_e}{T_p} = 2$, $\frac{T_\alpha}{T_p} = 2$

.

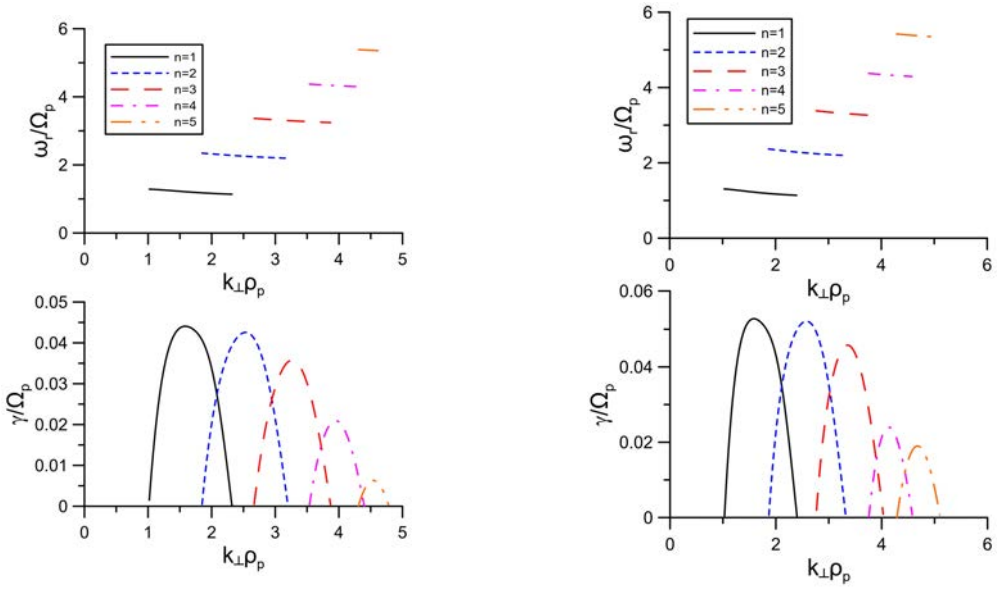

(a) $\frac{n_{0\alpha}}{n_{0e}} = 0.03$ (b) $\frac{n_{0\alpha}}{n_{0e}} = 0.07$

Figure 5.2: Normalized real frequency ω_r/Ω_p and growth rate γ/Ω_p for electrostatic proton cyclotron instability with respect to $k_\perp \rho_p$ for $\frac{n_{0\alpha}}{n_{0e}} = 0.03$ [panel (a)] and $\frac{n_{0\alpha}}{n_{0e}} = 0.07$ [panel (b)]. All other parameters are the same as in Fig. 5.1a

density of the helium ions. Thus, growth rate increases with increase in the number density of the helium ions.

In Fig. 5.3, the effect of the variation of $\frac{T_\alpha}{T_p}$ on the real frequency and growth rate is shown for the parameters of Fig. 5.1a and for $\frac{T_\alpha}{T_p} = 5$ (Fig. 5.3a) and $\frac{T_\alpha}{T_p} = 10$ (Fig. 5.3b). It is observed that the growth decreases slightly with the increase in $\frac{T_\alpha}{T_p}$.It has also to be noted that for $\frac{T_\alpha}{T_p} = 5$ & 10 only modes upto 4^{th} harmonic can be excited instead of 5^{th} harmonic. For each harmonic, the maximum normalized growth rate occurs for $\frac{T_\alpha}{T_p} = 2$ Fig. 5.1a (the maximum values of $\frac{\gamma}{\Omega_p}$ are 0.048, 0.042, 0.040 for $\frac{T_\alpha}{T_p} = 2, 5, 10$, respectively). The similar trend is observed for all other harmonics. Also, for a fixed value of $\frac{T_\alpha}{T_p}$, the peak value of the growth rate decreases continuously for higher harmonics.

We have analyzed the effect of electron streaming on the proton cyclotron harmonics in Fig. 5.4 on the normalized real frequency and growth rates for the parameters of Fig. 5.1a. The results are displayed in two panels, i.e., panel Fig. 5.4a ($\frac{U_b}{v_{te}} = 0.6$) and panel Fig. 5.4b ($\frac{U_b}{v_{te}} = 0.7$). It can be seen that for $\frac{U_b}{v_{te}} = 0.6$ Fig. 5.4a, only first two harmonics can be excited, with the peak value of growth rate of fundamental harmonic being 0.023 at $k\rho_p \sim 1.8$. On

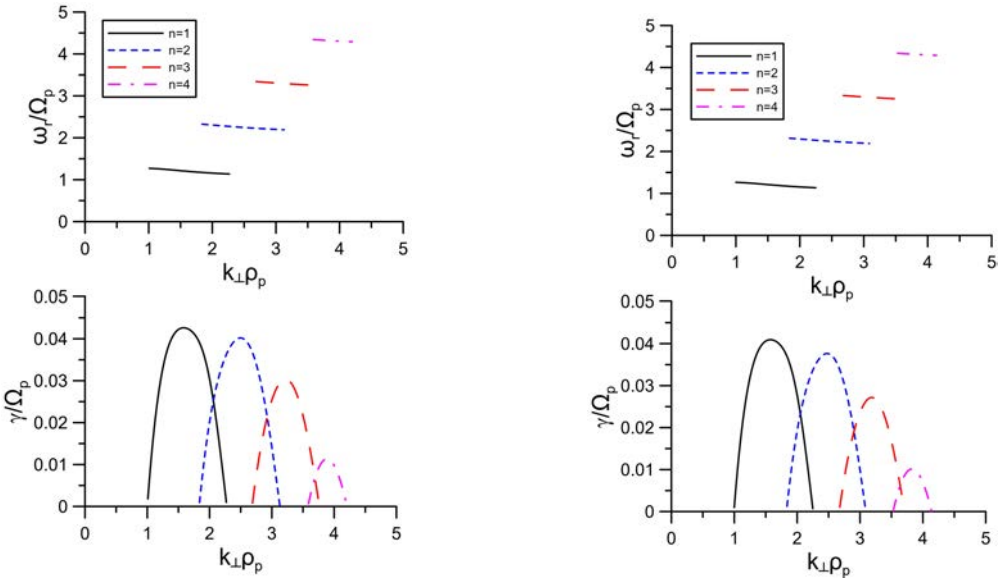

(a) $\frac{T_\alpha}{T_p} = 5$ (b) $\frac{T_\alpha}{T_p} = 10$

Figure 5.3: Normalized real frequency ω_r/Ω_p and growth rate γ/Ω_p for electrostatic proton cyclotron instability with respect to $k_\perp \rho_p$ for $\frac{T_\alpha}{T_p} = 5$ [panel (a)] and $\frac{T_\alpha}{T_p} = 10$ [panel (b)]. All other parameters are the same as in Fig. 5.1a

the other hand, for $\frac{U_b}{v_{te}} = 0.7$ (Fig. 5.4b), it is observed that upto 3$^{\text{rd}}$ harmonic can be excited. Further increase in $\frac{U_b}{v_{te}}$ value to 0.8 (refer to Fig. 5.1a) upto 5$^{\text{th}}$ harmonic become unstable. The peak value of growth rate for each harmonic increases with increase in the value of electron beam speed. It is also found that for each harmonic the peak value of growth rate occurs at smaller value of $k\rho_p$, e.g., peak value of $\frac{\gamma}{\Omega_p}$ for fundamental harmonic for $\frac{U_b}{v_{te}} = 0.6, 0.7, 0.8$ occurs at $k\rho_p \sim 1.8, \sim 1.7, \sim 1.5$, respectively. This is also true for all other harmonics. In the next subsection, numerical results on Helium cyclotron instability are discussed.

5.3.2 Helium cyclotron instability

In this subsection, the effect of various parameters on Helium cyclotron instability is studied. The frequencies are normalized with Helium cyclotron frequency, wavenumber with Larmor radius of Helium $\rho_\alpha = \frac{v_{th\alpha}}{\Omega_\alpha}$. The electron beam speed has been normalized with the thermal velocity of electron. The densities are normalized with total electron density at equilibrium. Here we have plotted the real frequency and growth rates versus $k_\perp \rho_\alpha$. The curves have been

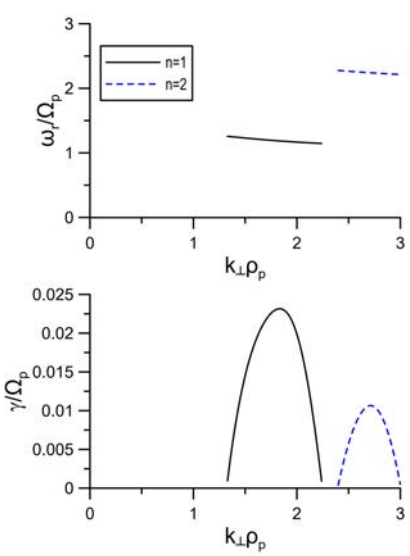

(a) $\frac{U_b}{v_{te}} = 0.6$

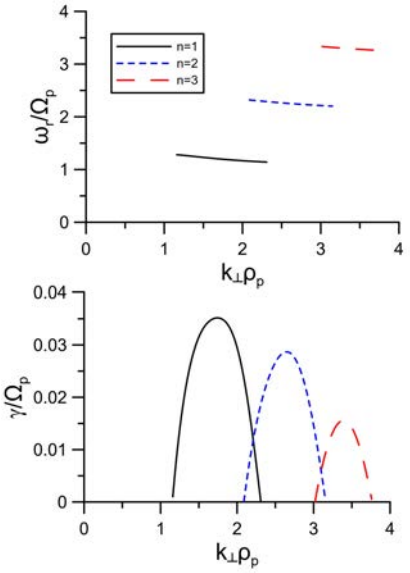

(b) $\frac{U_b}{v_{te}} = 0.7$

Figure 5.4: Normalized real frequency ω_r/Ω_p and growth rate γ/Ω_p for electrostatic proton cyclotron instability with respect to $k_\perp\rho_p$ for $\frac{U_b}{v_{te}} = 0.6$ [panel (a)] and $\frac{U_b}{v_{te}} = 0.7$ [panel (b)]. All other parameters are the same as in Fig. 5.1a

limited by the plasma conditions imposed on the argument of plasma dispersion function or wherever the damping occur. It is important to mention that heavier ion cyclotron instability or its harmonics are more difficult to excite than the proton cyclotron instability.

In Figs. 5.5a and 5.5b, normalized real frequency and growth rates are plotted for $\theta = 89.5^0$ and $\theta = 89.7^0$, respectively. The fixed plasma parameters are $z_\alpha = 2$, $\frac{\omega_p}{\Omega_p} = 60$, $\frac{U_b}{v_{te}} = 0.80$, $\frac{n_{0\alpha}}{n_{0e}} = 0.10$, $\frac{m_p}{m_\alpha} = 0.25$, $\frac{m_p}{m_e} = 1837$, $\frac{T_e}{T_p} = 10$, $\frac{T_\alpha}{T_p} = 0.6$. Interesting feature of Helium harmonic is that for all the variation that had been undertaken, only the odd harmonics are getting exited, unless stated otherwise. For $\theta = 89.5^0$, first harmonic and third harmonic are excited and for $\theta = 89.7^0$, first, third and fifth harmonics are excited. When the angle is increased from $\theta = 89.5^0$ to $\theta = 89.7^0$, it can be seen that the growth rate decreases substantially (Fig. 5.5). Also with increasing value of angle of propagation, the peak growth rate occurs at higher value of $k_\perp\rho_\alpha$. The peak growth rate for fundamental harmonic of helium for $\theta = 89.5^0$ is $\gamma/\Omega_i \approx 2.2 \times 10^{-3}$ at $k_\perp\rho_i \approx 1.2$. The corresponding absolute value of the argument of the plasma dispersion function, $\frac{\omega - \Omega_{p\alpha}}{\sqrt{2}k_\parallel v_{t\alpha}} \approx 4.8$ whereas it is larger for lower values of wavenumbers and decreases with increasing wave number. This pattern is seen for all the results presented.

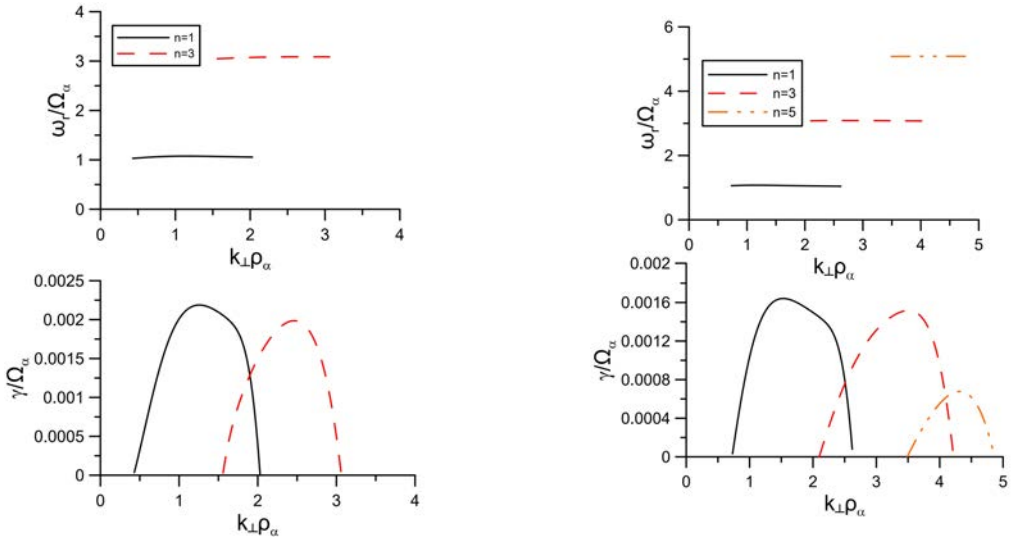

(a) $\theta = 89.5^0$ (b) $\theta = 89.7^0$

Figure 5.5: Normalized real frequency ω_r/Ω_p and growth rate γ/Ω_p for electrostatic Helium cyclotron instability with respect to $k_\perp \rho_\alpha$ for $\theta = 89.5^0$ [panel (a)] and $\theta = 89.7^0$ [panel (b)]. Fixed plasma parameters are $z_\alpha = 2, \frac{\omega_p}{\Omega_p} = 60, \frac{U_b}{v_{te}} = 0.80, \frac{n_{0\alpha}}{n_{0e}} = 0.10, \frac{m_p}{m_\alpha} = 0.25, \frac{m_p}{m_e} = 1837, \frac{T_e}{T_p} = 10, \frac{T_\alpha}{T_p} = 0.6$.

In Fig. 5.6, we have plotted the real frequency and growth rate for $\frac{n_{0\alpha}}{n_{0e}} = 0.08$ (Fig. 5.6a) and 0.12 (Fig. 5.6b) for parameters of Fig. 5.5b. For $\frac{n_{0\alpha}}{n_{0e}} = 0.08$, fundamental mode and third mode can be excited, however, for $\frac{n_{0\alpha}}{n_{0e}} = 0.10$ (Fig. 5.5b) 1st, 3rd and 5th harmonic can be excited. Finally, $\frac{n_{0\alpha}}{n_{0e}} = 0.12$, for the first time 2nd harmonic (even harmonic) can be excited along with 1^{st}, 3^{rd}, 5^{th} and 7^{th} harmonic. It is important to mention here that the growth rate increases substantially with the increase in Helium ion density. The numerical computations show that for helium harmonics, the contribution of the proton damping (second term in Eq. (5.17)) is negligible. However, damping due to helium ions (third term Eq. (5.17)) reduces with the increase in the number density of the helium ions. Thus, growth rate for Helium harmonics increases with increase in the number density of the helium ions.

The variation of $\frac{T_\alpha}{T_p}$ on the Helium cyclotron instability is shown in Fig. 5.7 for the parameters of Fig. 5.5b. It is observed that the growth rate decreases with increase in Helium ion temperature. Also, the number of harmonic that is getting excited decrease with increase in the Helium ion temperature.

In Fig. 5.8, the effect of variation of electron beam speed is shown on the Helium

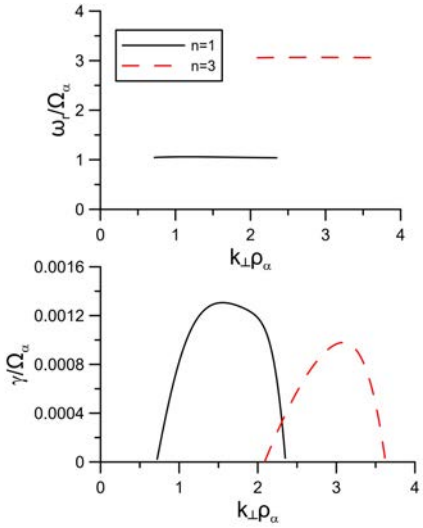

(a) $\frac{n_{0\alpha}}{n_{0e}} = 0.08$

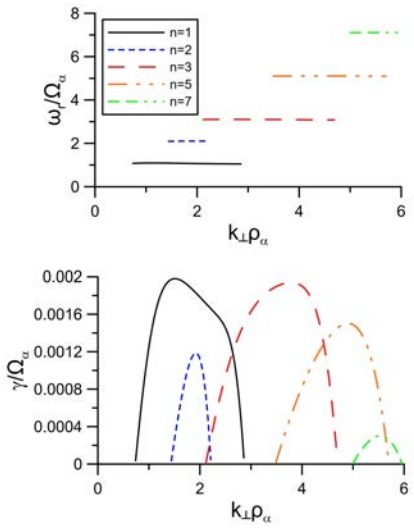

(b) $\frac{n_{0\alpha}}{n_{0e}} = 0.12$

Figure 5.6: Normalized real frequency ω_r/Ω_p and growth rate γ/Ω_p for electrostatic Helium cyclotron instability with respect to $k_\perp \rho_\alpha$ for $\frac{n_{0\alpha}}{n_{0e}} = 0.08$ [panel (a)] and $\frac{n_{0\alpha}}{n_{0e}} = 0.12$ [panel (b)]. All other parameters are the same as in Fig. 5.5b

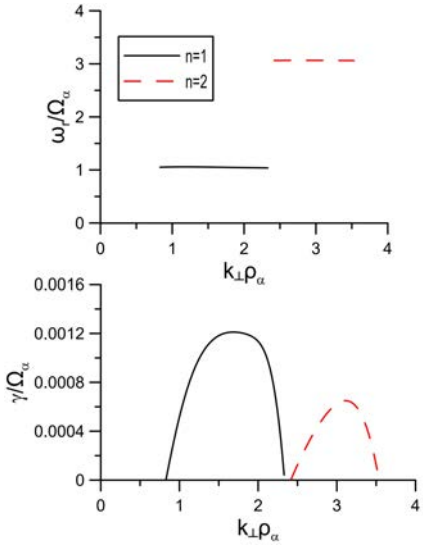

(a) $\frac{T_\alpha}{T_p} = 0.8$

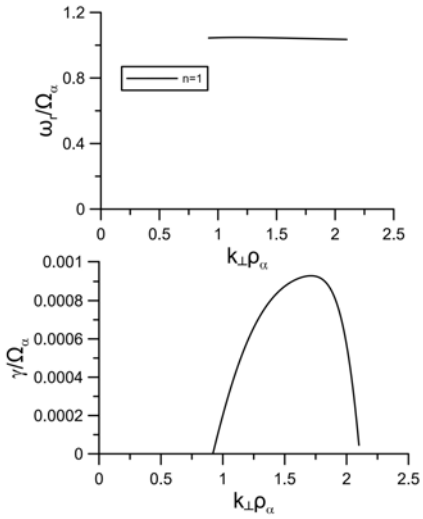

(b) $\frac{T_\alpha}{T_p} = 1.0$

Figure 5.7: Normalized real frequency ω_r/Ω_p and growth rate γ/Ω_p for electrostatic Helium cyclotron instability with respect to $k_\perp \rho_\alpha$ for $\frac{T_\alpha}{T_p} = 0.8$ [panel (a)] and $\frac{T_\alpha}{T_p} = 1.0$ [panel (b)]. All other parameters are the same as in Fig. 5.5b

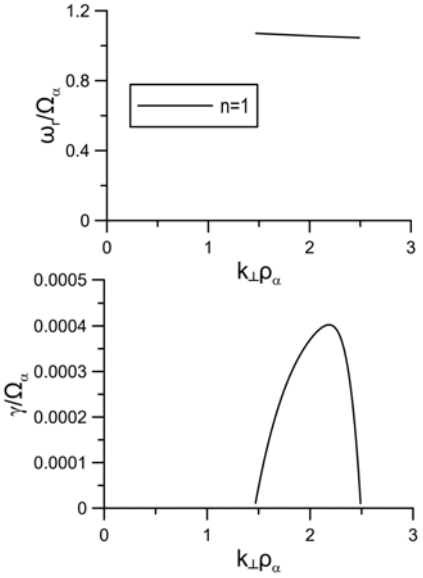

(a) $\frac{U_{be}}{b_{te}} = 0.4$

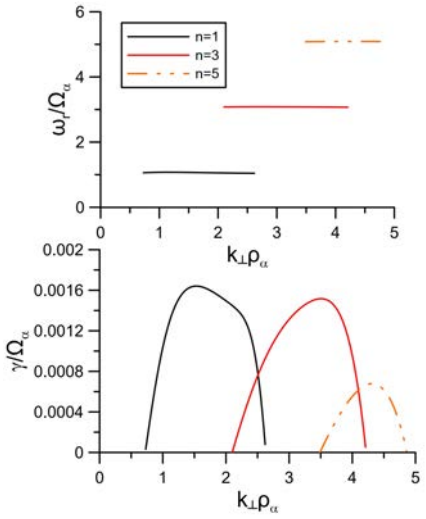

(b) $\frac{U_{be}}{b_{te}} = 0.8$

Figure 5.8: Normalized real frequency ω_r/Ω_p and growth rate γ/Ω_p for electrostatic Helium cyclotron instability with respect to $k_\perp \rho_\alpha$ for $\frac{U_{be}}{b_{te}} = 0.4$ [panel (a)] and $\frac{U_{be}}{b_{te}} = 0.8$ [panel (b)]. All other parameters are the same as in Fig. 5.5b

cyclotron instability. From Fig. 5.8a, it is seen that for $\frac{U_b}{v_{te}} = 0.4$ only fundamental mode is excited, however, at larger value of $\frac{U_b}{b_{te}} = 0.6$ (Fig. 5.5b) and $\frac{U_b}{b_{te}} = 0.8$ (Fig. 5.8b), not only growth rate increases but also upto second harmonic can be excited.

5.4 Conclusions

Electrostatic ion cyclotron instability associated with higher harmonics of proton and Helium cyclotron modes has been investigated. The magnetized plasma consists of three components: beam electron, protons and doubly charged Helium ions. The effect of various plasma parameters such as angle of propagation, number density and temperature of Helium ions and electron beam speed has been studied on the growth of proton and Helium cyclotron instability. In this study, we employed the method adopted by Kindel and Kennel (1971) and later on used by Rosenberg and Merlino (2009) to study the higher harmonics of electrostatic ion cyclotron waves. However, the method can not be applied at the exact proton and Helium harmonics, i.e., $\omega = n\Omega_p$ and $\omega = n\Omega_\alpha$.

It is found that growth rates decrease for both proton harmonics and Helium harmonics with increase in the angle of propagation, however a fewer number of proton harmonics and higher number of Helium harmonics are excited when the angle of propagation is increased. The conclusions drawn here are valid for both proton and Helium cyclotron instabilities.The extent of wavenumber for which both proton and Helium harmonics are unstable increases with increase in angle of propagation and the peak growth rate occurs at higher wave number. The increase in number density enhances the growth of the instability, however, temperature of ions has inverse effect on the instability. Further, as the electron beam speed is increased, the number excited harmonics increases and peak growth rate also increase and occur at the larger value of wave number. It is important to point out that heavy ion harmonics are difficult to excite.

Cluster observations of EIC waves in the nightside auroral region at $4R_E$ have been reported by Backrud et al. (2005a). They pointed out that these waves can be generated by electron beams. The total density of electrons was estimated to be 5cm^{-3} and proton cyclotron frequency, 7.6Hz. If we consider all ions as protons with small fraction of Helium ions, then, $\omega_p/\Omega_p \approx 60$ which we have assumed in our numerical calculations for all the figures presented here. For proton as well as Helium growth rate and real frequency calculations, we have taken $U_b/v_{te} = 0.8$. For the plasma parameters used in Fig. 5.1a, the peak growth rate for proton cyclotron fundamental mode comes out to be 360 mHz at $k_\perp \rho_p \approx 1.5$ and corresponding frequency is $\omega_r \approx 1.22\Omega_p = 9.3Hz$. Similarly, for Helium cyclotron fundamental mode (Fig. 5.5a), the peak growth rate is $\approx$ 16.6 mHz at $k_\perp \rho_\alpha \approx 1.2$ with corresponding frequency $\omega_r \approx 1.075\Omega_\alpha = 4.08$ Hz.

Here we have given an example of the auroral region where our results can be applied. However, the theory developed here is general in nature and can be applied to EIC observations in laboratory plasmas such as studied by Suszcynsky et al. (1989). The proton cyclotron waves and its harmonics have been observed in space plasmas. For example, proton cyclotron waves have been observed in auroral region by Cluster satellite (Backrud et al., 2005a), in magnetopause by THEMIS satellite (Tang et al., 2015). Proton cyclotron harmonics were observed by FAST satellite (Gavrishchaka et al., 2000).

Our results presented here and Rosenberg and Merlino (2009) results are similar in nature, e.g., they have reported that more number of harmonics can be generated with in-

crease in the heavy ion number density which we have also shown. Further, we have studied the effect of the variation of the more number of parameters, such as heavy ion temperature, angle of propagation, electron beam speed on the wave growth and harmonics. Our method can be applied to study the first and second harmonic of proton and fundamental harmonic of Helium cyclotron modes observed by the THEMIS satellite in the magnetopause Tang et al. (2015).

Chapter 6

Conclusions and scope for future work

6.1 Conclusions

The thesis addresses several aspects of the low-frequency waves in nonthermal plasmas where energetic particle distributions are used to model solar wind/lunar wake plasma. The coupling of electrostatic ion cyclotron (proton and helium) modes with fast and slow ion acoustic waves and electron-acoustic waves in multi component space plasmas is clearly brought out. The merging of two wave modes with each other forms an unstable region, thereby exciting one of the modes. Thesis also highlights this process and shown the generation of slow and fast ion acoustic waves by an electron beam in unmagnetised and magnetised solar wind and lunar wake regions. To study the coupling and merging processes a fluid theory approach has been used. The heavier ions such as doubly charged helium are the integral part of the solar wind/Lunar wake region and also can be found in magnetospheric regions such as auroral region. Using kinetic theory, the fundamental and higher order harmonics of proton as well as helium cyclotron waves are studied in the auroal region. These harmonics are generated by field aligned electron beam. The relevance of the theoretical results has been brought out in sync with observations in solar wind/lunar wake and magnetospheric plasmas. The highlight of the results is presented below:

6.1.1 Excitation of ion acoustic waves by electron beam in Lunar wake plasma

A linear theoretical model is developed to study the low frequency electrostatic waves in the lunar wake plasma taking inputs from Tao et al. (2012). The lunar wake plasma is modeled by fluid protons, fluid He^{++}, electron beam, and suprathermal electrons following kappa distribution. These results are presented in Chap. 2 and highlight is presented below:

- The numerical analysis of dispersion relation shows the existence of 6 modes. These are two electron acoustic modes (modes 1 and 6), two fast ion acoustic modes (modes 2 and 5), and two slow ion acoustic modes (modes 3 and 4). Modes 1, 2 and 3 have positive phase speed, while modes 4, 5, and 6 have negative phase speed.

- Mode 6 gets affected most with increase in electron beam velocity. In addition, phase speed turns from negative to positive with increase in electron beam velocity.

- Initially, mode 6 starts to merge with slow ion acoustic mode and then with fast ion acoustic mode generating the electron beam driven slow and fast ion acoustic waves, respectively. These modes are unstable with finite growth rate.

- It is seen that growth rate of electron beam driven slow ion-acoustic mode decreases with increase in number density and temperature of electron beam. An increase in number density of ions and temperatures of ions and protons increases the growth rate of the electron beam driven slow ion-acoustic mode.

- The growth of rate electron beam driven fast ion-acoustic mode increases with increase in electron beam density and decreases with an increase in ion number density and temperatures of the electron beam, ions, and protons.

- The frequency corresponding to the maximum growth rate of the electron beam driven slow ion-acoustic mode is $\omega_r = 0.03\omega_{pe}$ and for the electron beam driven fast ion-acoustic mode is $\omega_r = 0.2\omega_{pe}$. These frequency values agree very well with the observed low-frequency waves $\omega \approx 0.01\omega_{pe}$(WB1) and high frequency waves $\omega \approx$0.1 -0.4ω_{pe}(WB2/WB3) in the Lunar wake by Tao et al. (2012)

6.1.2 Electrostatic ion cyclotron and ion acoustic waves coupling in solar wind plasma

In this chapter (Chap. 3), the coupling of electrostatic ion cyclotron and ion acoustic waves is examined in three component magnetized plasma consisting of electrons, protons, and doubly charged Helium particles. The electrons are taken to be having superthermal kappa distribution. Protons and doubly charged Helium ions follow fluid equation. This model is used to examine the coupling of waves in solar wind plasma. The linear dispersion relation derived for the system is analyzed both analytically and numerically.

- The dispersion relation reveals that for parallel propagation, electrostatic ion cyclotron (proton and helium cyclotron) and ion acoustic (slow and fast) modes are decoupled.
- The coupling between acoustic waves and cyclotron wave is seen for oblique propagation.
- Increasing the angle of propagation increases the separation between acoustic and cyclotron modes indicating weakening of the strength of coupling.
- With the increase in angle of propagation to 90°, the acoustic modes vanish and only cyclotron modes remain in the system.
- For Helium cyclotron mode, increase in Helium ion concentration increases the wave frequency after $k\rho_p \geq 0.3$, whereas other modes do not show any change.
- Decrease in the value of κ decreases the frequencies of all modes for a certain $k\rho_p$ range, except for the slow ion acoustic modes where effect of superthermality is insignificant.
- Increase in the Helium ion temperature substantially increases the frequency of Helium cyclotron mode.

6.1.3 Excitation of electrostatic ion cyclotron waves and ion acoustic waves by electron beam in solar wind/Lunar wake plasma

The effect of magnetic field which was neglected in the theoretical model considered in Chap. 2 has been included in this chapter (Chap. 4). The inclusion of magnetic field and a finite beam increases the complexity of the dispersion relation, which can only be analyzed numerically.

- A general dispersion relation is derived for four component magnetized plasma comprising of fluid proton and doubly charged Helium ion, kappa electron and kappa beam electron.

- The numerical analysis of dispersion relation reveals the presence of electron, proton and Helium cyclotron modes and slow, fast ion and electron acoustic modes in the system. For parallel propagation without electron streaming, the dispersion curves are perfectly symmetrical about x-axis.

- When the dispersion relation is analyzed numerically for oblique propagation and by putting the beam velocity to zero, the coupling between various modes can be seen. Coupling occurs at 12 different places- compared to 8 different place in Chap. 3. The strength of coupling decreases with increase in the angle of propagation. For perpendicular direction, only cyclotron modes exist.

- When the dispersion relation is analyzed for various angles of propagation with finite electron beam velocity, the merging and coupling of various electrostatic modes are seen in this system.

- It is seen that for smaller angle of propagation, proton and helium cyclotron modes are excited. With increase in the angle of propagation, proton cyclotron mode is not excited, instead slow ion acoustic mode and Helium cyclotron mode are excited. Subsequent increase in the angle of propagation (for large oblique angles) drives both slow and fast ion acoustic modes unstable, while the Helium cyclotron mode is stable. The growth rate of fast and slow ion acoustic modes continuously diminishes beyond $\theta = 50^{\circ}$ and at perpendicular propagation, no modes ae excited.

6.1.4 Higher harmonic instability of electrostatic ion cyclotron waves in auroral plasma

In a three component magnetized plasma comprising of beam electrons, protons and doubly charged Helium ions, electrostatic ion cyclotron instability pertaining to the higher harmonics of proton and Helium cyclotron modes is investigated with the help of kinetic theory. These results are presented in Chap. 5 and salient findings are listed below:

- It is seen that with an increase in the angle of propagation fewer harmonics of proton cyclotron waves and higher number of harmonics of Helium cyclotron modes are excited. The growth rates for all these modes are reduced.
- The wave number regime in which proton and Helium harmonics become unstable increases with increase in the angle of propagation with growth rate peaking at higher wave number.
- Growth rate of both the instability increases with increase in number density of Helium ions. On the other hand, increase in temperature of Helium ions decreases it.
- With an increase in electron beam speed, the number of excited harmonics and its peak growth rate increases. Furthermore, growth rate peaks at higher value of wave number.
- Through our analysis, we could show that for two-component electron-ion plasma growth rate peaks at $k\rho_p \sim n$ (n being harmonic number) for each harmonic as suggested by Okuda et al. (1981b). However, in multi-component plasma growth rate is parameter dependent and so it does not necessarily always peaks at $k\rho_p \sim n$.
- A peculiar observation that came out from this study is that mainly odd harmonics of Helium cyclotron mode are excited for most of the parametric investigation that we have undertaken. This kind of behavior has not been observed or reported anywhere.

6.2 Suggestion for the future work

This thesis emphasize upon the use of energetic particles to understand various processes in space plasmas. The theoretical model developed in Chaps. 2 and 4 could be helpful in un-

derstanding the various linear waves that are observed in solar wind/Lunar wake plasma. As there is a renewal of interest in lunar wake region, our theoretical findings can be put to test with the help of data from upcoming lunar missions like Chandrayaan-2 (India), Chang'e-4 (China), Luna (Russia) etc. (Popel et al., 2015; Popel and Morozova, 2017). Furthermore, the plasma model discussed in Chaps. 2 and 4 can be modified to incorporate superthermal electron beam and kinetic theory to study the excitation of various plasma modes and compare results with simulation studies conducted by Tao et al. (2012). Theoretical model can be specifically developed to see the coupling of ion cyclotron and ion acoustic waves as reported by Tang et al. (2015). There one has to consider the multi-component plasma based on the observations by THEMIS. The electrostatic ion cyclotron (EIC) instability is useful to explain the heating of solar corona (Hinata, 1980; Luhn, 1984). Hinata (1980) has shown that coronal plasma is heated up to a temperature of a few million Kelvin degrees when the electron drift velocity is near or above the critical value for EIC instability. Energy transfer can take place between particle and waves, which results in heating of particle distribution depending upon the initial condition of nonlinearly coupled system of waves and gyrating ions (Luhn, 1984). Therefore, the model that is developed in Chap. 5 could be further extended to measure the ion heating associated with EIC waves from data that would be collected from recently launched Parkar Solar Probe. We have reported the excitation of odd harmonics of Helium cyclotron modes, which has not been observed anywhere. A rigorous data analysis may reveal existence of these wave modes. Further, for harmonic instability of ion cyclotron waves, we have considered Maxwellian particle distribution which can be extended to include nonthermal distribution.

Bibliography

R. R. Anderson, G. K. Parks, D. A. Eastman, T. E. andGurnett, and L. A. Frank. Plasma waves associated with energetic particles streaming into the solar wind from the earth's bow shock. *J. Geophys. Res. Space*, 86(A6), 1981. doi: 10.1029/ja086ia06p04493.

M. André. Dispersion surfaces. *J. Plasma Phys.*, 33(01), 1985. doi: 10.1017/s0022377800002270.

M. André, H. Koskinen, G. Gustafsson, and R. Lundin. Ion waves and upgoing ion beams observed by the viking satellite. *Geophys. Res. Lett.*, 14(4), 1987. doi: 10.1029/GL014i004p00463.

M. Backrud, M. André, A. Balogh, S. Buchert, N. Cornilleau-Wehrlin, and A. Vaivads. Identification of broad-band waves above the auroral acceleration region: Cluster observations. *Ann. Geophys.*, 22(12), 2004. doi: 10.5194/angeo-22-4203-2004.

M. Backrud, G. Stenberg, M. André, M. Morooka, Y. Hobara, S. Joko, K. Rönnmark, N. Cornilleau-Wehrlin, A. Fazakerley, and H. Rème. Cluster observations and theoretical identification of broadband waves in the auroral region. *Ann. Geophys.*, 23(12), 2005a. doi: 10.5194/angeo-23-3739-2005.

M. Backrud, A. Tjulin, A. Vaivads, M. André, and A. Fazakerley. Interferometric identification of ion acoustic broadband waves in the auroral region: CLUSTER observations. *Geophys. Res. Lett.*, 32(21), 2005b. doi: 10.1029/2005gl022640.

S. D. Bale, C. J. Owen, J.-L. Bougeret, K. Goetz, P. J. Kellogg, R. P. Lepping, R. Manning, and S. J. Monson. Evidence of currents and unstable particle distributions in an extended region around the lunar plasma wake. *Geophys. Res. Lett.*, 24(11), 1997. doi: 10.1029/97gl01193.

A. Barkan, N. D'Angelo, and R. L. Merlino. Laboratory experiments on electrostatic ion cyclotron waves in a dusty plasma. *Planet. Space Sci.*, 43(7), 1995. doi: 10.1016/0032-0633(94)00226-H.

B. Basu and N. J. Grossbard. Ion-cyclotron instability in current-carrying lorentzian (kappa) and maxwellian plasmas with anisotropic temperatures: A comparative study. *Phys. Plasmas*, 18(9), 2011. doi: 10.1063/1.3632974.

W. Baumjohann and R. A. Treumann. *Basic Space Plasma Physics*. Imperial College Press, 2012. ISBN 978-1-84816-895-4. doi: 10.1142/p850.

R. Bergmann. Electrostatic ion (hydrogen) cyclotron and ion acoustic wave instabilities in regions of upward field-aligned current and upward ion beams. *J. Geophys. Res. Space*, 89(A2), 1984. doi: 10.1029/ja089ia02p00953.

R. Bergmann, I. Roth, and M. K. Hudson. Linear stability of the H^+ - O^+ two-stream interaction in a magnetized plasma. *J. Geophys. Res. Space*, 93(A5), 1988. doi: 10.1029/ja093ia05p04005.

E. A. Bering. The plasma wave environment of an auroral arc: Electrostatic ion cyclotron waves in the diffuse aurora. *J. Geophys. Res. Space*, 89(A3), 1984. doi: 10.1029/JA089iA03p01635.

R. Bharuthram. Electron-acoustic instability driven by a field-aligned hot electron beam. *J. Plasma Phys.*, 46(1), 1991. doi: 10.1017/S0022377800015907.

J. H. Binsack. *Plasma Studies With The IMP-2 Satellite*. PhD thesis, Massachusetts Institute of Technology, 1966.

P. C. Birch and S. C. Chapman. Two dimensional particle-in-cell simulations of the lunar wake. *Phys. Plasmas*, 9(5), 2002. doi: 10.1063/1.1467655.

Paul C. Birch and Sandra C. Chapman. Particle-in-cell simulations of the lunar wake with high phase space resolution. *Geophys. Res. Lett.*, 28(2), 2001. doi: 10.1029/2000GL011958.

N. Borisov and U. Mall. Plasma distribution and electric fields behind the moon. *Phys. Lett. A*, 265(5-6), 2000. doi: 10.1016/s0375-9601(99)00852-x.

J. E. Borovsky and S. P. Gary. How important are the alpha-proton relative drift and the electron heat flux for the proton heating of the solar wind in the inner heliosphere? *J. Geophys. Res. Space*, 119(7), 2014. doi: 10.1002/2014ja019758.

J. M. Bosqued, N. Lormant, H. Rème, C. d'Uston, R. P. Lin, K. A. Anderson, C. W. Carlson, R. E. Ergun, D. Larson, J. McFadden, M. P. McCarthy, G. K. Parks, T. R. Sanderson, and K.P. Wenzel. Moon-solar wind interactions: First results from the wind/3dp experiment. *Geophys. Res. Lett.*, 23(10), 1996. doi: 10.1029/96GL00303.

R. Bruno and V. Carbone. The solar wind as a turbulence laboratory. *Living Rev. Solar Phys.*, 2, 2005. doi: 10.12942/lrsp-2005-4.

R. Bruno and V. Carbone. The solar wind as a turbulence laboratory. *Living Rev. Solar Phys.*, 10(1), 2013. doi: 10.12942/lrsp-2013-2.

J. Castro, P. McQuillen, and T. C. Killian. Ion acoustic waves in ultracold neutral plasmas. *Phys. Rev. Lett.*, 105(6), 2010. doi: 10.1103/physrevlett.105.065004.

C. Cattell. The relationship of field-aligned currents to electrostatic ion cyclotron waves. *J. Geophys. Res. Space*, 86(A5), 1981. doi: 10.1029/ja086ia05p03641.

C. Cattell, R. Bergmann, K. Sigsbee, C. Carlson, C. Chaston, R. Ergun, J. McFadden, F. S. Mozer, M. Temerin, R. Strangeway, R. Elphic, L. Kistler, E. Moebius, L. Tang, D. Klumpar, and R. Pfaff. The association of electrostatic ion cyclotron waves, ion and electron beams and field-aligned currents: Fast observations of an auroral zone crossing near midnight. *Geophys. Res. Lett*, 25(12), 1998. doi: 10.1029/98GL00834.

C. A. Cattell, F. S. Mozer, I. Roth, R. R. Anderson, R. C. Elphic, W. Lennartsson, and E. Ungstrup. ISEE 1 observations of electrostatic ion cyclotron waves in association with ion beams on auroral field lines from ∼2.5 to 4.5re. *J. Geophys. Res. Space*, 96(A7), 1991. doi: 10.1029/91ja00378.

A. K. Chattopadhyay, S. V. Kulkarni, R. Srinivasan, and Et Al. Second-harmonic ion cyclotron resonance heating scenarios of aditya tokamak plasma. *Pramana*, 85(4), 2015. doi: 10.1007/s12043-014-0908-1.

F. F. Chen. *Introduction to Plasma Physics and Controlled Fusion*, volume 1. Springer US, 1984. ISBN 978-1-4757-5595-4. doi: 10.1007/978-1-4757-5595-4.

C. Chiuderi and M. Velli. *Basics of Plasma Astrophysics*. Springer-Verlag Mailand, 2015. ISBN 978-88-470-5279-6. doi: 10.1007/978-88-470-5280-2.

K. Chotoo, N. A. Schwadron, G. M. Mason, T. H. Zurbuchen, G. Gloeckler, A. Posner, L. A. Fisk, A. B. Galvin, D. C. Hamilton, and M. R. Collier. The suprathermal seed population for corotating interaction region ions at 1 au deduced from composition and spectra of h+, he++, and he+ observed on wind. *J. Geophys. Res. Space*, 105(A10), 2000. doi: 10.1029/1998ja000015.

V. W. Chow and M. Rosenberg. Electrostatic ion cyclotron instability in dusty plasmas. *Planet. Space Sci.*, 43(5), 1995. doi: 10.1016/0032-0633(94)00134-d.

V. W. Chow and M. Rosenberg. Electrostatic ion-cyclotron waves in a plasma with negative ions. *Phys. Plasmas*, 1(12), 1996. doi: 10.1063/1.859049.

S. Chowdhury, S. Biswas, N. Chakrabarti, and R. Pal. Experimental observation of electron-acoustic wave propagation in laboratory plasma. *Phys. Plasmas*, 24(6), 2017. doi: 10.1063/1.4985680.

Michael R. Collier, D. C. Hamilton, G. Gloeckler, P. Bochsler, and R. B. Sheldon. Neon-20, oxygen-16, and helium-4 densities, temperatures, and suprathermal tails in the solar wind determined with WIND/MASS. *Geophys. Res. Lett.*, 23(10), 1996. doi: 10.1029/96gl00621.

Sir. W. Crookes. *On radiant matter a lecture delivered to the British Association for the Advancement of Science, at Sheffield, Friday, August 22, 1879 /.* London :[s.n.],, 1879. URL `https://www.biodiversitylibrary.org/item/77297`.

D. R Dakin, T. Tajima, G. Benford, and N. Rynn. Ion heating by the electrostatic ion cyclotron instability: theory and experiment. *J. Plasma Physics*, 15(02), 1976. doi: 10.1017/S0022377800019723.

N. D'Angelo and R. W. Motley. Electrostatic oscillations near the ion cyclotron frequency. *Phys. Fluids*, 5(5), 1962. doi: 10.1063/1.1706672.

N. D'Angelo, S. v. Goeler, and T. Ohe. Propagation and damping of ion waves in a plasma with negative ions. *Phys. Fluids*, 9(8), 1966. doi: 10.1063/1.1761904.

C. Darwin. *Narrative of the surveying voyages of His Majesty's Ships Adventure and Beagle between the years 1826 and 1836, describing their examination of the southern shores of South America, and the Beagle's circumnavigation of the globe.*, volume 3. Henry Colburn, London, 1839. URL `https://books.google.co.in/books?id=WNlCAQAAMAAJ`.

H. Derfler and T. C. Simonen. Higher-order landau modes. *Phys. Fluids*, 12(2), 1969. doi: 10.1063/1.1692477.

S. Devanandhan, S. V. Singh, and G. S. Lakhina. Electron acoustic solitary waves with kappa-distributed electrons. *Phys. Scripta*, 84(2), 2011a. doi: 10.1088/0031-8949/84/02/025507.

S. Devanandhan, S. V. Singh, G. S. Lakhina, and R. Bharuthram. Electron acoustic solitons in the presence of an electron beam and superthermal electrons. *Nonlinear Proc. Geoph.*, 18(5), 2011b. doi: 10.5194/npg-18-627-2011.

S. Devanandhan, S. V. Singh, G. S. Lakhina, and R. Bharuthram. Electron acoustic waves in a magnetized plasma with kappa distributed ions. *Phys. Plasmas*, 19(8), 2012. doi: 10.1063/1.4743015.

S. Devanandhan, S.V. Singh, G. S. Lakhina, and R. Bharuthram. Small amplitude electron acoustic solitary waves in a magnetized superthermal plasma. *Ccmmun. Nonlinear. Sci.*, 22(1-3), 2015. doi: 10.1016/j.cnsns.2014.07.026.

M. B. Dhanya, A. Bhardwaj, A. Alok, Y. Futaana, S. Barabash, M. Wieser, M. Holmström, and P. Wurz. First observation of transport of solar wind protons scattered from magnetic anomalies into the near lunar wake: Observations by SARA/chandrayaan-1. *Geophys. Res. Lett.*, 45(17), 2018. doi: 10.1029/2018gl079330.

S. Sh. Dolginov, E. G. Eroshenko, L. N. Zhuzgov, N. V. Pushkov, and L. O. Tyurmina. Magnetic measurements on the second cosmic rocket. *ARS Journal*, 31(11), 1961. doi: 10.2514/8.5864.

SH. SH. Dolginov, E. G. Yeroshenko, L. N. Zhuzgov, and N. V. Pushkov. Investigation of the magnetic field of the moon. *AIAA Journal*, 1(2), 1963. doi: 10.2514/3.1589.

W. E. Drummond and Marshall N. Rosenbluth. Anomalous diffusion arising from microinstabilities in a plasma. *Phys. Fluids*, 5(12), 1962. doi: 10.1063/1.1706559.

N. Dubouloz, R. Pottelette, M. Malingre, G. Holmgren, and P. A. Lindqvist. Detailed analysis of broadband electrostatic noise in the dayside auroral zone. *J. Geophys. Res. Space*, 96(A3), 1991a. doi: 10.1029/90JA02355.

N. Dubouloz, R. Pottelette, M. Malingre, and R. A. Treumann. Generation of broadband electrostatic noise by electron acoustic solitons. *Geophys. Res. Lett.*, 18(2), 1991b. doi: 10.1029/90gl02677.

P. B. Dusenbery, R. F. Martin, and R. M. Winglee. Ion-ion waves in the auroral region: Wave excitation and ion heating. *J. Geophys. Res.*, 93(A6), 1988. doi: 10.1029/ja093ia06p05655.

W. M. Farrell, R. J. Fitzenreiter, C. J. Owen, J. B. Byrnes, R. P. Lepping, K. W. Ogilvie, and F. Neubauer. Upstream ulf waves and energetic electrons associated with the lunar wake: Detection of precursor activity. *Geophys. Res. Lett.*, 23(10), 1996. doi: 10.1029/96GL01355.

W. M. Farrell, M. L. Kaiser, and J. T. Steinberg. Electrostatic instability in the central lunar wake: A process for replenishing the plasma void? *Geophys. Res. Lett.*, 24(9), 1997. doi: 10.1029/97gl00878.

W. M. Farrell, M. L. Kaiser, J. T. Steinberg, and S. D. Bale. A simple simulation of a plasma void: Applications to wind observations of the lunar wake. *J. Geophys. Res. Space*, 103 (A10), 1998. doi: 10.1029/97JA03717.

U. Feldman, E. Landi, and N. A. Schwadron. On the sources of fast and slow solar wind. *J. Geophys. Res. Space*, 110(A7), 2005. doi: 10.1029/2004JA010918.

B. D. Fried and R. W. Gould. Longitudinal ion oscillations in a hot plasma. *Phys. Fluids*, 4 (1), 1961. doi: 10.1063/1.1706174.

S. A. Fuselier, S. P. Gary, M. F. Thomsen, S. J. Bame, and D. A. Gurnett. Ion beams and the ion/ion acoustic instability upstream from the earth's bow shock. *J. Geophys. Res. Space*, 92(A5), 1987. doi: 10.1029/ja092ia05p04740.

Y. Futaana, S. Barabash, M. Wieser, M. Holmström, A. Bhardwaj, M. B. Dhanya, R. Sridharan, P. Wurz, A. Schaufelberger, and K. Asamura. Protons in the near-lunar wake observed by the sub-keV atom reflection analyzer on board chandrayaan-1. *J. Geophys. Res. Space Physics*, 115(A10), 2010. doi: 10.1029/2010ja015264.

G. Ganguli, Y. C. Lee, and P. J. Palmadesso. Kinetic theory for electrostatic waves due to transverse velocity shears. *Phys. Fluids*, 31(4), 1988. doi: 10.1063/1.866818.

G. Ganguli, S. Slinker, V. Gavrishchaka, and W. Scales. Low frequency oscillations in a plasma with spatially variable field-aligned flow. *Phys. Plasmas*, 9(5), 2002. doi: 10.1063/1.1445181.

S. P. Gary. The electron/electron acoustic instability. *Phys. Fluids*, 30(9), 1987. doi: 10.1063/1.866040.

S. P. Gary and N. Omidi. The ion-ion acoustic instability. *J. Plasma Phys.*, 37(01), 1987. doi: 10.1017/s0022377800011983.

S. P. Gary and R. L. Tokar. The electron-acoustic mode. *Phys. Fluids*, 28(8), 1985. doi: 10.1063/1.865250.

V. V. Gavrishchaka, M. E. Koepke, and G. I. Ganguli. Ion cyclotron modes in a two-ion-component plasma with transverse-velocity shear. *J. Geophys. Res. Space*, 102(A6), 1997. doi: 10.1029/97ja00639.

V. V. Gavrishchaka, S. B. Ganguli, and G. I. Ganguli. Electrostatic oscillations due to filamentary structures in the magnetic-field-aligned flow: The ion-acoustic branch. *J. Geophys. Res. Space*, 104(A6), 1999. doi: 10.1029/1999ja900094.

V. V. Gavrishchaka, G. I. Ganguli, W. A. Scales, S. P. Slinker, C. C. Chaston, J. P. McFadden, R. E. Ergun, and C. W. Carlson. Multiscale coherent structures and broadband waves due to parallel inhomogeneous flows. *Phys. Rev. Lett.*, 85(20), 2000. doi: 10.1103/physrevlett.85.4285.

T. Gold. Motions in the magnetosphere of the earth. *J. Geophys. Res.*, 64(9), 1959. doi: 10.1029/JZ064i009p01219.

M. Goossens. *An Introduction to Plasma Astrophysics and Magnetohydrodynamics*. Kluwer Academic Publishers, 2003. ISBN 1402014333. doi: 10.1007/978-94-007-1076-4.

D. A. Gurnett and L. A. Frank. Ion acoustic waves in the solar wind. *J. Geophys. Res. Space*, 83(A1), 1978. doi: 10.1029/JA083iA01p00058.

D. A. Gurnett, E. Marsch, W. Pilipp, R. Schwenn, and H. Rosenbauer. Ion acoustic waves and related plasma observations in the solar wind. *J. Geophys. Res. Space*, 84(A5), 1979. doi: 10.1029/JA084iA05p02029.

D. A. Gurnett, G. B. Hospodarsky, W. S. Kurth, D. J. Williams, and S. J. Bolton. Fine structure of langmuir waves produced by a solar electron event. *J. Geophys. Res. Space*, 98(A4), 1993. doi: 10.1029/92ja02838.

F. Hadi, Ata ur Rahman, and A. Qamar. Landau damping of electrostatic modes in nonthermal plasmas. *Phys. Plasmas*, 24(10), 2017. doi: 10.1063/1.5006802.

J. S. Halekas, V. Angelopoulos, D. G. Sibeck, K. K. Khurana, C. T. Russell, G. T. Delory, W. M. Farrell, J. P. McFadden, J. W. Bonnell, D. Larson, R. E. Ergun, F. Plaschke, and K. H. Glassmeier. First results from ARTEMIS, a new two-spacecraft lunar mission: Counter-streaming plasma populations in the lunar wake. *Space Sci. Rev.*, 165(1-4), 2011. doi: 10.1007/s11214-010-9738-8.

J. S. Halekas, A. R. Poppe, and J. P. McFadden. The effects of solar wind velocity distributions on the refilling of the lunar wake: ARTEMIS observations and comparisons to one-dimensional theory. *J. Geophys. Res. Space*, 119(7), 2014. doi: 10.1002/2014ja020083.

J. K. Hargreaves. *The Solar-Terrestrial Environment An Introduction to Geospace - the Science of the Terrestrial Upper Atmosphere, Ionosphere, and Magnetosphere*. Cambridge University Press, 1992. ISBN 9780511628924. doi: 10.1017/CBO9780511628924.

A. Hasegawa. *Plasma Instabilities and Nonlinear Effects*. Springer-Verlag Berlin Heidelberg, 1975. ISBN 978-3-642-65982-9. doi: 10.1007/978-3-642-65980-5.

K. Hashimoto, M. Hashitani, Y. Kasahara, Y. Omura, M. N. Nishino, Y. Saito, S. Yokota, T. Ono, H. Tsunakawa, H. Shibuya, M. Matsushima, H. Shimizu, and F. Takahashi. Electrostatic solitary waves associated with magnetic anomalies and wake boundary of the moon observed by KAGUYA. *Geophys. Res. Lett.*, 37(19), 2010. doi: 10.1029/2010gl044529.

J. P. Hauck, H. Böhmer, N. Rynn, and G. Benford. Ion beam excitation of ion-cyclotron waves and ion heating in plasmas with drifting electrons. *J. Plasma Phys.*, 19(02), 1978. doi: 10.1017/s0022377800023229.

M. A. Hellberg and R. L. Mace. Generalized plasma dispersion function for a plasma with a kappa-maxwellian velocity distribution. *Phys. Plasmas*, 9(5), 2002. doi: 10.1063/1.1462636.

D. Henry and J. P. Trguier. Propagation of electronic longitudinal modes in a non-maxwellian plasma. *J. Plasma Phys.*, 8(3), 1972. doi: 10.1017/S0022377800007169.

R. J. Hess, R. A. andMacDowall, B. Goldstein, M. Neugebauer, and R. J. Forsyth. Ion acoustic-like waves observed by ulysses near interplanetary shock waves in the three-dimensional heliosphere. *J. Geophys. Res. Space*, 103(A4), 1998. doi: 10.1029/97ja03395.

S. Hinata. Electrostatic ion-cyclotron heating of solar atmosphere. *Astrophys. J.*, 235, 1980. doi: 10.1086/157629.

E. W. Hones. The earth's magnetotail. *Sci. Am.*, 254(3), 1986. doi: 10.1038/scientificamerican0386-40.

A. J. Hundhausen. *Introduction to Space Physics*, chapter The Solar Wind, pages 91–128. Cambridge university press, 1995. ISBN 9780521457149.

K. E. J. Huttunen, S. D. Bale, T. D. Phan, M. Davis, and J. T. Gosling. Wind/WAVES observations of high-frequency plasma waves in solar wind reconnection exhausts. *J. Geophys. Res. Space*, 112(A1), 2007. doi: 10.1029/2006ja011836.

R. Ichiki, M. Shindo, S. Yoshimura, T. Watanabe, and Y. Kawai. Ion acoustic waves in one- and two-negative ion species plasmas. *Phys. Plasmas*, 8(10), 2001. doi: 10.1063/1.1396843.

U. S. Inan and M. Gołkowski. *Principles of Plasma Physics for Engineers and Scientists*. Cambridge University Press, 2010. ISBN 978-0-521-19372-6. doi: 10.1017/CBO9780511761621.

W. D. Jones, A. Lee, S. M. Gleman, and H. J. Doucet. Propagation of ion-acoustic waves in a two-electron-temperature plasma. *Phys. Rev. Lett.*, 35(20), 1975. doi: 10.1103/physrevlett.35.1349.

M. N. Kadijani, H. Abbasi, and H. H. Pajouh. Influence of superthermal electrons on obliquely propagating ion-acoustic solitons in magnetized plasmas. *Plasma Phys. Contr. F.*, 53(2), 2010. doi: 10.1088/0741-3335/53/2/025004.

R. L. Kaufmann, G. R. Ludlow, H. L. Collin, W. K. Peterson, and J. L. Burch. Interaction of upgoing auroral H^+ and O^+beams. *J. Geophys. Res. Space*, 91(A9), 1986. doi: 10.1029/ja091ia09p10080.

L. Kay, S. Palen, and G. Blumenthal. *21st Century Astronomy*. W. W. Norton & Company, 2016. ISBN 978-0-393-91878-6. URL `http://books.wwnorton.com/books/webad.aspx?id=4294990550`.

Paul J. Kellogg, Keith Goetz, Steven J. Monson, J.-L. Bougeret, Robert Manning, and M. L. Kaiser. Observations of plasma waves during a traversal of the moon's wake. *Geophys. Res. Lett.*, 23(10), 1996. doi: 10.1029/96gl00376.

S. H. Kim, J. R. Heinrich, and R. L. Merlino. Electrostatic ion-cyclotron waves in a plasma with heavy negative ions. *Planet. Space Sci.*, 56(11), 2008. doi: 10.1016/j.pss.2008.07.020.

S. Kimura and T. Nakagawa. Electromagnetic full particle simulation of the electric field structure around the moon and the lunar wake. *Earth, Planets Space*, 60(6), 2008. doi: 10.1186/bf03353122.

J. M. Kindel and C. F. Kennel. Topside current instabilities. *J. Geophys. Res.*, 76(13), 1971. doi: 10.1029/JA076i013p03055.

P. M. Kintner, M. C. Kelley, and F. S. Mozer. Electrostatic hydrogen cyclotron waves near one earth radius altitude in the polar magnetosphere. *Geophys. Res. Lett.*, 5(2), 1978. doi: 10.1029/GL005i002p00139.

P. M. Kintner, M. C. Kelley, R. D. Sharp, A. G. Ghielmetti, M. Temerin, C. Cattell, P. F. Mizera, and J. F. Fennell. Simultaneous observations of energetic (kev) upstreaming and electrostatic hydrogen cyclotron waves. *J. Geophys. Res. Space*, 84(A12), 1979. doi: 10.1029/JA084iA12p07201.

C. A. Kletzing, J. D. Scudder, E. E. Dors, and C. Curto. Auroral source region: Plasma properties of the high-latitude plasma sheet. *J. Geophys. Res.*, 108(A10), 2003. doi: 10.1029/2002ja009678.

J. Kono, M. andVranjes and N. Batool. Electrostatic ion cyclotron and ion plasma waves in a symmetric pair-ion plasma cylinder. *Phys. Rev. Lett.*, 112(10), 2014. doi: 10.1103/physrevlett.112.105001.

N. A. Krall and A. W. Trivelpiece. *Principles Of Plasma Physics*. McGraw-hill Book Company, 1973. ISBN 0-07-035346-8.

M. J. Kurian, S. Jyothi, S. K. Leju, M. Isaac, C. Venugopal, and G. Renuka. Stability of electrostatic ion cyclotron waves in a multi-ion plasma. *Pramana*, 73(6), 2009. doi: 10.1007/s12043-009-0171-z.

G. S. Lakhina. Low-frequency electrostatic noise due to velocity shear instabilities in the regions of magnetospheric flow boundaries. *J. Geophys. Res. Space*, 92, 1987. doi: 10.1029/JA092iA11p12161.

G. S. Lakhina and S. V. Singh. Generation of weak double layers and low-frequency electrostatic waves in the solar wind. *Sol. Phys.*, 290(10), 2015. doi: 10.1007/s11207-015-0773-1.

G. S. Lakhina, S. V. Singh, A. P. Kakad, F. Verheest, and R. Bharuthram. Study of nonlinear ion- and electron-acoustic waves in multi-component space plasmas. *Nonlinear Proc. Geoph.*, 15(6), 2008. doi: 10.5194/npg-15-903-2008.

G. S. Lakhina, S. V. Singh, and A. P. Kakad. Ion acoustic solitons/double layers in two-ion plasma revisited. *Phys. Plasmas*, 21(6), 2014. doi: 10.1063/1.4884791.

A. Lang and H. Boehmer. Electron current disruption and parallel electric fields associated with electrostatic ion cyclotron waves. *J. Geophys. Res. Space*, 88(A7), 1983. doi: 10.1029/JA088iA07p05564.

I. Langmuir. Oscillations in ionized gases. *Proc. Natl. Acad. Sci. U.S.A.*, 14(8), 1928. doi: 10.1073/pnas.14.8.627.

K. F Lee. Ion cyclotron instability in current-carrying plasmas with anisotropic temperatures. *J. Plasma Physics*, 8(3), 1972. doi: 10.1017/S0022377800007224.

L. C. Lee and J. R. Kan. Nonlinear ion-acoustic waves and solitons in a magnetized plasma. *Phys. Fluids*, 24(3), 1981. doi: 10.1063/1.863389.

C. S. Lin, J. L. Burch, S. D. Shawhan, and D. A. Gurnett. Correlation of auroral hiss and upward electron beams near the polar cusp. *J. Geophys. Res. Space*, 89(A2), 1984. doi: 10.1029/JA089iA02p00925.

N. Lin, P.J. Kellogg, R.J. MacDowall, and S.P. Gary. Ion acoustic waves in the heliosphere. *Space Sci. Rev.*, 97(1), 2001. doi: 10.1023/A:1011823505395.

G. Livadiotis. Introduction to special section on origins and properties of kappa distributions: Statistical background and properties of kappa distributions in space plasmas. *J. Geophys. Res. Space*, 120(3), 2015. doi: 10.1002/2014JA020825.

A. Luhn. Selective heating of minority ions in the lower solar corona by electrostatic ion cyclotron waves. *Adv. Space Res.*, 4(2-3), 1984. doi: 10.1016/0273-1177(84)90308-9.

R. L. Lysak, M. K. Hudson, and M. Temerin. Ion heating by strong electrostatic ion cyclotron turbulence. *J. Geophys. Res. Space*, 85(A2), 1980. doi: 10.1029/JA085iA02p00678.

S. K. Maharaj, R. Bharuthram, S. V. Singh, and G. S. Lakhina. Existence domains of slow and fast ion-acoustic solitons in two-ion space plasmas. *Phys. Plasmas*, 22(3), 2015. doi: 10.1063/1.4916319.

M. Maksimovic, V. Pierrard, and P. Riley. Ulysses electron distributions fitted with kappa functions. *Geophys. Res. Lett.*, 24(9), 1997. doi: 10.1029/97gl00992.

M. Maksimovic, I. Zouganelis, J.-Y. Chaufray, K. Issautier, E. E. Scime, J. E. Littleton, E. Marsch, D. J. McComas, C. Salem, R. P. Lin, and H. Elliott. Radial evolution of the electron distribution functions in the fast solar wind between 0.3 and 1.5 AU. *J. Geophys. Res. Space*, 110(A9), 2005. doi: 10.1029/2005ja011119.

A. Mangeney, C. Salem, C. Lacombe, J.-L. Bougeret, C. Perche, R. Manning, P. J. Kellogg, K. Goetz, S. J. Monson, and J.-M. Bosqued. WIND observations of coherent electrostatic waves in the solar wind. *Ann. Geophys.*, 17(3), 1999. doi: 10.1007/s00585-999-0307-y.

E. Marsch. Kinetic physics of the solar corona and solar wind. *Living Rev. Solar Phys.*, 3 (1), 2006. doi: 10.12942/lrsp-2006-1.

E. Marsch, K. H. Mühlhäuser, H. Rosenbauer, R. Schwenn, and F. M. Neubauer. Solar wind helium ions: Observations of the helios solar probes between 0.3 and 1 AU. *J. Geophys. Res. Space*, 87(A1):35, 1982. doi: 10.1029/ja087ia01p00035.

J. D. Menietti, P. Schippers, O. Santolík, D. A. Gurnett, F. Crary, and A. J. Coates. Ion cyclotron harmonics in the saturn downward current auroral region. *J. Geophys. Res. Space*, 116(A12), 2011. doi: 10.1029/2011ja017102.

R. L. Merlino. Electrostatic ion-cyclotron waves driven by parallel velocity shear. *Phys. Plasmas*, 9(5), 2002. doi: 10.1063/1.1465418.

F. C. Michel. Lunar wake at large distances. *J. Geophys. Res.*, 73(23), 1968. doi: 10.1029/JA073i023p07277.

M. K. Mishra and R. S. Chhabra. Ion-acoustic compressive and rarefactive solitons in a warm multicomponent plasma with negative ions. *Phys. Plasmas*, 3(12), 1996. doi: 10.1063/1.872063.

A. P. Misra, N. C. Adhikary, and P. K. Shukla. Ion-acoustic solitary waves and shocks in a collisional dusty negative-ion plasma. *Phys. Revi. E*, 86(5), 2012. doi: 10.1103/physreve.86.056406.

M. Moldwin. *An Introduction to Space Weather*. Cambridge University Press, 2008. ISBN 978-0-521-71112-8. doi: 10.1017/CBO9780511801365.

Michael D. Montgomery, S. J. Bame, and A. J. Hundhausen. Solar wind electrons: Vela 4 measurements. *J. Geophys. Research. Space*, 73(15), 1968. doi: 10.1029/ja073i015p04999.

A. I. Morozov. *Introduction to Plasma Dynamics*. CRC Press, 2013. ISBN 978-1-4398-8133-0.

S. R. Mosier and D. A. Gurnett. Ionospheric observation of VLF electrostatic noise related to harmonics of the proton gyrofrequency. *Nature*, 223(5206), 1969. doi: 10.1038/223605a0.

R. W. Motley and N. D'Angelo. Excitation of electrostatic plasma oscillations near the ion cyclotron frequency. *Phys. Fluids*, 6(2), 1963. doi: 10.1063/1.1706728.

F. S. Mozer, R. Ergun, M. Temerin, C. Cattell, J. Dombeck, and J. Wygant. New features of time domain electric-field structures in the auroral acceleration region. *Phys. Rev. Lett.*, 79(7), 1997. doi: 10.1103/PhysRevLett.79.1281.

T. Nakagawa, Y. Takahashi, and M. Iizima. GEOTAIL observation of upstream ULF waves associated with lunar wake. *Earth, Planets Space*, 55(9), 2003. doi: 10.1186/bf03351789.

N. F. Ness. The magnetohydrodynamic wake of the moon. *J. Geophys. Res.*, 70(3), 1965. doi: 10.1029/JZ070i003p00517.

N. F. Ness. *Solar-Terrestrial Physics/1970*, volume 11, chapter Interaction of the Solar Wind with the Moon, pages 347–393. Springer, Dordrecht, 1972. doi: https://doi.org/10.1007/978-94-009-3693-5_21.

D. C. Nicholls, M. A. Dopita, and R.S. Sutherland. Resolving the electron temperature discrepancies in h ii regions and planetary nebulae: κ-distributed electrons. *Astrophys. J.*, 752(2), 2012. doi: 10.1088/0004-637x/752/2/148.

D. R. Nicholson. *Introduction to Plasma Theory*. Wiley, 1983. ISBN 047109045X.

M. B. M. Niyat, S. M. Khorashadizadeh, and A. R. Niknam. Electrostatic ion cyclotron instability in a plasma with q-nonextensive distributions. *Phys. Plasmas*, 23(12), 2016. doi: 10.1063/1.4971810.

F. Nsengiyumva, M. A. Hellberg, F. Verheest, and R. L. Mace. Stopbands in the existence domains of acoustic solitons. *Phys. Plasmas*, 21(10), 2014. doi: 10.1063/1.4896707.

K. Ogasawara, V. Angelopoulos, M. A. Dayeh, S. A. Fuselier, G. Livadiotis, D. J. McComas, and J. P. McFadden. Characterizing the dayside magnetosheath using energetic neutral atoms: IBEX and THEMIS observations. *J. Geophys. Res. Space*, 118(6), 2013. doi: 10.1002/jgra.50353.

K. W. Ogilvie, J. T. Steinberg, R. J. Fitzenreiter, C. J. Owen, A. J. Lazarus, W. M. Farrell, and R. B. Torbert. Observations of the lunar plasma wake from the WIND spacecraft on december 27, 1994. *Geophys. Res. Lett.*, 23(10), 1996. doi: 10.1029/96gl01069.

T. Ohnuma, S. Miyake, T. Watanabe, T. Watari, and T. Sato. Coupling between electrostatic ion cyclotron waves and ion acoustic waves. *Phys. Rev. Lett.*, 30(12), 1973. doi: 10.1103/PhysRevLett.30.535.

H. Okuda and M. Ashour-Abdalla. Formation of a conical distribution and intense ion heating in the presence of hydrogen cyclotron waves. *Geophys. Res. Lett.*, 8(7), 1981. doi: 10.1029/GL008i007p00811.

H. Okuda and K.-I. Nishikawa. Ion-beam-driven electrostatic hydrogen cyclotron waves on auroral field lines. *J. Geophys. Res. Space*, 89(A2), 1984. doi: 10.1029/ja089ia02p01023.

H. Okuda, C. Z. Cheng, and W. W Lee. Anomalous diffusion and ion heating in the presence of electrostatic hydrogen cyclotron instabilities. *Phys. Rev. Lett.*, 46(6), 1981a. doi: 10.1103/PhysRevLett.46.427.

H. Okuda, C. Z. Cheng, and W. W. Lee. Numerical simulations of electrostatic hydrogen cyclotron instabilities. *Phys. Fluids*, 24(6), 1981b. doi: 10.1063/1.863484.

S. Olbert. *Physics of the Magnetosphere*, chapter Summary of experimental results from M.I.T. detector on IMP-1, pages 641–659. Springer Netherlands, 1968. doi: 10.1007/978-94-010-3467-8.

C. P. Olivier, S. K. Maharaj, and R. Bharuthram. Ion-acoustic solitons, double layers and supersolitons in a plasma with two ion- and two electron species. *Phys. Plasmas*, 22(8), 2015. doi: 10.1063/1.4928884.

C. J. Owen, R. P. Lepping, K. W. Ogilvie, J. A. Slavin, W. M. Farrell, and J. B. Byrnes. The lunar wake at 6.8 RL: WIND magnetic field observations. *Geophys. Res. Lett.*, 23(10), 1996. doi: 10.1029/96gl01354.

G. K. Parks. *Physics Of Space Plasmas An Introduction*. Westview Press, 2 edition, 2004. ISBN 0813341299.

F. W. Perkins. Ion-streaming instabilities: Electromagnetic and electrostatic. *Phys. Fluids*, 19(7), 1976. doi: 10.1063/1.861597.

A. Piel. *Plasma Physics- An Introduction to Laboratory, Space, and Fusion Plasmas*. Springer International Publishing, 2017. ISBN 978-3-319-63425-8. doi: 10.1007/978-3-319-63427-2.

V. Pierrard and M. Lazar. Kappa distributions: Theory and applications in space plasmas. *Sol. Phys.*, 267(1), 2010. doi: 10.1007/s11207-010-9640-2.

W. G. Pilipp, H. Miggenrieder, M. D. Montgomery, K. H. Mühlhäuser, H. Rosenbauer, and R. Schwenn. Characteristics of electron velocity distribution functions in the solar wind derived from the helios plasma experiment. *J. Geophys. Res. Space*, 92(A2), 1987. doi: 10.1029/ja092ia02p01075.

N. F. Pisarenko, E. Yu. Budnik, Yu. I. Ermolaev, I. P. Kirpichev, V. N. Lutsenko, E. I. Morozova, and E. E. Antonova. The ion differential spectra in outer boundary of the ring current: November 17, 1995 case study. *J. Atmos. Sol. Terr. Phys.*, 64(5-6), 2002. doi: 10.1016/s1364-6826(02)00015-9.

S. I. Popel and T. I. Morozova. Wave processes during the interaction of the earth's magnetotail with dusty plasma near the lunar surface. *Plasma Phys. Rep.*, 43(5), 2017. doi: 10.1134/s1063780x17050075.

S. I. Popel, G. E. Morfill, P. K. Shukla, and H. Thomas. Waves in a dusty plasma over the illuminated part of the moon. *J. Plasma Phys.*, 79(6), 2013. doi: 10.1017/S0022377813001001.

S. I. Popel, L. M. Zelenyi, and B. Atamaniuk. Dusty plasma sheath-like structure in the region of lunar terminator. *Phys. Plasmas*, 22(12), 2015. doi: 10.1063/1.4937368.

E. R. Priest. *Introduction to Space Physics*, chapter The Sun and Its Magnetohydrodynamics, pages 58–90. Cambridge university press, 1995. ISBN 9780521457149.

Aman-ur Rehman, M. Ahmad, S. Ali Shan, and T. Majeed. Kinetic theory of ion acoustic waves in a q-nonextensive distributed ions and electrons plasma. *Physica A*, 506, 2018a. doi: 10.1016/j.physa.2018.05.038.

S. ur Rehman, Q. ul Haque, and A. Shah. Interplanetary ion acoustic wave in solar wind plasma. *Phys. Plasmas*, 25(8), 2018b. doi: 10.1063/1.5028338.

M. Rosenberg and R. L. Merlino. Instability of higher harmonic electrostatic ion cyclotron waves in a negative ion plasma. *J. Plasma Physics*, 75(4), 2009. doi: 10.1017/S0022377808007642.

A. Roux, S. Perraut, J. L. Rauch, C. de Villedary, G. Kremser, A. Korth, and D. T. Young. Wave-particle interactions near ω_{He^+} observed on board geos 1 and 2: 2. generation of ion cyclotron waves and heating of He^+ ions. *J. Geophys. Res. Space*, 87(A10), 1982. doi: 10.1029/JA087iA10p08174.

R. Rubia, S. V. Singh, and G. S. Lakhina. Existence domains of electrostatic solitary structures in the solar wind plasma. *Phys. Plasmas*, 23(6), 2016. doi: 10.1063/1.4953892.

R. Rubia, S. V. Singh, and G. S. Lakhina. Occurrence of electrostatic solitary waves in the lunar wake. *J. Geophys. Res. Space*, 122(9), 2017. doi: 10.1002/2017ja023972.

R. Rubia, S. V. Singh, and G. S. Lakhina. Existence domain of electrostatic solitary waves in the lunar wake. *Phys. Plasmas*, 25(3), 2018. doi: 10.1063/1.5017638.

C. T. Russell. *Space Weather*, chapter Solar Wind and Interplanetary Magnetic Field: A Tutorial, pages 73–89. American Geophysical Union (AGU), 2013. ISBN 9780875909844. doi: 10.1029/GM125p0073.

N. Sato. Production of negative ion plasmas in a q machine. *Plasma Sources Sci. T.*, 3(3), 1994. doi: 10.1088/0963-0252/3/3/024.

F. Scarf. *Plasma Waves and Instabilities at Comets and in Magnetospheres*, volume 53, chapter Plasma Wave Observations at Comets Giacobini-Zinner and Halley, pages 31–40. American Geophysical Union, 1989. doi: 10.1029/GM053p0031.

F. L. Scarf, F. V. Coroniti, C. F. Kennel, D. A. Gurnett, W. Ip, and E. J. Smith. Plasma wave observations at comet giacobini-zinner. *Science*, 232(4748), 1986. doi: 10.1126/science.232.4748.377.

P. Schippers, M. Blanc, N. André, I. Dandouras, G. R. Lewis, L. K. Gilbert, A. M. Persoon, N. Krupp, D. A. Gurnett, A. J. Coates, S. M. Krimigis, D. T. Young, and M. K. Dougherty. Multi-instrument analysis of electron populations in saturn's magnetosphere. *J. Geophys. Res. Space*, 113(A7), 2008. doi: 10.1029/2008ja013098.

D. Schriver and M. Ashour-Abdalla. Broadband electrostatic noise due to field-aligned currents. *Geophys. Res. Lett.*, 16(8), 1989. doi: 10.1029/GL016i008p00899.

C. E. Seyler and J. E. Wahlund. Theory of nearly perpendicular electrostatic plasma waves and comparison to freja satellite observations. *J. Geophys. Res. Space*, 101(A10), 1996. doi: 10.1029/96ja02041.

M. Shahmansouri and M. Tribeche. Propagation properties of ion acoustic waves in a magnetized superthermal bi-ion plasma. *Astrophys. Space Sci.*, 350(2), 2014. doi: 10.1007/s10509-014-1794-1.

A. S. Sharma, M. Mohan, and M. Y. Yu. The electron-acoustic-drift instability. *Phys. Lett. A*, 97(9), 1983. doi: 10.1016/0375-9601(83)90671-0.

J. Sharma and S. C. Sharma. Excitation of electrostatic ion-cyclotron waves by an ion beam in a two-ion component plasma. *Phys. Plasmas*, 17(12), 2010. doi: 10.1063/1.3522876.

J. Sharma, S. C. Sharma, V. K. Jain, and A. Gahlot. Higher harmonics generation by a spiraling ion beam in collisionless magnetized plasma. *J. Plasma Physics*, 79(5), 2013. doi: 10.1017/S002237781300007X.

J. Sharma, S. C. Sharma, and D. Kaur. Instability of ion beam driven electrostatic ion-cyclotron waves in collisional magnetized two-ion component plasma. *Pr. Electromag. Res. Lett.*, 54, 2015. doi: 10.2528/pierl15042703.

R. D. Sharp, R. G. Johnson, and E. G. Shelley. Satellite measurements of auroral alpha particles. *J. Geophys. Res. Space*, 79(34), 1974. doi: 10.1029/ja079i034p05167.

N. Singh, J. R. Conrad, and R. W. Schunk. Electrostatic ion cyclotron, beam-plasma, and lower hybrid waves excited by an electron beam. *J. Geophys. Res. Space*, 90(A6), 1985. doi: 10.1029/ja090ia06p05159.

S. V. Singh and G. S. Lakhina. Generation of electron-acoustic waves in the magnetosphere. *Planet. Space Sci.*, 49(1), 2001. doi: 10.1016/S0032-0633(00)00126-4.

B. Song, D. Suszcynsky, N. D'Angelo, and R. L. Merlino. Electrostatic ion-cyclotron waves in a plasma with negative ions. *Phys. Plasmas*, 1(12), 1989. doi: 10.1063/1.859049.

B. Song, N. D'Angelo, and R. L. Merlino. Ion-acoustic waves in a plasma with negative ions. *Phys. Fluids B Plasma*, 3(2), 1991. doi: 10.1063/1.859736.

T. Sreeraj, S. V. Singh, and G. S. Lakhina. Coupling of electrostatic ion cyclotron and ion acoustic waves in the solar wind. *Phys. Plasmas*, 23(8), 2016. doi: 10.1063/1.4960657.

T. Sreeraj, S. V. Singh, and G. S. Lakhina. Electrostatic waves driven by electron beam in lunar wake plasma. *Phys. Plasmas*, 25(5):052902, 2018. doi: 10.1063/1.5032141.

T. H. Stix. *Waves in Plasmas*. American Institute of Physics, 1992. ISBN 978-0-88318-859-0.

S. Sultana, I. Kourakis, N. S. Saini, and M. A. Hellberg. Oblique electrostatic excitations in a magnetized plasma in the presence of excess superthermal electrons. *Phys. Plasmas*, 17 (3), 2010. doi: 10.1063/1.3322895.

D. Summers and R. M. Thorne. The modified plasma dispersion function. *Phys. Fluids B Plasma*, 3(8), 1991. doi: 10.1063/1.859653.

D. M. Suszcynsky, N. D'Angelo, and R. L. Merlino. An experimental study of electrostatic ion cyclotron waves in a two-ion component plasma. *J. Geophys. Res. Space*, 94(A7), 1989. doi: 10.1029/ja094ia07p08966.

D. G. Swanson. *Plasma Waves*. CRC Press, 2003. ISBN 9780750309271.

X. Tang, C. Cattell, R. Lysak, L. B. Wilson III, L. Dai, and S. Thaller. Themis observations of electrostatic ion cyclotron waves and associated ion heating near the earth's dayside magnetopause. *J. Geophys. Res. Space*, 120(5), 2015. doi: 10.1002/2015JA020984.

J. B. Tao, R. E. Ergun, D. L. Newman, J. S. Halekas, L. Andersson, V. Angelopoulos, J. W. Bonnell, J. P. McFadden, C. M. Cully, H.-U. Auster, K.-H. Glassmeier, D. E. Larson, W. Baumjohann, and M. V. Goldman. Kinetic instabilities in the lunar wake: ARTEMIS observations. *J. Geophys. Res. Space*, 117(A3), 2012. doi: 10.1029/2011ja017364.

M. Temerin, M. Woldorff, and F. S. Mozer. Nonlinear steepening of the electrostatic ion cyclotron wave. *Phys. Rev. Lett.*, 43(26), 1979. doi: 10.1103/PhysRevLett.43.1941.

J. V. Thompson. *Zoological Researches and Illustration; Or, Natural History of Nondescript Or Imperfectly Known Animals, in a Series of Memoirs*. Number 1. King and Ridings, 1828. URL `https://books.google.co.in/books?id=aJFPAQAAMAAJ`.

R. M. Thorne and D. Summers. Landau damping in space plasmas. *Phys. Fluids B Plasma*, 3(8), 1991. doi: 10.1063/1.859624.

A. Tjulin. *Waves in Space Plasmas. Lower hybrid cavities and simple pole distribution function.* PhD thesis, Uppsala University, 2003.

R. L. Tokar and S. P. Gary. Electrostatic hiss and the beam driven electron acoustic instability in the dayside polar cusp. *Geophys. Res. Lett.*, 11(12), 1984. doi: 10.1029/gl011i012p01180.

L. Tonks and I. Langmuir. Oscillations in ionized gases. *Phys. Rev.*, 33(2), 1929. doi: 10.1103/PhysRev.33.195.

P. Trávníček, P. Hellinger, D. Schriver, and S. D. Bale. Structure of the lunar wake: Two-dimensional global hybrid simulations. *Geophys. Res. Lett.*, 32(6), 2005. doi: 10.1029/2004gl022243.

B. T. Tsurutani and R. M. Thorne. Diffusion processes in the magnetopause boundary layer. *Geophys. Res. Lett.*, 9(11), 1982. doi: 10.1029/gl009i011p01247.

E. Ungstrup, D. M. Klumpar, and W. J. Heikkila. Heating of ions to superthermal energies in the topside ionosphere by electrostatic ion cyclotron waves. *J. Geophys. Res. Space*, 84 (A8), 1979. doi: 10.1029/JA084iA08p04289.

J. A. Van Allen. *Encyclopedia of physics*, chapter Radiation Belts, pages 1009–1010. VCH Publishers, 1991. ISBN 0-89573-752-3.

V. M. Vasyliunas. A survey of low-energy electrons in the evening sector of the magnetosphere with ogo 1 and ogo 3. *J. Geophys. Res.*, 73(9), 1968. doi: 10.1029/JA073i009p02839.

J. -P. Villain, C. Hanuise, R. A. Greenwald, K. B. Baker, and J. M. Ruohoniemi. Obliquely propagating ion acoustic waves in the auroral e region: Further evidence of irregularity production by field-aligned electron streaming. *J. Geophys. Res. Space*, 95(A6), 1990. doi: 10.1029/ja095ia06p07833.

J. Vranjes. New features of ion acoustic waves in inhomogeneous and permeating plasmas. *Astron. Astrophys.*, 554(A90), 2013. doi: 10.1051/0004-6361/201221020.

J. E. Wahlund, P. Louarn, T. Chust, H. de Feraudy, A. Roux, B. Holback, B. Cabrit, A. I. Eriksson, P. M. Kintner, M. C. Kelley, J. Bonnell, and S. Chesney. Observations of ion acoustic fluctuations in the auroral topside ionosphere by the FREJA S/C. *Geophys. Res. Lett.*, 21(17), 1994. doi: 10.1029/94gl01290.

J. E. Wahlund, A. I. Eriksson, B. Holback, M. H. Boehm, J. Bonnell, P. M. Kintner, C. E. Seyler, J. H. Clemmons, L. Eliasson, D. J. Knudsen, P. Norqvist, and L. J. Zanetti. Broadband ELF plasma emission during auroral energization: 1. slow ion acoustic waves. *J. Geophys. Res. Space*, 103(A3), 1998. doi: 10.1029/97ja02008.

K. Watanabe and T. Taniuti. Electron-acoustic mode in a plasma of two-temperature electrons. *J. Phys. Soc. Jpn.*, 43(5), 1977. doi: 10.1143/JPSJ.43.1819.

E. S. Weibel. Ion cyclotron instability. *Phys. Fluids*, 76(13), 1970. doi: 10.1063/1.1692893.

S. Wiehle, F. Plaschke, U. Motschmann, K.-H. Glassmeier, H. U. Auster, V. Angelopoulos, J. Mueller, H. Kriegel, E. Georgescu, J. Halekas, D. G. Sibeck, and J. P. McFadden. First lunar wake passage of ARTEMIS: Discrimination of wake effects and solar wind fluctuations by 3d hybrid simulations. *Planet. Space Sci.*, 59(8), 2011. doi: 10.1016/j.pss.2011.01.012.

R. A. Wolf. *Introduction to Space Physics*, chapter Magnetospheric configuration, pages 288–329. Cambridge university press, 1995. ISBN 9780521457149.

L. Xie, L. Li, Y. Zhang, and D. L. De Zeeuw. Three-dimensional MHD simulation of the lunar wake. *Sci. China Earth Sci.*, 56(2), 2013. doi: 10.1007/s11430-012-4383-6.

N. Yadav and R. P. Sharma. Nonlinear interaction of 3d kinetic alfvén waves and ion acoustic waves in solar wind plasmas. *Sol. Phys.*, 289(5), 2013. doi: 10.1007/s11207-013-0436-z.

M. Yamada, S. Seiler, H. W. Hendel, and H. Ikezi. Electrostatic ion cyclotron instabilities driven by parallel ion beam injection. *Phys. Fluids*, 76(13), 1977. doi: 10.1063/1.861882.

S. Yoshimura, Y. Nakamura, T. Watanabe, and Y. Kawai. Excitation characteristics of ion waves in a negative ion plasma. *J. Phys. Soc. Jpn.*, 66(12), 1997. doi: 10.1143/jpsj.66.3842.

D. T. Young, S. Perraut, A. Roux, C. D. Villedary, R. Gendrin, A. Korth, G. Kremser, and D. Jones. Wave-particle interactions near ω_{He^+} observed on board geos 1 and 2: 1. propagation of ion cyclotron waves in He^+- rich plasma. *J. Geophys. Res. Space*, 86(A8), 1981. doi: 10.1029/JA086iA08p06755.

M. Y. Yu and P. K. Shukla. Linear and nonlinear modified electron-acoustic waves. *J. Plasma Phys.*, 29(3), 1983. doi: 10.1017/S0022377800000866.

W. F. A. Zimmermann. *Naturwunder im Reiche der Luft. Eine populäre Belehrung über die Atmosphäre der Erde, etc. [With illustrations.]*. 1868. URL `https://books.google.co.in/books?id=NDVWAAAAcAAJ`.

B. Zolesi and L. R. Cander. *Ionospheric Prediction and Forecasting*. Springer-Verlag Berlin Heidelberg, 2014. ISBN 978-3-642-38429-5. doi: 10.1007/978-3-642-38430-1.

(T. Sreeraj) (Prof. Satyavir Singh)

Candidate Guiding Teacher

SYNOPSIS OF THE THESIS TO BE SUBMITTED

TO THE

UNIVERSITY OF MUMBAI

FOR THE DEGREE OF

DOCTOR OF PHILOSOPHY IN PHYSICS

IN THE FACULTY OF

SCIENCE

TITLE OF THE THESIS:	GENERATION OF LOW FREQUENCY WAVES BY ENERGETIC PARTICLES IN SPACE PLASMAS
NAME OF THE CANDIDATE:	T. SREERAJ
NAME OF THE GUIDE:	Prof. SATYAVIR SINGH
PLACE OF RESEARCH:	INDIAN INSTITUTE OF GEOMAGNETISM, PLOT NO. 5, SECTOR - 18, KALAM-BOLI HIGHWAY, NEW PANVEL (W), NAVI MUMBAI- 410 218, INDIA
NUMBER AND DATE OF REGISTRATION:	28/02-12-2016
DATE OF SUBMISSION:	03-10-2018

SIGNATURE OF STUDENT:

SIGNATURE OF GUIDE:

Synopsis

Plasma, a word derived from the Greek word meaning 'moldable substance', is the fourth state of matter, after solid, liquid and gas. Plasma is a collection of charged particles and neutral particles that exhibits collective behavior, due to long range coulomb forces. In simple terms, plasma can be considered as ionized gas. Though, almost all gases contains a small amount of ionization (as dictated by Saha's ionization formula), but these cannot be called as a plasma. A qualitative, but rigorous definition of plasma is (Chen, 2016):

A plasma is a quasineutral gas of charged and neutral particles which exhibits collective behavior

Current estimated composition of Universe is 69% dark energy, 27% dark matter, and 1% ordinary matter (Chen, 2016) and 99% of ordinary matter is in plasma state (Baumjohann and Treumann, 2012). Since the plasma is a collection of particles, both charged and neutral, one can speculate that a statistical approach will be the best way to describe the system and indeed, it is. The kinetic theory, which has roots in statistical mechanics, provides the comprehensive treatment of plasma and takes into the consideration effects of all the particle in the system. In this method, collision-less Boltzmann equation or Vlasov equation serves as the fundamental equation. A further simplified, yet efficient, description of plasma can be achieved by taking velocity moments of the Vlasov equation, which gives the time and spatial evolution of macroscopic variables, such as number density, bulk velocity, temperature and pressure. These equations are reminiscent of the fluid equation that is employed in fluid dynamics and hence this approach is called as fluid theory.

Waves are the carrier of energy and information in any medium. Like any other medium, plasma support a wide range of waves which are linear and non-linear in nature. The linear waves are those whose equations which describes the oscillating quantities have linear relationship under the action of small external influences. The waves are characterized by certain frequency and wave vector and the relation between wave vector and frequency is called the dispersion relation. Solution of dispersion relation or it's roots (as it is called), represent the various plasma wave modes that can be sustained in the given plasma model. The plasma waves are broadly classified into electrostatic and electromagnetic waves. Electrostatic waves are the material waves which exist in plasma which arises due to oscillation

of one or other plasma species. These are the waves which propagate longitudinally with reference to oscillating electric field and these will not have any oscillation in the magnetic field. On the other hand, electromagnetic waves have oscillation in the electric & magnetic field and which moves transversely with reference to oscillating electric and magnetic field. Apart from these classification, based on the frequency scale, the plasma waves are classified as high frequency and low frequency waves. High frequency waves are usually associated with electron motion. Since electrons are comparatively lighter than the ions, it can oscillate much faster and leads to high frequency waves. Examples are Langmuir waves, electron cyclotron waves, electron acoustic waves, whistler waves etc. On the other hand, the motions of ions always contribute to low frequency waves. Examples are ion acoustic waves, electrostatic ion cyclotron waves, electromagnetic ion cyclotron waves etc. As far as unmagnetized plasma is concerned, low frequency waves points to the condition $\omega \lessapprox \omega_{pi}$ while high frequency waves have $\omega \gtrapprox \omega_{pe}$, where ω_{pi} and ω_{pe} are plasma frequency of ions and electrons respectively. For a magnetized plasma, the frequency goes like : $\Omega_i << \omega_{pi} << \omega_{pe} < \Omega_e$ or $\Omega_i << \omega_{pi} << \omega_e < \Omega_{pe}$ depending upon the region. In this scenario, the low frequency implies $\omega \lessapprox \Omega_i$ and other modes are named as low frequency and high frequency based upon the waves being considered (Nicholson, 1983).

In magnetized plasmas, electrostatic ion cyclotron (EIC) waves have gained much attention due to the fact that instability associated with these waves, which is known as electrostatic ion cyclotron instability (EICI), have the lowest threshold among various current driven instabilities (Kindel and Kennel, 1971). The EIC waves serve as one of the source of ion heating in magnetosphere. EIC waves propagates nearly perpendicular to the ambient magnetic field and have frequencies near to the cyclotron frequency of the corresponding species, i.e., proton or heavier ions in the plasma. EIC waves was first observed by D'Angelo and Motley (1962) in laboratory plasma and subsequently it was observed in high latitude ionosphere by Mosier and Gurnett (1969). Free energy for this instability is provided by field aligned currents (Kintner et al., 1979), ion beams (Kindel and Kennel, 1971), velocity shear (Ganguli et al., 2002), relative streaming between ions (Bergmann et al., 1988), electron drifts (Chow and Rosenberg, 1996) and density gradients (Tang et al., 2015). A recent study by Tang et al. (2015) from analyzing the data from THEMIS satellite gathered at magnetopause region has identified the gradients in the plasma density which acts as a pos-

sible source of free energy for EIC waves. Numerical simulation undertaken by Okuda et al. (1981) in two component plasma concluded that harmonics of EIC waves satisfy the condition $\omega \approx n\Omega_i$ with the growth rate peaking at $k_\perp \rho_i \approx n$, where n is the number of harmonic. Kinetic analysis of EICI involving the dust particle has been carried out in a three component plasma by Rosenberg and Chow (1999) and they have shown that with the increase in dust density there is a decrease in the critical drift of ions required to excite the instability. In four component magnetized plasma comprising of electrons, hydrogen (H^+), positively charged oxygen(O^+) and negatively charged oxygen (O^-), it was shown that temperature anisotropy of the oxygen ions only slightly enhance the growth rates (Kurian et al., 2009). In a non-thermal plasma, Niyat et al. (2016) have derived dispersion relation for EIC waves that has non-extensive electrons drifting with respect to stationary ions. They found that minimum value of the critical drift velocity decreases with decrease in the non-extensivity parameter of electrons, whereas larger temperature anisotropy of ions weakens the instability and increases the minimum value of the critical drift velocity. In the magnetospheric cusp region, Slapak et al. (2017) have shown the presence of EIC waves and it's harmonics with the aid of Cluster- 4 satellite. They have shown excitation of the fundamental mode as-well-as it's harmonics, which enhances the ion heating. Using fast satellite observations, Cattell et al. (1998) have shown presence of EIC waves near the cyclotron frequencies of H +, O +, and He + in the auroral zone. The numerical analysis of the electrostatic dispersion relation shows that observed ion-beams do not drive the EIC waves but relative drifts of various ion species can drive the waves unstable. Moreover, the observed modes matches with the simulation prediction. However, they have also cautioned that in the simulation studies, though the ion beams and up flowing electrons are well modelled by Maxwellian distribution, the up-flowing electrons are non-Maxwellian. The multiple harmonics of Hydrogen cyclotron waves have also been observed by FAST satellite (Gavrishchaka et al., 2000). These observations were associated with spatial transverse gradient in the ion flow parallel to the magnetic field. Harmonics of EIC waves in the Saturn downward current auroral region have also been observed (Menietti et al., 2011).

Another low frequency electrostatic wave, i.e., ion acoustic wave was a subject of study from the early days of plasma physics. Ion acoustic wave is a fundamental mode in unmagnetized plasma. This mode was extensively studied by many people and is observed

in many regions of magnetosphere and throughout solar system (Gurnett and Frank, 1978; Scarf et al., 1979; Lee and Kan, 1981; Lin et al., 2001; Hellberg and Mace, 2002; Sultana et al., 2010). Ion acoustic waves were invoked to explain various plasma phenomena, such as transport phenomenon in Sun (Cranmer et al., 2007) as well as auroral particle acceleration processes in the Earth's ionosphere (Koepke, 2002). Replicating the plasma model that is seen in the Saturn's magnetosphere, which comprises of single charged cool adiabatic ions, kappa distributed cool and hot electrons and an ultra-low density ion beam, Koen et al. (2014) has carried out paricle-in-cell simulation studies. They showed that with the increase in the hot electron density, the growth rate of the ion acoustic mode increases. Recently, modelling solar wind plasma with singly ionized drifting helium ions, protons, and electrons, Rehman et al. (2018) has shown that beam velocity enhances the phase velocity of IAW significantly more than that of density and temperature of plasma species. It has also been proved theoretically and experimentally that in a two ion component plasma there exist two different types of ion acoustic modes- namely fast ion acoustic mode and slow ion acoustic mode. They are distinguished by difference their in phase speeds (D'Angelo, 1966; Wong et al., 1975; Sato, 1994). The fast ion-acoustic mode is the usual ion-acoustic mode as in two component electron-ion plasma and slow ion acoustic mode is an ion-ion hybrid mode that requires essentially two ion species to have different thermal speeds.

Electron counter part of this wave, namely electron acoustic wave, was discovered by Fried and Gould (1961). This was shown to be a heavily damped electrostatic wave mode in unmagnetized electron-ion plasma. Weakly damped electron acoustic waves can occur when there are electrons with different temperatures (Watanabe and Taniuti, 1977). In unmagnetized plasma comprising of hot & cold electron and ions, Yu and Shukla (1983) have found out the existence of electron acoustic mode which satisfies the phase velocity condition $v_{tc} << \omega/k << v_{ti} << v_{th}$. This mode has been incorporated to explain various wave phenomena occurring in different parts of magnetosphere. A notable mention is that of Broadband electrostatic Noise or BEN. BEN emissions are observed throughout the magnetosphere and it's frequency extends from ion cyclotron/lower hybrid frequency to electron plasma frequency and above (Singh and Lakhina, 2001, 2004). Using kinetic theory, Singh and Lakhina (2001) has invoked the electron acoustic mode to explain the high-frequency part of the BEN.

A system under thermodynamic equilibrium arranges the particle in Maxwell-Boltzmann distribution. Maxwell-Boltzmann distribution is the most preferred way of arranging the particle of a system as this have the least entropy, which have a Gaussian type bell curved plot. The earlier studies on plasma waves mainly focused on the Maxwellian particle distribution. However, new high time resolution observations in space plasmas reveals that the particle distributions are characterized by power law decrease, rather than exponential decrease as dictated by Maxwell-Boltzmann distribution. This means most of the space plasma reside in a state which is not in thermal equilibrium with surroundings. The distribution function that is used to describe this state is called non-thermal distribution function or Lorentzian distribution function or Kappa distribution function. The concept of Kappa distribution was introduced by Olbert (1968) which he used to account for the electric current produced by electrons in the magnetosheath. Later on, it was used by Vasyliunas (1968) to fit the electron number data in the magnetosphere by OGO 1 (Orbiting Geophysical Observatory) and OGO 3 satellite. Ever since there had been a numerous observations of this type of distribution function space plasmas [for an extensive review, see Livadiotis (2015)].

In this thesis, low frequency waves such as electrostatic ion cyclotron waves, ion acoustic wave and electron-acoustic waves in multi component space plasmas are studied. Fluid as well as kinetic theory of plasma waves is used to study the coupling of ion-acoustic & ion cyclotron waves and electron-acoustic & electron-cyclotron waves and their generation in Maxwellian and non-thermal plasmas. The harmonic generation of light and heavy ion cyclotron waves has also been studied by using kinetic theory. The relevance of the theoretical results has been brought out in sync with observations in solar wind/lunar wake and magnetospheric plasmas. The thesis is divided into six chapters and detailed description of subject matter discussed in each chapter is given below:

Chapter I

The first chapter deals with the general introduction to the subject of plasma physics including basic definitions and the fundamental principles. The brief description of natural sources of plasma starting from the Sun, solar wind, magnetospheric regions, ionosphere and lunar wake is provided. The theoretical approaches both fluid and kinetic that are used to study the

plasma system are discussed in detail. In space plasmas, often particle distribution departs from Maxwellian and these distributions are known as non-thermal distribution. A brief introduction of kappa distribution, a non-thermal particle distribution frequently observed in space plasmas, is presented. The motivation leading to the research carried out in the thesis and extensive literature survey about the ion & electron-acoustic and ion & electron cyclotron waves and their importance has been discussed thoroughly.

Chapter II

The moon obstructs the flow of solar wind and on the other side creates a cavity that is devoid of plasma. This region is known as lunar wake and this is a region of interesting plasma wave activity. The initial study of Lunar wake plasma dates back to time of Apollo missions. Ever since, there has been a growing interest in the lunar wake region. Lunar wake extends up-to 6.8 R_L, where R_L stands for Lunar radius (Farrell et al., 1998; Ogilvie et al., 1996). ARTEMIS (Acceleration, Reconnection, Turbulence and Electrodynamics of the Moons Interaction with the Sun) mission is a new two-probe lunar mission derived from the THEMIS (Time History of Events and Macroscale Interactions during Substorms) mission. This now consist of ARTEMIS P1 (formerly known as THEMIS-B) and ARTEMIS P2 (formerly known as THEMIS-C). Using the data derived from ARTEMIS P1, a comprehensive analysis of electrostatic waves were undertaken by Tao et al. (2012). Using the 1-D Vlasov simulation techniques of plasma modeled by protons, a suprathermal electron beam and suprathermal electrons, they tried to explain various features of observed electrostatic waves.

In this chapter, we have developed a linear theoretical model to study the low frequency electrostatic waves in the Lunar wake plasma taking inputs from Tao et al. (2012). The lunar wake plasma is modeled by fluid protons, fluid He^{++}, electron beam, and suprathermal electrons following kappa distribution. The effect of magnetic field is neglected here. Using linear- fluid theory, the dispersion relation for the system is derived. Numerical analysis of the dispersion relation hints the existence of six modes in the system: two electron acoustic modes, two fast ion acoustic modes, and two slow ion acoustic modes. The three modes have positive phase speed and other three have negative phase speed are observed.

With an increase in electron beam speed, the electron beam mode gets affected the most and the phase speed turns positive from negative. The electron beam generates beam driven fast and slow ion acoustic waves which are unstable with a finite growth by merging with the fast ion acoustic wave and slow ion acoustic wave, respectively. The electron beam driven slow ion-acoustic waves occur at lower wave-numbers, whereas fast ion-acoustic waves occur at a large value of wave-numbers. We have applied this analysis to the electrostatic waves observed in lunar wake during the first flyby of the ARTEMIS mission. From numerical analysis, it is shown that the frequency corresponding to the maximum growth rate of the electron beam driven slow ion-acoustic mode is $\omega_r = 0.03\omega_{pe}$ and for the electron beam driven fast ion acoustic mode it is $\omega_r = 0.2\omega_{pe}$. These frequency estimates agree very well with the observed low-frequency waves $\omega = 0.01\omega_{pe}$ and high frequency waves $\omega = 0.1 - 0.4\omega_{pe}$ in the lunar wake. The various other parametric variation which affects electron beam driven fast and slow ion acoustic modes are studied in detail.

Chapter III

Introducing magnetic field into any plasma system increase the complexity in the system. As a first step, we have included the magnetic field into our three component model: fluid protons, fluid He^{++}, and suprathermal electrons following kappa distribution. Since magnetic field is included in this system, the wave modes will become dependent on the angle of propagation. In the initial stage, the dispersion relation for the three component plasma is simplified by neglecting the ion contribution. The dispersion relation obtained from this simplification is similar to the one that is observed by Hellberg and Mace (2002); Kadijani et al. (2010); Sultana et al. (2010) for two component plasma. Thereafter, the numerical analysis of this dispersion relation is carried out indicating the existence of coupling of acoustic modes as well as cyclotron modes. The individual wave modes have been studied extensively, however, the coupling of these wave modes was not studied in particular, eventhough, the satellite observations hints the possible coupling (Tang et al., 2015). The above mentioned analysis is extended with the inclusion of fluid ions. Analytically, it is shown that for parallel propagation four different types of modes are present in the plasma: proton cyclotron mode, helium-cyclotron mode, fast ion-acoustic and slow ion-acoustic mode. This

fact is also verified from numerical analysis. Further, when the wave is propagating with finite angle with the magnetic field (say, at 5°), the proton cyclotron mode couples with two modes, i.e., fast ion-acoustic mode at $k\rho_p \approx 0.45$ and slow ion-acoustic mode at $k\rho_p \approx 0.8$ and Helium cyclotron mode couples with fast ion-acoustic mode at $k\rho_p \approx 0.24$ and slow ion-acoustic mode at $k\rho_p \approx 0.41$. With further increase in the angle of propagation, the strength of coupling (which is gauged by the widening of gaps) decreases and finally for perpendicular propagation only cyclotron modes are seen. This chapter also describes in detail the effects of number density of helium ions, superthermality index and temperature of ions.

Chapter IV

Introduction of magnetic field implies the fact that there is a preferred direction in plasma, which in-turn allows the waves to propagate at a finite angle. In this chapter, we have extended the model used in the Chapter II to include the magnetic effects. The dispersion relation predicts the existence of electron cyclotron mode, proton cyclotron mode as well as Helium cyclotron mode along with electron acoustic modes, fast ion acoustic modes, and slow ion acoustic modes. All of these modes have 2 different phase speeds: positive and negative phase speed. This means that for parallel propagation and with zero beam velocity, the dispersion plot looks perfectly symmetrical; there will be six modes with positive phase speed and six will be in negative phase speed. With the increase in the angle of propagation to 1° and without streaming, the dispersion plot show complicated coupling which happening at 6 places (instead of 4 places as described in Chapter III) between these modes: at $k\rho_p \approx 0.05$, mode electron acoustic mode & Helium cyclotron mode: at $k\rho_p \approx 0.10$, mode electron acoustic mode & proton cyclotron mode; at $k\rho_p \approx 0.25$, mode fast ion acoustic mode & Helium cyclotron mode; at $k\rho_p \approx 0.40$, mode slow ion acoustic mode & Helium cyclotron mode; at $k\rho_p \approx 0.45$, mode fast ion acoustic mode & proton cyclotron mode; at $k\rho_p \approx 0.80$, mode slow ion acoustic mode & proton cyclotron mode. The numerical analysis becomes much more complicated when there is finite beam velocity as well as the waves are propagating at an oblique angle as there will be coupling and merging of different waves. This chapter details the results carried out for this problem.

Chapter V

EIC waves are observed in various regions of magnetosphere and has also been studied in various laboratory conditions. However, the studies pertaining to harmonics of ion cyclotron waves are limited. There are indication of presence of double charged alpha particle (He^{++}) which is precipitating into night side auroral zone (Sharp et al., 1974). The origin of these alpha particle is from solar wind. Theoretically, there has not been any study on EICI involving He^{++}. So in this chapter, excitation of EIC waves and it's harmonic is studied with the aid of kinetic theory.

A three-component magnetized plasma consisting of beam electrons, protons and doubly charged Helium ions is considered to model the auroral plasma. The dispersion relation is derived under the suitable approximation of plasma dispersion function. The dispersion relation so obtained in much more general than what was derived by Rosenberg and Merlino (2009) in the sense that calculation of instability includes the damping arising due to proton and helium ions. We have found that this inclusion significantly alter the nature of harmonics which can be sustained in plasma. We have cross checked our results with Okuda et al. (1981) and Rosenberg and Merlino (2009) by putting the density of He^{++} to be zero. It is seen that though the growth rate for fundamental mode peaks near $k\rho_p \sim 1$ in both the cases with $\omega/\Omega_p \approx 1$ as pointed out by Okuda et al. (1981) for two-component plasma, However, this condition is easily violated when there is a slight variation of the plasma parameters. The numerical analysis indicates that with the increase in the angle of propagation, fewer harmonics of proton cyclotron waves with decreased growth rates and higher number of Helium harmonics with decreased growth rates are excited. The interesting feature of this analysis reveals that largely odd Helium harmonics are excited. The theory that is developed is general in nature and can be applied not only to any particular magnetospheric region, even in the solar corona (Luhn, 1984; Hinata, 1980).

Chapter VI

The results obtained in Chapters II-V are summarized and the future scope of the work is also discussed in this chapter.

Bibliography

W. Baumjohann and R. A. Treumann. *Basic Space Plasma Physics*. Imperial College Press, 2012. ISBN 978-1-84816-895-4. doi: 10.1142/p850.

R. Bergmann, I. Roth, and M. K. Hudson. Linear stability of the h+ - o+ two-stream interaction in a magnetized plasma. *J. Geophys. Res.- Space*, 93(A5):4005, 1988. doi: 10.1029/ja093ia05p04005.

C. Cattell, R. Bergmann, K. Sigsbee, C. Carlson, C. Chaston, R. Ergun, J. McFadden, F. S. Mozer, M. Temerin, R. Strangeway, R. Elphic, L. Kistler, E. Moebius, L. Tang, D. Klumpar, and R. Pfaff. The association of electrostatic ion cyclotron waves, ion and electron beams and field-aligned currents: FAST observations of an auroral zone crossing near midnight. *Geophys. Res. Lett.*, 25(12):2053–2056, 1998. doi: 10.1029/98gl00834.

F. F. Chen. *Introduction to Plasma Physics and Controlled Fusion*. Springer International Publishing, 2016. ISBN 978-3-319-22309-4. doi: 10.1007/978-3-319-22309-4.

V. W. Chow and M. Rosenberg. Electrostatic ion cyclotron instabilities in negative ion plasmas. *Phys. Plasmas*, 3(4):1202–1211, 1996. doi: 10.1063/1.871744.

S. R. Cranmer, A. A. van Ballegooijen, and R. J. Edgar. Self-consistent coronal heating and solar wind acceleration from anisotropic magnetohydrodynamic turbulence. *Astrophys. J. Supp. S.*, 171(2):520–551, 2007. doi: 10.1086/518001.

N. D'Angelo. Propagation and damping of ion waves in a plasma with negative ions. *Phys. of Fluids*, 9(8):1605, 1966. doi: 10.1063/1.1761904.

N. D'Angelo and R. W. Motley. Electrostatic oscillations near the ion cyclotron frequency. *Phys. Fluids*, 1962. doi: 10.1063/1.1706672.

W. M. Farrell, M. L. Kaiser, J. T. Steinberg, and S. D. Bale. A simple simulation of a plasma void: Applications to wind observations of the lunar wake. *J. Geophys. Res.- Space*, 103 (A10):23653–23660, 1998. ISSN 2156-2202. doi: 10.1029/97JA03717.

B. D. Fried and R. W. Gould. Longitudinal ion oscillations in a hot plasma. *Phys. Fluids*, 4 (1):139–147, 1961. doi: 10.1063/1.1706174.

G. Ganguli, S. Slinker, V. Gavrishchaka, and W. Scales. Low frequency oscillations in a plasma with spatially variable field-aligned flow. *Phys. Plasmas*, 9(5):2321–2329, 2002. doi: 10.1063/1.1445181.

V. V. Gavrishchaka, G. I. Ganguli, W. A. Scales, S. P. Slinker, C. C. Chaston, J. P. McFadden, R. E. Ergun, and C. W. Carlson. Multiscale coherent structures and broadband waves due to parallel inhomogeneous flows. *Phys. Rev. Lett.*, 85(20):4285–4288, 2000. doi: 10.1103/physrevlett.85.4285.

D. A. Gurnett and L. A. Frank. Ion acoustic waves in the solar wind. *J. Geophys. Res.- Space*, 83(A1):58–74, 1978. ISSN 2156-2202. doi: 10.1029/JA083iA01p00058.

M. A. Hellberg and R. L. Mace. Generalized plasma dispersion function for a plasma with a kappa-maxwellian velocity distribution. *Phys. Plasmas*, 9(5):1495–1504, 2002. doi: 10.1063/1.1462636.

S. Hinata. Electrostatic ion-cyclotron heating of solar atmosphere. *Astrophys. J.*, 235:258, jan 1980. doi: 10.1086/157629.

M Nouri Kadijani, H Abbasi, and H Hakimi Pajouh. Influence of superthermal electrons on obliquely propagating ion-acoustic solitons in magnetized plasmas. *Plasma Phys. Contr. F.*, 53(2):025004, 2010. doi: 10.1088/0741-3335/53/2/025004.

J. M. Kindel and C. F. Kennel. Topside current instabilities. *J. Geophys. Res.- Space*, 76 (13):3055–3078, 1971. doi: 10.1029/JA076i013p03055.

P. M. Kintner, M. C. Kelley, R. D. Sharp, A. G. Ghielmetti, M. Temerin, C. Cattell, P. F. Mizera, and J. F. Fennell. Simultaneous observations of energetic (keV) upstreaming and electrostatic hydrogen cyclotron waves. *J. Geophys. Res.- Space*, 84(A12):7201, 1979. doi: 10.1029/ja084ia12p07201.

E. J. Koen, A. B. Collier, S. K. Maharaj, and M. A. Hellberg. Particle-in-cell simulations of ion-acoustic waves with application to saturn‘s magnetosphere. *Phys. Plasmas*, 21(7): 072122, 2014. doi: 10.1063/1.4891320.

M. E. Koepke. Contributions of q-machine experiments to understanding auroral particle acceleration processes. *Phys. Plasmas*, 9(5):2420–2427, 2002. doi: 10.1063/1.1456068.

M. J. Kurian, S. Jyothi, S. K. Leju, M. Isaac, C. Venugopal, and G. Renuka. Stability of electrostatic ion cyclotron waves in a multi-ion plasma. *Pramana*, 73(6):1111–1122, 2009. doi: 10.1007/s12043-009-0171-z.

L. C. Lee and J. R. Kan. Nonlinear ion-acoustic waves and solitons in a magnetized plasma. *Phys. Fluids*, 24(3):430–433, 1981. doi: 10.1063/1.863389.

N. Lin, P.J. Kellogg, R.J. MacDowall, and S.P. Gary. Ion acoustic waves in the heliosphere. *Space Sci. Rev.*, 97(1):193–196, 2001. ISSN 1572-9672. doi: 10.1023/A:1011823505395.

G. Livadiotis. Introduction to special section on origins and properties of kappa distributions: Statistical background and properties of kappa distributions in space plasmas. *J. Geophys. Res.- Space*, 120(3):1607–1619, 2015. doi: 10.1002/2014ja020825.

A. Luhn. Selective heating of minority ions in the lower solar corona by electrostatic ion cyclotron waves. *Adv. Space Res.*, 4(2-3):165–168, jan 1984. doi: 10.1016/0273-1177(84)90308-9.

J. D. Menietti, P. Schippers, O. Santolík, D. A. Gurnett, F. Crary, and A. J. Coates. Ion cyclotron harmonics in the saturn downward current auroral region. *J. Geophys. Res.- Space*, 116(A12):n/a–n/a, 2011. doi: 10.1029/2011ja017102.

S. R. Mosier and D. A. Gurnett. Ionospheric observation of vlf electrostatic noise related to harmonics of the proton gyrofrequency. *Nature*, 1969. doi: 10.1038/223605a0.

D. R. Nicholson. *Introduction to plasma theory*. John Wiley, 1983. ISBN 047109045X.

M. Barati Moqadam Niyat, S. M. Khorashadizadeh, and A. R. Niknam. Electrostatic ion cyclotron instability in a plasma with q-nonextensive distributions. *Phys. Plasmas*, 23 (12):122110, 2016. doi: 10.1063/1.4971810.

K. W. Ogilvie, J. T. Steinberg, R. J. Fitzenreiter, C. J. Owen, A. J. Lazarus, W. M. Farrell, and R. B. Torbert. Observations of the lunar plasma wake from the wind spacecraft on december 27, 1994. *Geophys. Res. Lett.*, 23(10):1255–1258, 1996. ISSN 1944-8007. doi: 10.1029/96GL01069.

H. Okuda, C. Z. Cheng, and W. W. Lee. Numerical simulations of electrostatic hydrogen cyclotron instabilities. *Phys. Fluids*, 24(6):1060, 1981. doi: 10.1063/1.863484.

S. Olbert. *Summary of Experimental Results from M.I.T. Detector on IMP-1*. Springer Netherlands, 1968. ISBN 978-94-010-3467-8.

S. ur Rehman, Q. ul Haque, and A. Shah. Interplanetary ion acoustic wave in solar wind plasma. *Physics of Plasmas*, 25(8):084503, 2018. doi: 10.1063/1.5028338.

M. Rosenberg and V. W. Chow. Collisional effects on the electrostatic dust cyclotron instability. *J. Plasma Physics*, 1999.

M Rosenberg and RL Merlino. Instability of higher harmonic electrostatic ion cyclotron waves in a negative ion plasma. *J. Plasma Physics*, 75(04):495–508, 2009. doi: 10.1017/S0022377808007642.

N. Sato. Production of negative ion plasmas in a q machine. *Plasma Sources Sci. T.*, 3(3): 395–399, 1994. doi: 10.1088/0963-0252/3/3/024.

F. L. Scarf, D. A. Gurnett, and W. S. Kurth. Jupiter plasma wave observations: An initial voyager 1 overview. *Science*, 204(4396):991–995, 1979. ISSN 0036-8075. doi: 10.1126/science.204.4396.991.

R. D. Sharp, R. G. Johnson, and E. G. Shelly. Satellite measurements of auroral alpha particles. *J. Geophys. Res.- Space*, 79(34):5167–5170, 1974. doi: 10.1029/JA079i034p05167.

S. V. Singh and G. S. Lakhina. Electron acoustic solitary waves with non-thermal distribution of electrons. *Nonlinear Proc. Geoph.*, 11(2):275–279, 2004. URL `https://hal.archives-ouvertes.fr/hal-00302331`.

S.V. Singh and G. S. Lakhina. Generation of electron-acoustic waves in the magnetosphere. *Planet. Space Sci.*, 49(1):107–114, 2001. doi: https://doi.org/10.1016/S0032-0633(00)00126-4.

R. Slapak, H. Gunell, and M. Hamrin. Observations of multiharmonic ion cyclotron waves due to inverse ion cyclotron damping in the northern magnetospheric cusp. *Geophys. Res. Lett.*, 44(1):22–29, 2017. doi: 10.1002/2016gl071680.

S. Sultana, I. Kourakis, N. S. Saini, and M. A. Hellberg. Oblique electrostatic excitations in a magnetized plasma in the presence of excess superthermal electrons. *Phys. Plasmas*, 17 (3):032310, 2010. doi: 10.1063/1.3322895.

X. Tang, C. Cattell, R. Lysak, L. B. Wilson III, L. Dai, and S. Thaller. Themis observations of electrostatic ion cyclotron waves and associated ion heating near the earth's dayside magnetopause. *J. Geophys. Res.- Space*, 120(5):3380–3392, 2015. doi: 10.1002/2015JA020984.

J. B. Tao, R. E. Ergun, D. L. Newman, J. S. Halekas, L. Andersson, V. Angelopoulos, J. W. Bonnell, J. P. McFadden, C. M. Cully, H.-U. Auster, K.-H. Glassmeier, D. E. Larson, W. Baumjohann, and M. V. Goldman. Kinetic instabilities in the lunar wake: Artemis observations. *J. Geophys. Res.- Space*, 117(A3), 2012. doi: 10.1029/2011JA017364.

V. M. Vasyliunas. A survey of low-energy electrons in the evening sector of the magnetosphere with ogo 1 and ogo 3. *J. Geophys. Res.- Space*, 73(9):2839–2884, 1968. doi: 10.1029/JA073i009p02839.

K. Watanabe and T. Taniuti. Electron-acoustic mode in a plasma of two-temperature electrons. *J. Phys. Soc. Jpn.*, 43(5):1819–1820, 1977. doi: 10.1143/JPSJ.43.1819.

A. Y. Wong, D. L. Mamas, and D. Arnush. Negative ion plasmas. *Phys. Fluids*, 18(11):1489, 1975. doi: 10.1063/1.861034.

M. Y. Yu and P. K. Shukla. Linear and nonlinear modified electron-acoustic waves. *J. Plasma Phys.*, 29(3):409–413, 1983. doi: 10.1017/S0022377800000866.

(T. Sreeraj) (Prof. Satyavir Singh)

Candidate Guiding Teacher